SAI/2000-029/Rp

3rd ISO POST-OPERATIONS CROSS-CALIBRATION STATUS REPORT

v1.0

June 8, 2000

P. García-Lario

Contents

1 Introduction

1.1 Scope

This is the third of a series of Reports generated every six months by the ISO Data Centre (IDC, hereafter) which tries to summarize the up-to-date status (as of June 2000) of (cross-)calibration activities during the ISO Post-Operations Phase (POPS, hereafter).

It includes information on the latest achievements in the calibration of all four ISO instruments with special emphasis on cross-calibration aspects as well as an assessment of the progress made in the last six months within the framework of the POPS Cross-Calibration Plan.

The previous (First and Second) Status Reports can be found respectively at:

`http://www.iso.vilspa.esa.es/users/expl_lib/ISO/1st_status_report_ext.ps.gz`

and

`http://www.iso.vilspa.esa.es/users/expl_lib/ISO/2nd_status_report_ext.ps.gz`

This series of Status Reports will culminate in the Final POPS Cross-Calibration Status Report to be issued in April 2001.

1.2 Structure of cross-calibration activities

The global IDC strategy for approaching cross-calibration during the Post-Operations phase, as described in the ISO POPS Cross-Calibration Plan, is based on topic-oriented Working Groups, each one of them addressing one specific calibration topic.

Working Groups are formed by members from the IDC and from the different NDCs. They are also open to contributions from external individuals interested in actively participating in ISO calibration activities.

Currently, eight Working Groups (WGs, hereafter) have been created and are actively working on:

- Beam Profiles/Pointing
- Glitches
- Line profiles
- Photometric calibration
- Polarisation
- Spectral Matching and RSRF
- Transients
- Interactive Analysis

Of course, the topics addressed by each of these WGs overlap in many cases since many cuts through the calibration issue are possible. For example, studies of *Transients* are fundamental to a full understanding of the instruments' photometric calibration, which is the main goal of the *Photometric Calibration* WG.

The WG scheme provides them with a platform to exchange their knowledge and to progress with respect to their own subject.

It is the responsibility of cross-calibration manpower to maintain an overview of the work of the several Working Groups, cooperate with instrument-specific calibration manpower in efforts to understand inconsistencies of calibration relevant to more than one instrument and establish links between the different Working Groups when necessary favouring a fluid exchange of useful information.

An up-to-date overview of the composition of each of these WGs can be found at:

`http://www.iso.vilspa.esa.es/users/expl_lib/ISO/WG_COMPOSITION_3.PS`

Note that the chair of the Polarisation WG has now left ESA. The work of that WG is considered to have been largely completed with the release of the ESA SP series proceedings *"ISO Polarisation Observations"* ESA SP-435, December 1999. No further work is planned on CAM polarisation calibration. Update notes will be provided for PHT as appropriate.

1.3 Final Goals: General

The objectives of cross-calibration can be summarized as follows:

- Compare the results of different ISO instruments and verify the errors quoted for each instrument-specific calibration. Where these results appear to be inconsistent seek to understand and to eliminate those differences.

- Compare ISO results with external data (e.g. ground based observations, KAO data, IRAS, MSX, COBE,..). Where results appear to be inconsistent seek to understand and to eliminate those differences.

- Verify that, from a more global point of view, the calibrations of the individual ISO instruments are correct, and ensure a certain level of homogeneity and consistency of the data and how they were calibrated (e.g. compatibility of models, bandpass zero-points, and of calibration philosophy and procedures).

The intention is to have a flexible plan/strategy with these goals as a reference which is materialized in a detailed schedule of cross-calibration activities for each of the Working Groups listed above.

Responsibility for cross-calibration planning is with the IDC in close interaction with the NDCs, which are responsible for instrument-specific calibration.

1.4 Final Goals: per Working Group

1.4.1 Beam Profiles/Pointing

· Characterization of the instruments' beam profiles.

- Address common problems (asymmetries, vignetting, ghosts,..) and their possible relation to the ISO telescope point spread function (PSF).
- Allow cross-fertilisation of models available.
- Evaluation of common deconvolution tools, to apply to extended source data, once beam profile calibration files become available.
- Support improvement of ISO pointing reconstruction in OLP.

1.4.2 Glitches

- Statistical analysis and characterization of glitches in the four ISO instruments. Study of the relation with the space radiation environment.
- Compare glitch statistics and glitch height distributions with model predictions and simulations.
- Enhance the quality of the reduced ISO data, improving the de-glitching and de-tailing algorithms in the pipeline and/or IA.
- Keep the knowledge on the radiation environment and its effects on the detectors, so that it can be applied to future missions.

1.4.3 Line profiles

- Characterize the SWS and LWS observed instrumental profiles.
- Study the stability of these instrumental profiles as a function of time, forward and backward scans, detector, line strength and point-like versus extended sources.
- Analysis and interpretation of deviations found from line profile definition; recommendations and caveats.
- Comparison with theoretical instrumental profiles and resolution.

1.4.4 Photometric calibration

- Definition of the photometric system and description of calibration sources/ models used in ISO data reduction.
- Characterization of the photometric accuracies achieved by each ISO AOT (and the corresponding photometric 'error budget').
- Make periodic 4-instrument photometric comparisons on selected sample targets and extend this comparison to calibration models and to photometric results obtained with other facilities (DIRBE/IRAS/MSX/KAO, ground-based,..) using OLP data products.

· Make similar comparisons on a subsample of targets using data reduced with the latest available versions of the instrument IAs and compare this with OLP photometric accuracies.

· Testing of photometric improvements as new algorithms or calibration files become available stimulating their inclusion into the corresponding IAs first and eventually into the pipeline.

· Identification and analysis of photometric calibration problems affecting OLP data products providing recommendations and caveats to the users of the ISO Legacy Archive.

1.4.5 Polarisation

· Characterization of the polarimetric capabilities of ISO. Angles, detection limits, wavelength dependency, internal consistency (PHT,CAM) and comparison with external data.

1.4.6 Spectral Matching and RSRF

· Analysis of spectral matching between LWS and SWS in the overlapping region. Same with CAM-CVF and PHT-S spectra. Comparison with models.

· Identification of possible systematic errors in the measured spectral response to extended sources by comparing the observations from a variety of instruments. Effects on the determination of spectral line fluxes.

· Expansion of cross-calibration between the instruments beyond the wavelength regions which they have in common.

· Characterization of the Relative Spectral Response Function (RSRF) for all ISO spectroscopic modes.

1.4.7 Transients

· Characterize transient effects in the 4 ISO instruments and determine the best correction method as a function of detector type, observing mode and characteristics of the source, and estimation of effects on photometric accuracy.

· Stimulate the development and implementation of S/W tools to detect and correct transient effects in IAs first and eventually in the pipeline.

1.4.8 Interactive Analysis

· Coordinate the information flow between developers of the different instruments' IAs, making sure that each team is aware of what other teams are doing and that S/W tools developed by one of the teams are made available to other teams if they consider it useful.

· Stimulate the implementation of new S/W tools in the four ISO instruments' IAs.

· Raise the profile of the various IA packages as means to enhance data reduction.

· Investigate communication channels between the IA users and IA developers in both directions.

2 Review of Cross-Calibration Plan

2.1 Overview of Working Group activities

As it is defined in the ISO POPS Cross-Calibration Plan, the WGs should:

- look at major calibration issues across instrument boundaries
- identify problems, (interim-)goals and milestones (usually linked to OLP milestones)
- trigger/recommend further work, and recognise imperatives in their area
- establish and pursue relevant contacts in NDCs
- identify good calibration sources and strategies.

2.2 Report on actions on-going and/or closed

A number of actions proposed in the last version (2.0) of the ISO POPS Cross-Calibration Plan, have been closed in the last six months. In the following, a summary of the main results found and conclusions reached is provided, sorted by WG. In some cases, the activities described below were not directly carried out by members of the WG but they are included because they might be relevant for the future planning of the WG or to illustrate a progress on the current understanding of a problem under analysis by a specific WG. Reports on other actions closed before December 1999 can be found in the previous issues of this document (First and Second Cross-Calibration POPS Status Reports).

2.2.1 Beam Profiles/Pointing :

```
BP: Proceedings of the Workshop:  "ISO Beyond point sources:
     studies of extended  infrared emission" held at VILSPA
     (September 14-17, 1999)
```

The organisation of this Meeting at VILSPA in September 14-17, 1999 was undoubtfully a major milestone in the activities of this WG.

The aim was to bring together scientists working on ISO programmes in which the analysis of extended emission was important, to exchange results and experiences.

The analysis of extended sources requires expertise in surface brightness calibration, map construction, and source flux extraction to arrive at reliable results and interpretation.

More than 40 astronomers attended the Workshop and now the Proceedings of this Workshop are about to be published in volume 455 of the ESA Special Publication Series.

Before it becomes available, the final programme and abstracts of the presentations given can be found at:

`http://www.iso.vilspa.esa.es/meetings/isobeyond/fourth_announcement.html`

`BP: ISO telescope asymmetric PSF model revision`

The model is reviewed in detail in the document: *"The ISO point spread function and CAM beam profile"* by Koryo Okumura, presented at the "ISO Beyond point sources: studies of extended infrared emission" Workshop above mentioned. In this document the Point Spread Function (PSF) of the ISO telescope as seen by CAM is analysed and compared with the theoretical PSF computed using two independent methods (Fast Fourier Transform of the telescope aperture and ray-tracing using coherent light). Obviously the CAM's PSFs suffer from instrumental effects (Figure 1). The asymmetry observed in the PSF is especially noticeable on its first ring and arises either from the telescope or the camera. Unfortunately, it is difficult to separate the instrumental contribution from the PSF of the telescope, but the asymmetry is not reproduced by the simple aperture model in Fourier space, unless a certain phase information is added in the complex aperture together with its amplitude. This non-zero phase in the aperture corresponds to a slight offset of the secondary mirror of the telescope from its nominal position. This is also verified using the ray-tracing model of the PSF. PSF models with an offset equivalent to a lateral displacement in the position of the secondary mirror of just 0.3 mm combined with a small displacement along the optical axis (they have complementary effects) are found to be consistent with the asymmetry enhancement observed at shorter wavelengths. However, the models tend to produce a stronger wavelength dependency than observed.

It may be worth to note also that the measured PSFs have a FWHM consistent with the observed value for all filters except for the LW1 filter, which shows a larger FWHM than the predicted value. This might be explained as

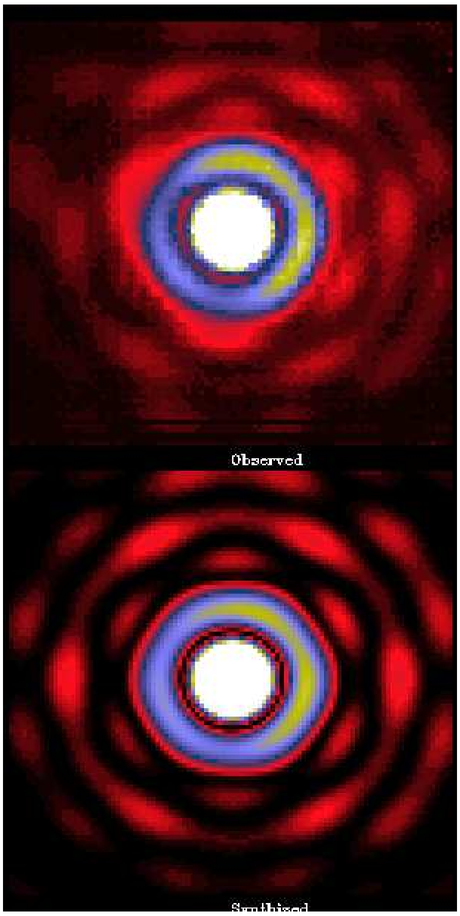

Figure 1: Observed (top) and synthesized (bottom) PSFs: 1.5″ pixel field of view at LW9 (15 μm) - Koryo Okumura

a transient effect in the PSF microscan for this low-background filter, but this possibility has not been checked.

`BP: Ghosts correction: revision of status`

One of the instrumental contributions which causes most difficulties in the extended source calibration of ISOCAM data is the presence of ghost images generated by multi-reflections inside the instrument (between the detector plane and the filter plane). Using calibration observations performed during the mission with the specific purpose of measuring this effect it can be estimated that the errors induced by ghosts in the photometry can amount up to 35% in the worst cases. The error contribution also depends on the wavelength. The effect

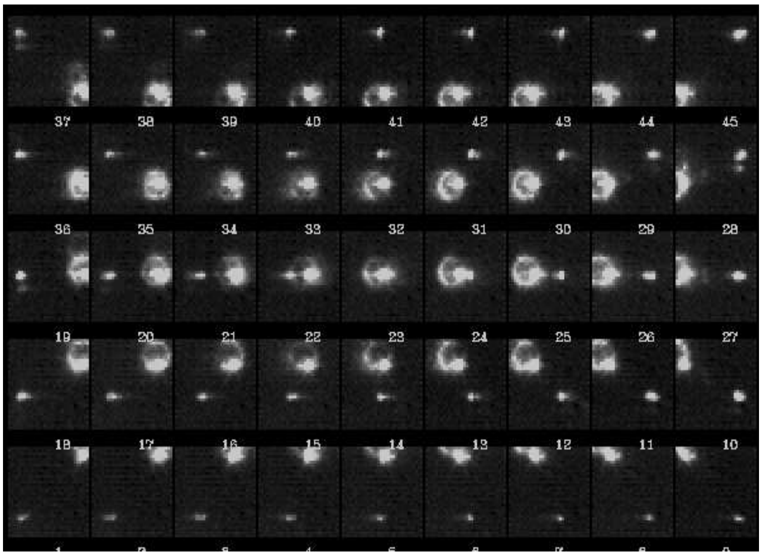

Figure 2: Global behaviour of ghosts (ring-like feature) when a point source (small spot) moves over the detector (CVF at 7 μm with a pixel feld of view of $6''$ in revolution 531) - Koryo Okumura

in any case is stronger when using the CVF than for broad band filters, and has its maximum intensity for objects observed at the edges of the detector (Figure 2).

The latest review on the ghost problem and corrections so far available can be found in the document *"The ISO point spread function and CAM beam profile"* by Koryo Okumura.

The optical model at the present stage can reproduce qualitatively the brightness distribution of the ghosts but it is still not able to predict the quantitative impact of the ghosts on the photometry.

A tentative correction has been derived for the ghost of a uniformly extended source, such as the Zodiacal light, which is expected to be contaminated by ghosts all over the image. Extended sources show a characteristic pattern, lung-like (Figure 3), interpreted as due to reflections on different parts of the CVF with different reflection coefficient.

By adjusting the coefficients of the brightest and faintest parts of the lung-like pattern, one can obtain a reasonable correspondance between the wavelength dependence of this pattern with that observed in the case of point sources. Spectra of the zodiacal light obtained with CAM CVF can then be corrected up to a level where residuals are of the order of 10% (LW) to 20% (SW). The spectrum before and after correcting for ghosts is shown in Figure 4, where we can see that the broad feature observed at 10 μm, previously interpreted as

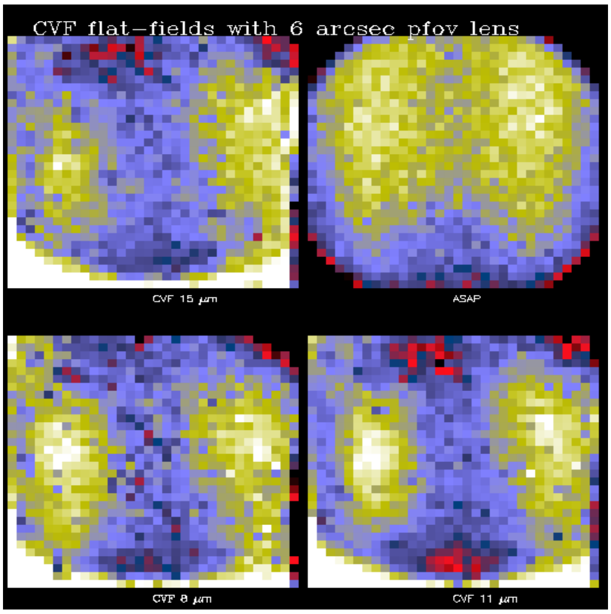

Figure 3: Flat fields given by the zodiacal light observed at 3 wavelengths of the CVFs compared to the flat field produced by a ray-tracing model (upper right panel) - Koryo Okumura

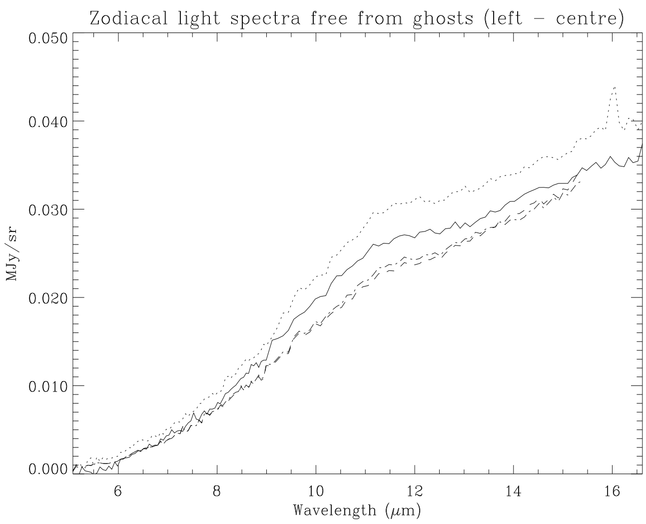

Figure 4: Zodiacal light spectra measured on the detector central region (solid line), on the left 'lung' (dashed line) and ghost corrected spectra of forward and backward CVF scans (dashed-dotted line) - Koryo Okumura

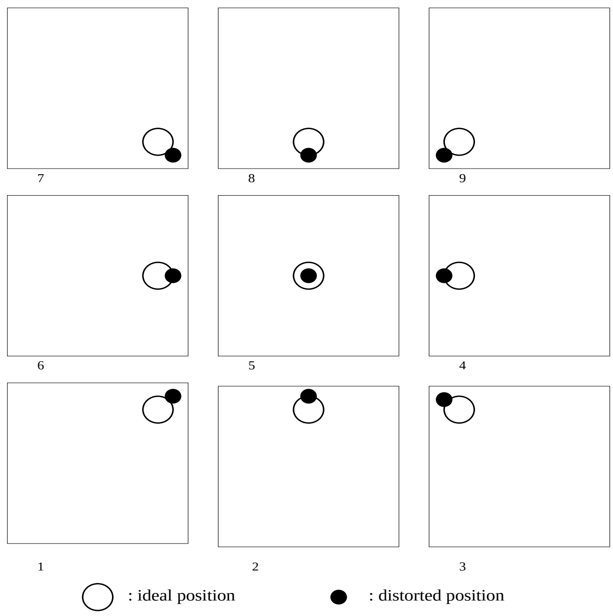

Figure 5: Distorted raster observation of a point source with ISOCAM - ISO CAM Handbook

silicates, tends to be reduced by this ghost correction.

Before any correction for ghosts is made available either in CIA or the pipeline for CAM-CVF, the user must be aware that since the Spectral Response Function of CAM-CVF was derived without including the ghost flux into the estimation of the total flux from a star, for consistency they should not include the ghost flux in the estimation of the total flux of a given source.

`BP: Field distortion corrections in ISOCAM data`

Distortions in the ISOCAM field of view have to be taken into account in order to fill the gap of the calibration data. The differences between the ideal positions and the real measurements (Figure 5) are known to occur because of all the optical elements encountered in the beam path.

For a detailed description of the current status of the problem the document *"ISOCAM LW Channel Field of View Distortion"* by Hervé Aussel (1998) is available at:

`http://www.iso.vilspa.esa.es/users/expl_lib/CAM/distortion.ps.gz`

Field distortion increases with the pixel field of view (p.f.o.v., hereafter) and has been derived for the LW channel $6''$ and $3''$ lenses, from particular CAM

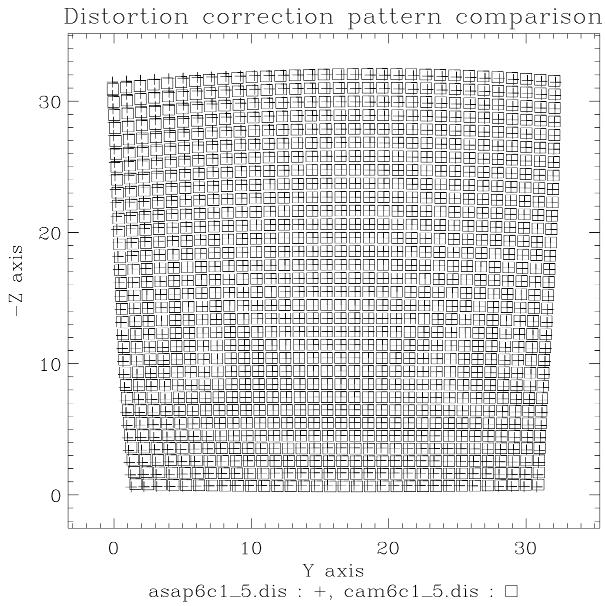

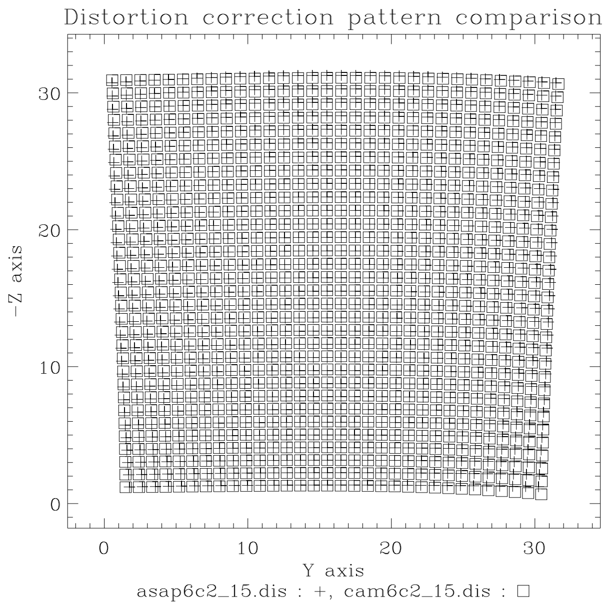

Figure 6: Comparison between observations (squares) and model (crosses) for CVF1 at 5 μm (top) and for CVF2 (bottom) at 15 μm both through $6''$ pixel field of view - Koryo Okumura

data sets using calibration observations of fields that contained many stars. No measurements have been made for the 1.5$''$ lens because the distortion is in general cases small and the measurements too difficult to perform as the amplitude of the satellite jitter is of the order of the quantities to be measured.

The raster pattern size also increases with wavelength (∼4.5 % from 4 to 15 μm) and can be modelled with a suitable choice of the refractive index.

For CAM images taken with the 6$''$ and 3$''$ p.f.o.v., third order polynomial coefficients have been derived which are able to reproduce the distortions observed (see Figure 6). They are found to depend also on lens position. Currently, a distortion correction is implemented in CIA which uses the coefficients corresponding to the nearest configuration. However, the distortion seems to be different also for different filters with the same configuration.

Optical models can help to derive a complete set of polynomials taking this into account, even when no calibration observations are available. We know that there are several elements playing a role in creating distortion effects. First, the field mirror tilt, which creates a deformation with trapezoidal form; second, the lens aberration, which creates a pin cushion distortion; and third, the filter width, which has an effect on the magnification.

The final goal of this investigation is to develop a tool based on this optical model able to correct quantitatively for field distortion for any CAM configuration. Observations and model now basically agree but some further fine tuning is still required. Efforts are currently on-going trying to describe the distortions observed at different wavelengths by a single parameter K and determine the effect of lens wheel positioning uncertainty. This 'distortion parameter' K depends on the choice of the origin of coordinates of the polynomials and represents the displacement of the optical axis of ISOCAM with respect to the detector centre.

`BP: Implementation of SWS beam profile calibration files in SWS IA`

The SWS beam profile model generated by Douwe Beintema (see previous Status Report) has been used as input for the production of the corresponding calibration files. They were generated by covering an area of 12$'\times$12$'$ with a spacing of 1$''$. These new Cal-G files are expected to be of extraordinary help in the calibration of extended sources and bad-pointed observations. They are now being implemented in SWS IA and will be distributed together with the SWS version 9.5 pipeline data products (to be released in September 2000).

The idea is now to compare the beam profile model with the telescope PSF model provided by Koryo Okumura and check for consistency.

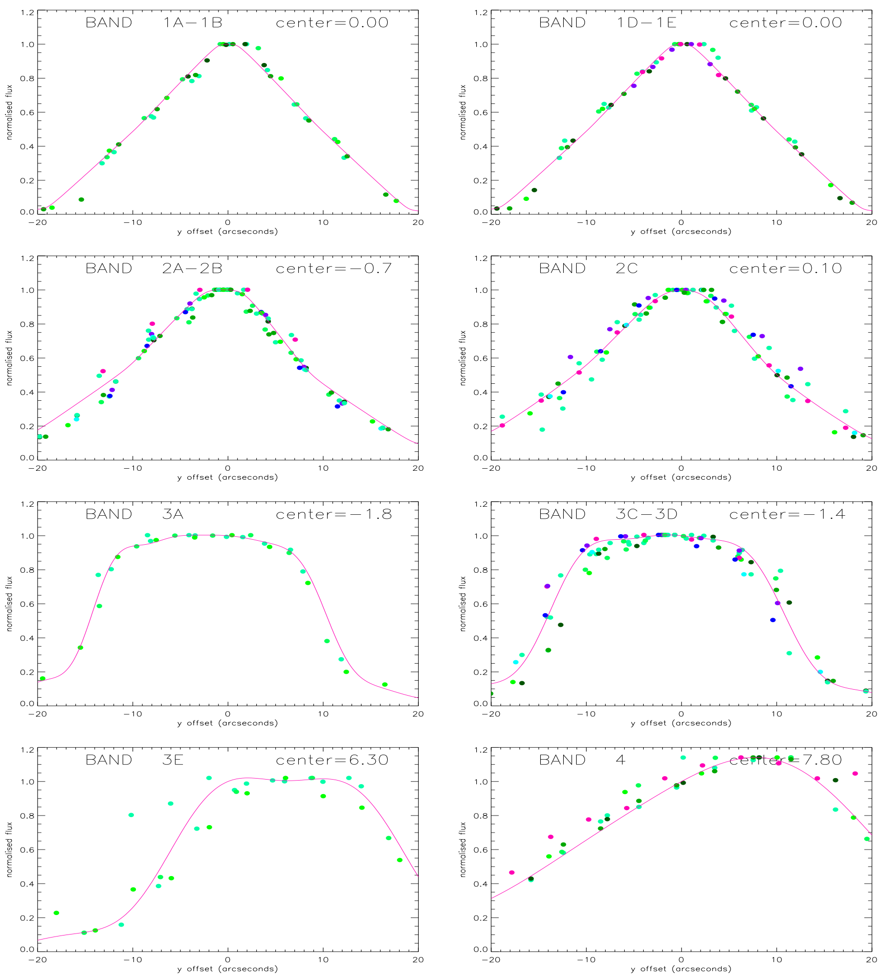

Figure 7: SWS beam profiles. Comparison between model and observations in the y-axis for the different SWS bands - Douwe Beintema + Rosario Lorente

`BP: Implementation of SWS pointing correction tool in SWS IA`

As we have already mentioned, the SWS beam profiles provided by Douwe Beintema, fine tuned to fit merged data sets of calibration observations consisting of rasters made on several point sources are now available. Model and observations were compared for the different SWS bands and axis with a general good agreement.

The beams, as it can clearly be seen in Figure 7, are in many cases far from flat-topped. This makes SWS very sensitive to small pointing offsets. In addition, there are internal detector misalignments which can reach up to $8''$ and produce mismatches between different bands.

In order to correct for the effects produced in SWS spectra by these detector misalignments and peaked profiles, a pointing correction tool has been generated and it is now being implemented in SWS IA, which is able to correct for absolute pointing offsets up to $10''$ with a resolution of $0.1''$.

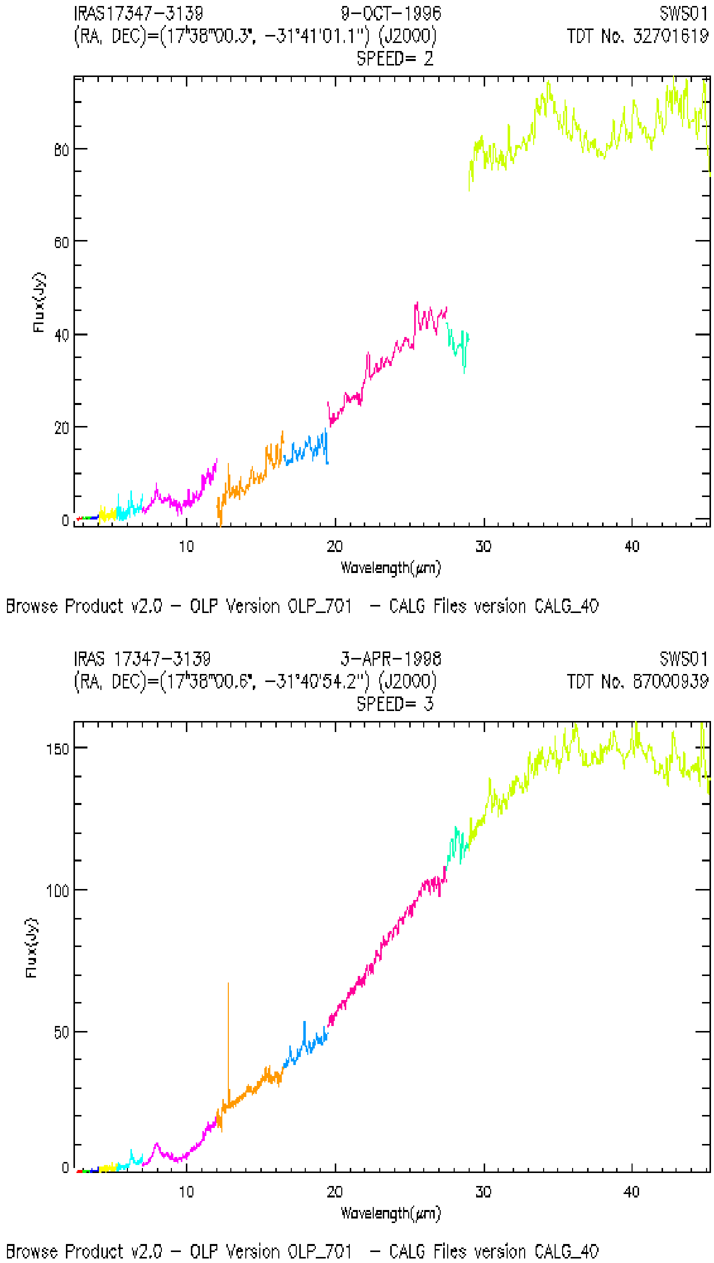

Figure 8: Example of a bad pointed SWS observation (top) compared to the SWS spectrum of the same source taken with the correct coordinates (bottom).

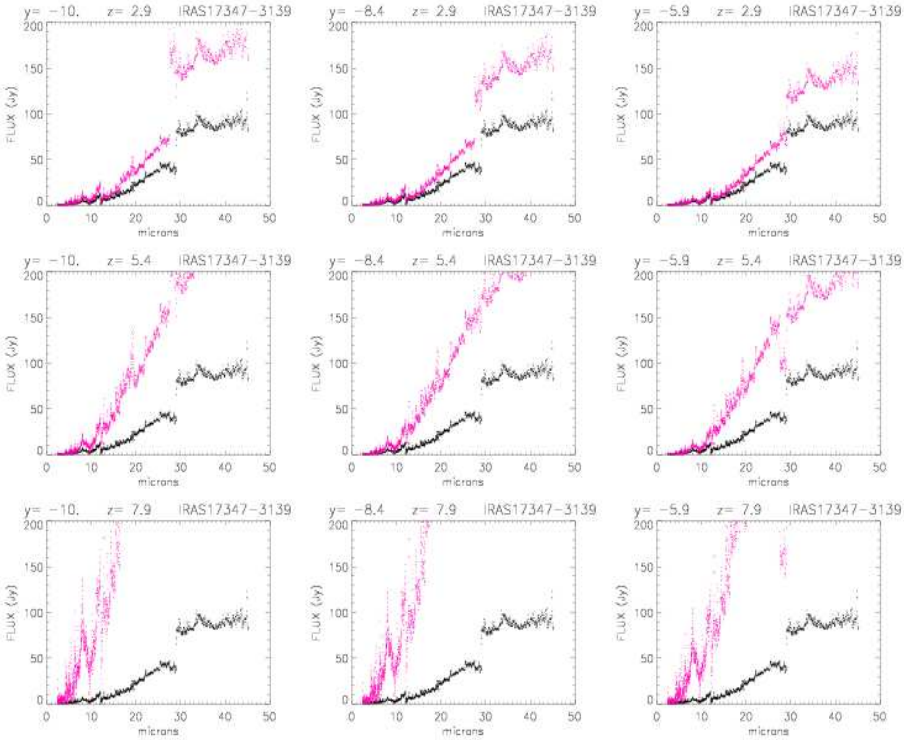

Figure 9: Example of the use of the pointing correction tool: an offset of (y=−8″; z=+5″) is able to remove the band mismatches and bring the flux level into agreement with the on-target measurement - Alberto Salama

In Figure 8 we show the SWS spectrum of a source observed off-centre compared to the SWS spectrum of the same source taken with the correct coordinates. As expected, the bad pointed observation shows strong band mismatches and a much lower flux level.

Figure 9 shows how the pointing correction tool is able to completely remove the mismatches observed between the SWS bands and bring the flux level into a much better agreement (20%) with the on-target measurement for an offset of (y=−8″; z=+5″), which exactly corresponds to the actual offset existing between the two observations shown in Figure 8, as derived from the input coordinates.

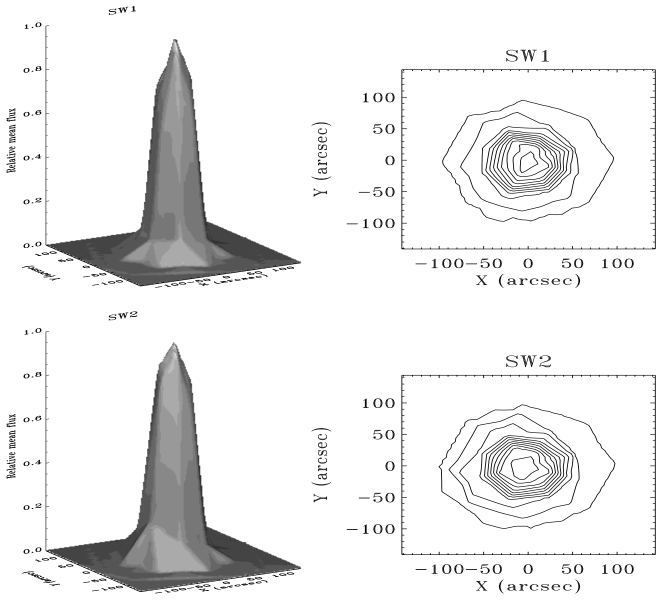

Figure 10: 3-D and contour plots of the beam profile of the LWS detectors SW1 and SW2 - Chris Lloyd

`BP: Characterisation of LWS beam profiles`

As for the other ISO instruments, the flux calibration of LWS is made on the basis of point-like sources. This means that if we want to derive the surface brightness of an extended source measured with ISO, conversion factors are needed to transform point source fluxes (Jy) into extended source fluxes (MJy/sr).

This can be made in the case of an infinitely extended and homogeneous source via the knowledge of the beam profiles. A description of the methodology followed to derive these conversion factors for the four ISO instruments is given in the paper *"ISO Beam Profiles and extended source flux calibration"* by Alberto Salama presented also at the "ISO Beyond point sources: studies of extended infrared emission" Workshop.

Concernig LWS, conversion factors from point source to extended source fluxes were derived by Chris Lloyd from the LWS mean beam profile (averaged over radial directions) and IDL routines to compute the mean beam as a function of position have recently been implemented in version 2.0 of ISAP.

Application of these conversion factors to a few LWS rasters scans on extended sources significantly improves the level of agreement of ISO calibration with the flux derived from IRAS maps of the same positions in the sky at 100 μm (up to the 10% level).

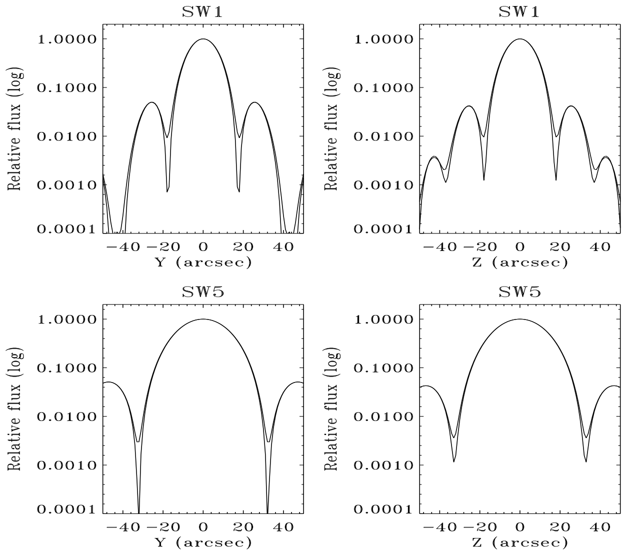

Figure 11: The effect of a finite size for Mars on the telescope PSF is shown for the telecope coordinates Y and Z for the LWS detectors SW1 and SW5. Note how this leads to a smoothing of the PSF pattern - Chris Lloyd

The basic problem before was the understanding of the core beam width, $40''$ instead of the previously assumed $50''$. This discrepancy seems to be related to the M2 entrance mirror of the LWS.

Efforts have concentrated in the last few months on the comparison of the LWS beam model with the telescope PSF model by Okumura. No major differences are found when the simpler model developed by Bruce Swinyard is used, however.

Some fine tuning was also made to the beam model, based on a series of grating observations of Mars.

1) The outer scans of the Mars measurements presented conspicuous fringing. It has been found that there is little difference in taking an average flux per detector (as done previously) or defringe the spectrum first for the determination of the beam profile.

2) Taking into account the real dimension of Mars ($6''$, previously a delta function had been taken), the sharp cuts in the model PSF are smoothed and there is a better agreement with the observations (Figure 11).

3) An elliptical (instead of circular) aperture is now taken, with eccentricity=0.93, in accordance to the optical diagram of the M2 mirror system ("Coupe B").

The resulting beam has now a FWHM dependency on wavelength not as pronounced as in the earlier modelling. The LW4 and LW5 values agree better.

Concerning fringing, it is now well established that it is always observed in the case of extended sources and sometimes when point sources are observed off-axis, with the amplitude of the fringing increasing towards longer wavelengths. The map of the fringe amplitude is consistent with the interpretation that the fringes are due to interference between the light reflected from the M2 mirror and its substrate.

Regarding the fracturing of the spectra on one side of the Mars scans (observed together with an apparent simultaneous reduction in fringing) one plausible interpretation is in terms of specular reflections on the M2 mirror system for off-axis incoming radiation. Additional work is still on-going on this subject.

The latest review describing the LWS beam profile characteristics is available as part of the "ISO Beyond Point Sources" Conference Proceedings in the paper *"An investigation of the ISO LWS beam profile and fringing"* by Chris Lloyd.

`BP: Characterisation of ISOPHOT-P aperture profiles`

With regard to ISOPHOT, PHT-C and PHT-S, beam profiles and effective solid angles are now well characterised and the consistency of ISO data with COBE/DIRBE is found to be better than 25% typically.

In addition, theoretical footprints are now available for all filters of P2 and P3 detectors, as well as for C100 and C200, in Cal-G files v5.4.

However, a small fraction of observations (2%) are multi-aperture measurements made with ISOPHOT using P filters which display in many cases an abnormal behaviour. Thus, this mode (PHT04) is not yet scientifically validated. The main reason for this is the strong assymetry observed in the aperture profiles, especially in filters associated to P1 detectors which cover the spectral range between 3.3 and 16 μm (see Figures 12 and 13).

The effect is that aperture profile measurements made with a point source placed at various positions within the aperture produce quite different signals. Moreover, assuming a strong gradient in these aperture profiles is not enough to explain the peculiar behaviour of the aperture sequences on the sky background. We must consider also a shift in the aperture centres of a few arcsec relative to each other for modelling the measured signal.

The results have implications for sky measurements in the so-called non-standard apertures, since the measured background fluxes do not scale with the corresponding aperture area. Due to the gradients in the aperture profiles, observations of extended structures depend on the roll-angle of the satellite. And last, but not least, photometry of point sources are affected if the objects are observed a few arcsec off-centre.

The full report on this effect can be found in the paper: *"ISOPHOT aperture profiles and background measurements"* by Thomas Müller.

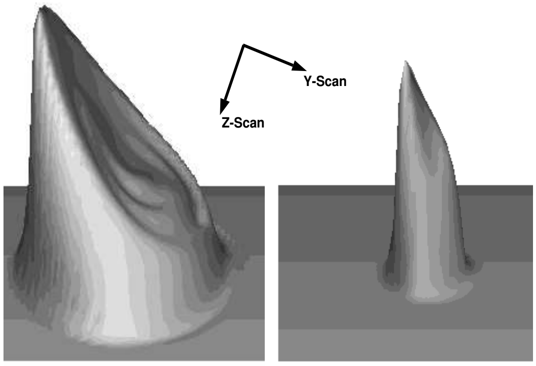

Figure 12: Constructed 3-D aperture profile at 12.0 μm for the 180$''$ aperture (left) and for the 52$''$ aperture (right) from two perpendicular scans parallel to the S/C y and z-axis - Thomas Müller

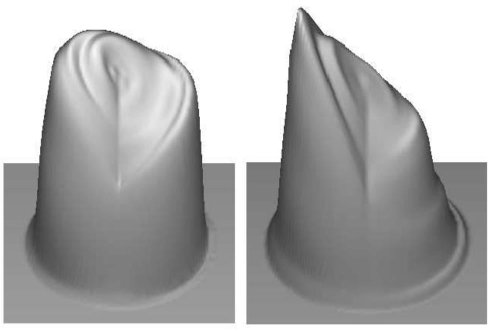

Figure 13: Constructed 3-D aperture profile at 7.3 μm (left), and at 16 μm (right), using the 180$''$ aperture from two perpendicular scans parallel to the S/C y and z-axis- Thomas Müller

Recommendations to deal with PHT04 observations and ways around to determine the background contribution and to distinguish clearly between point and extended sources (and even determine the extension of a source on arcsec scale) are provided in *"ISOPHOT aperture sequences on point- and extended sources"* also written by Thomas Müller. Both papers will soon be available as part of the "ISO Beyond Point Sources" Conference Proceedings.

BP: Analysis of pointing effects on PHT-S measurements

During the ISO mission it was observed that some PHT-S spectra showed remarkable flux jumps at pixels 31/32 and pixels 95/96, which correspond exactly to the junctions of the order sorting filters, mounted in front of the detector blocks (see Figure 14). The strength of this instrumental artifact is known to depend on the centering of the source within the PHT-S aperture of $24'' \times 24''$ and it was probably produced during the pre-launch fixing of the filters, which had to be glued manually and with great care in a process which, apparently, was not completely successful.

Following the confirmation of a strong dependency on pointing by Peter Ábrahám some time ago, Sybille Peschke recently carried out a survey on the ISO Data Archive trying to find out how many mispointed PHT-S observations were actually contained in the Archive which might be affected by this problem.

For this, the coordinates provided by the observers were compared with the actual positions observed by ISO. In principle, only observations with deviations from the correct pointing larger than $2''$and smaller than $12''$ are susceptible to be corrected either because the central part of the beam profile is not well enough known, or because the object is already outside the geometrical aperture of PHT-S.

With the assumption that the user input coordinates were accurate, no more than 5% of the PHT-S observations could be corrected due to mispointing. However, there is evidence for a large number of observations with coordinates provided by the observers in the ISO Data Archive which are affected by large uncertainties (i.e. those taken from the IRAS catalogues, known to be acccurate only to about $10''$-$15''$).

Thus, it was recommended that any pointing correction tool should be implemented only in PIA, for interactive analysis, but not as part of the automated pipeline.

Such tool already exists in PIA and its use is recommended for those specific observations showing the kind of artifacts above described. Note that, in some cases, flux jumps are detected between different order filters which amount up to 40% of the total flux for just a few arcsec offset.

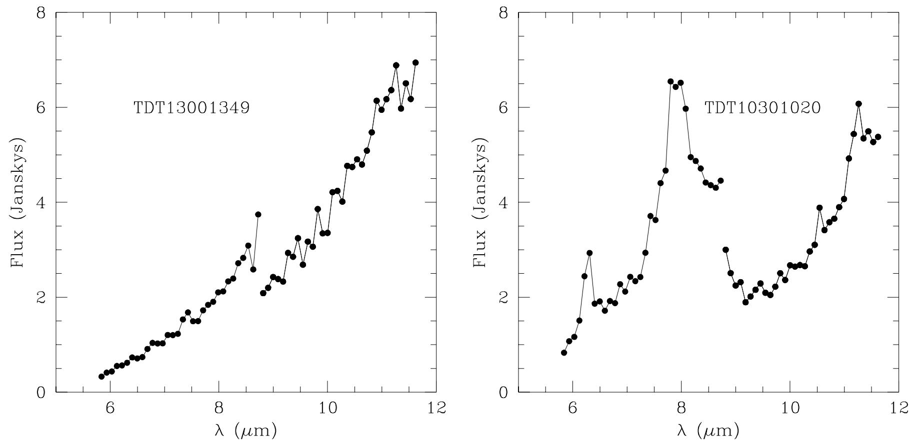

Figure 14: Example of the effect of mispointing in PHT-S. Note the jumps between pixels 95 and 96 at 8.8 μm.

BP: Analysis of a possible synchronization problem between ISO pointing files and recorded data

A possible synchronization problem between ISO pointing files and LWS parallel mode science data found by Florence Vivares was reported in a previous meeting of this WG consisting in a shift of 0.75 s. During operations a similar shift of $\sim$0.7 s was also found for SWS science data and for PHT serendipitous mode data. The issue was discussed with Fokker in the past but no satisfactory explanation was found. With the new synchronization problem found by LWS, the issue was re-opened again.

The origin of the problem is still unknown. Time offsets had already been placed some time ago in the PHT Serendipity Mode Analysis Software. A consistent delay of 700$\pm$30 ms is found when the coordinates of a point source found during a slew, as derived from the IIPH (Instrument Instantaneous Pointing History) file, are compared with the known optical position of the source, The source signal is always seen before it is expected from this reference position. Possible courses of action to correct for this effect in ISO data products affected by the problem are being investigated.

BP: Description of final status of ISO Pointing and improvements during Post-Operations

In the first months of the ISO mission it was found that errors up to 4 arcseconds could be present in the ISO pointing, depending on the target observed. The pointing appeared to be much better than the specifications (Absolute

Pointing Error of 11.7$''$, but it was suspected that some systematics could be present, which could therefore be corrected for.

Thus, a specific calibration programme was designed and executed in revolution 137, by which a number of point-like sources were observed with ISOCAM. 79 stars were selected from the Ground-Based Preparatory Programme (GBPP) list of calibration standards and observed in the LW9 filter (at 15 μm). The centroids of all these images were derived with good determinations in 54 cases. These were correlated with (i) the position of the guide star in the STR (Star TRacker), (ii) star ecliptic and galactic coordinates, (iii) the Solar Aspect Angle, and (iv) guide star magnitudes. A possible correlation was found only with the position of the guide star in the STR field of view, indicative of a possible improvement in the ISO pointing.

A second attempt was done in revolution 264, with a more accurate star selection procedure based on the improved Hipparcos star catalogue coordinates and an ad-hoc empirical colour-colour relation between visual magnitude and the expected flux in the CAM LW9 filter. After analysis of the results obtained, the correlation between pointing offset and position of the guide star in the STR was confirmed.

An independent investigation was then initiated based on the absolute pointing reconstruction as given by the confirmation star, a second guide star used at the start of every revolution. It appeared that a recalibration of the STR was possible, via the introduction of a focal length dependence on the angle of incidence of the visible radiation coming from the guide star. The model was applied to predict the offsets measured in revolution 264 with excellent results.

A verification exercise was performed in revolution 368, based on a series of SWS02 observations on and around HR 6705. With the new calibration, the measured offsets were decreased substantially, being only $+2.4''$and $-1.0''$ along the Y and Z axis respectively. Further to this, the go ahead was given to the uplink implementation of the STR recalibration which became operative as of revolution 369.

A second, but lower magnitude, improvement in the ISO pointing was obtained by increasing the sampling of the Sun ephemerides as used by the onboard software of the AOCS. As of revolution 453, a new so-called Sun model was introduced, and the improved algorithm was also introduced in the downlink in OLP v6.1.

The most recent ISO Pointing model now considers the effects of differential aberration, proper motion and parallax of the guide stars used.

While aberration was thought to be corrected for ISO observations by the fact that guidestars are always close ($\leq 2.5^0$) to the observed target, the differential aberration effect can cause pointing errors up to 0.9$''$ (if ISO's velocity is considered as well, this can become even larger).

On top of aberration two other significant sources of residual pointing errors were addressed, parallax and proper motion of guidestars. The effects are smaller ($\leq$0.4$''$) but still significant in some cases, fortunately only affecting few nearby guidestars.

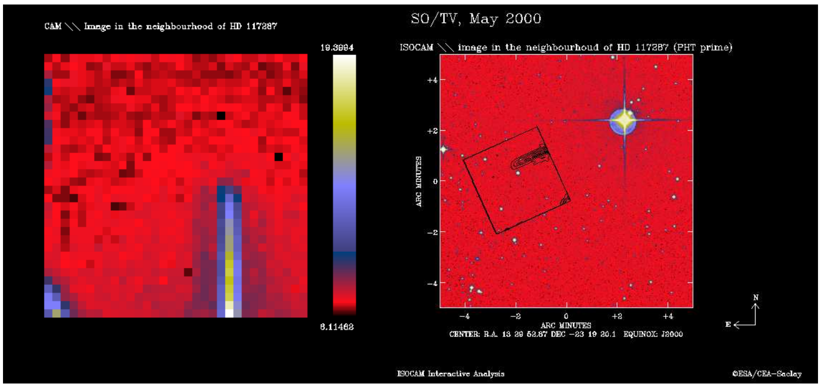

Figure 15: Straylight observed in a CAM parallel image in the neighbourhood of the bright Mira variable HD 117287 (left). The distance to this source from the centre of the image is about 4′ - Stephan Ott

New Cal-G files were generated which correct for the Pointing Correction effects above refered and they have already been implemented in OLP v8.6.

Now, after all these improvements have been introduced in the pipeline and in order to get a quantitative assessment of the ISO Pointing Accuracy, a scientific validation exercise has been carried out, using the stars observed in revolution 264 experiment as test cases. The main conclusion obtained is that the Absolute Pointing Error for ISO is found to be 1.4′′, a value which exceeds all expectations.

A minor limitation still exists which comes from the fact that the CAM PSFs used for the determination of the centroids of the stars observed is sampled with a step of 0.5′′, resulting in an uncertainty in the determination of the position of the stars in the CAM images which could be slightly improved in the future.

The full story is documented in "The ISO Absolute Pointing Accuracy" by Alberto Salama and Andy Pollock, available at

`http://www.iso.vilspa.esa.es/users/expl_lib/ISO/pointing.ps.gz`

`BP: Straylight effects in CAM parallel data and PHT observations`

In several cases, straylight has been detected in CAM parallel images and PHT observations taken close to bright infrared sources in the sky.

In the case of CAM parallel, images taken in the neighborhood of bright sources show bands of illuminated pixels pointing towards the direction where

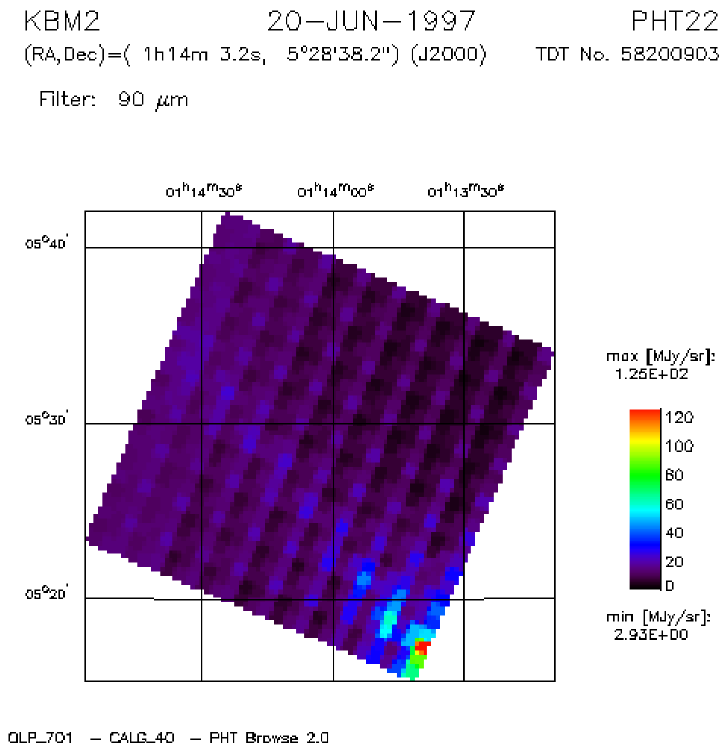

Figure 16: Straylight observed in a PHT22 raster map taken in the vicinity of Saturn. The planet is located at a distance of 4.5′ outside the displayed field close to the lower corner of the image and exactly in the direction indicated by the stripe - Thomas Müller

the bright source is located. The effect is seen in some cases at distances of several arcminutes (see Figure 15).

In addition, a stripe of emission found by C. Kiss and P. Ábrahám at MPIA in a PHT raster map has recently been identified by Thomas Müller as produced by straylight coming from Saturn, which was located at the time when the map was obtained at a distance of 15′ (see Figure 16).

In order to fully characterise these effects, investigation is on-going trying to identify other data sets which might be affected by the problem (with a bright source in the vicinities). Results will be presented at the next WG Meeting and reported in the next issue of this Status Report.

2.2.2 Glitches:

`GL: Glitches Working Group: General status`

An overview on the effect of glitches in ISO Detectors can be found in the document: *"The ISO Detectors and the Space Radiation Environment"* by Ana Heras et al., available at:

`ftp://astro.estec.esa.nl/pub/aheras/iso_gwg/spweather.ps`

It presents a statistical study of the glitch rates and glitch characteristics as derived from the data of the four instruments on board of ISO, and compare the results obtained for each instrument and for different detector materials with the available models. The evolution of glitch rates and some instrument performance parameters are analysed as a function of time in the mission and ISO's position in orbit.

The observed glitch rates are found to be 1.5−4 times higher than the value predicted by the CREME96 model for the cosmic ray integral flux. Moreover, when comparing the deposited energy distribution associated with the observed glitches and the results from ray-tracing simulations including only direct cosmic rays, it is found that the contribution from the lower deposited energy hits is larger than in purely cosmic-ray based models (although there is a good agreement for the higher energies in Ge detectors).

It is concluded that between 30% and 75% of the observed glitches are caused by δ-rays and other secondary particles produced in the detector and in the instrument and satellite shields.

The production of secondaries has been modelled more recently by Petteri Nieminen (LWS) and by Hervé Dzitko and Arnaud Claret (CAM) using the GEANT3.21 Monte-Carlo particle transport simulation code.

The discrepancies in LWS glitch statistics with models that were previously reported (contribution from high energy impacts lower than for other instruments) are confirmed. The glitch height distribution histograms are expected to be affected through the conversion factors from glitch height to energy deposited. The largest uncertainty here is the photoconductive gain G. It is interesting to note that already in ground tests the spike height values were smaller than expected from the conversion of particle energy to number of electron-hole pairs. The averaged spike heights measured differed by a factor of four between the two unstressed Ge:Ga detectors tested. Different G-values were assumed to explain these discrepancies (see M. Price's Thesis, sections 5.5.2 and 5.5.4). A recalculation of the pulse height spectra has been proposed in order to investigate the problem more in detail.

With respect to CAM, the Monte-Carlo simulations were carried out by Arnaud Claret and Hervé Dzitko (Figure 17). The glitch size, glitch rate and energy properties were predicted this way and compared with in-flight data.

Counting rates induced by secondary nuclear interaction particles can be estimated through an analytical approach, assuming the geometrical interaction cross section and the average multiplicity of the interaction, and considering also the secondary particles emitted by the shield near the detector.

A mean number of 8.48 ± 0.46 pixels/glitch and a glitch rate of 0.83 ± 0.12 glitches/sec were derived.

Experimentally, ∼1 glitch/sec is detected, close to the mean value (if we consider the errors) of ∼0.83 glitches/sec derived.

Details on improved de-glitching techniques per instrument are given below.

`GL: PHT status: Implementation of the two-threshold de-glitching method in OLP v10.0`

Concerning PHT de-glitching, no additional improvements are expected in PIA.

With regard to pipeline data products and, as already reported in the previous Status Report, the implementation in the pipeline of the more sophisticated, two-threshold de-glitching method which works at ERD level was postponed to OLP version 10.0 since it requires a quite different approach to the problem (the correction is applied at read-out level and not at ramp level).

The implementation of the two-threshold deglitching in the OLP is dependent on the feasibility to fit it into the structure of the OLP code which is optimized for fast processing, which might be hindering its straight forward implementation.

The description of the two-threshold de-glitching method can be found in the document *"De-glitching methods by the ISOPHOT Interactive Analysis (PIA)"* by Carlos Gabriel and José Acosta available at:

`ftp://astro.estec.esa.nl/pub/aheras/iso_gwg/PHT_degl.ps`

`GL: SWS status: Improvements of glitch detection in SWS data`

A list of modules have been planned to be updated or added to SWS pipeline processing, most likely for OLPv10. Some of them have a direct impact on glitch detection since they will lead to a better linearization of the SWS integration ramps.

The glitch detection algorithm itself has been tuned by adapting the detector specific calibration files and by fitting a higher order polynomial to the data just for glitch detection purposes.

A further improvement for glitch detection in OLP was achieved by including the full reset interval for the search for glitches and a cross-talk correction (25% of the glitches in SWS band 4 are due to this effect).

In particular, the future inclusion of the pulse shape correction module (see more details on this calibration problem under the *Transients WG* subsection of

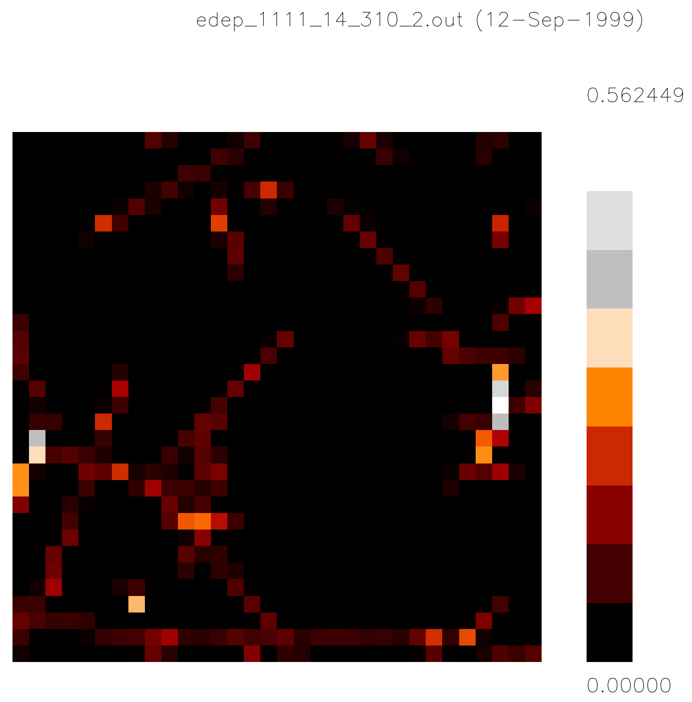

number of particles (type 14) = 1.00000e+06 of 310 MeV
number of glitches = 29
% of interacting particles = 0.00290000

energy band (MeV) = 257−375
particle flux (sec−1) = 1278.31
obs. duration (sec) = 782.285
number of images = 372

<number of glitches / image> = 0.0779570
0.00000 2.00000 0.0779570 0.00000 0.287458

<number of pixels / glitch> = 8.75862
1.00000 38.0000 8.75862 7.00000 7.83298

<energy / glitch> = 0.660784 MeV
0.0153769 2.54824 0.660784 0.448071 0.606038
<energy / pixel> = 0.0754438 MeV

Figure 17: Example of synthetic glitches produced using the GEANT code applied to CAM data - Arnaud Claret

this document) in OLP v9.5 will make possible to simplify the glitch detection algorithm and to increase the detection efficiency.

Concerning glitch removal, a slight modification of the algorithm will be implemented in OLP v9.5. The original algorithm skipped two samples after a detected glitch. The new algorithm checks whether a point after a detected glitch has a standard deviation greater than a certain value in order to discard it or not for the ramp slope calculation. As a consequence, more points are considered in the calculation of each glitch affected slope.

De-tailing SWS glitches in band 2, by using the 'dynadark' module, which models the memory effects in these detectors, is under study. Concerning the study of the statistics on SWS tails, and due to manpower limitations, it has been postponed after the delivery of next OLP v10.0. Thus, possible improvements in de-tailing derived from this analysis will only be implemented in OSIA at a later stage.

`GL: CAM status: Investigation on new de-glitching methods for ISOCAM data`

Concerning simulations, no further work has been done in the last few months. The results derived from Monte-Carlo simulations will be presented at the NSREC (Nuclear and Space Radiation Effects Conference) next July in Grenoble. The resulting document will be made available through the ISO web pages as soon as possible and a reference to it will be provided hopefully in the next Status Report (December 2000).

Currently, work is concentrated at the ISO Data Centre on the development and improvement of new CAM de-glitching techniques (Figure 18). As already mentioned in our last Status Report, several de-glitching methods have been developed by Stephan Ott for application to ISOCAM data.

The idea is to take advantage of valuable information about ISOCAM's current configuration, glitch distribution, flux level and redundancy in the raster or beam-swith observation, ignored by currently existing standard de-glitching techniques (multi-resolution, sigma clipping,..). This leads to badly chosen thresholds, which result in too high noise level due to un-suppressed glitches, masked out sources or gradients and no deglitching for observations with few read-outs.

In the last few months some of these new de-glitching methods have been improved (like those used for faint sources and low redundancy data in CAM parallel) giving very satisfactory results.

A detailed description of all these techniques, together with examples of results obtained and a list of application fields and caveats to take into account in each case can be found in the document *"ISOCAM Faint Source Report"* by Bruno Altieri et al. available at:

`http://www.iso.vilspa.esa.es/users/expl_lib/CAM/fs_report.ps.gz`

and in the document *"Innovative Cosmic Ray Rejection in ISOCAM data"* by Stephan Ott et al. which can be found at:

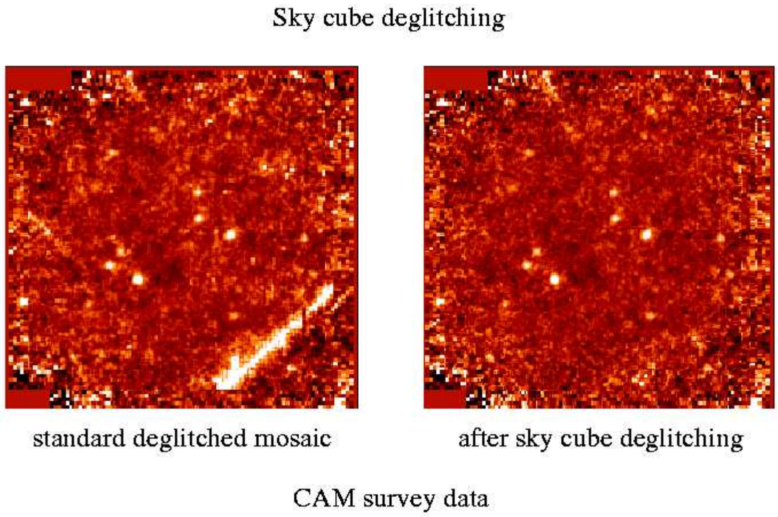

Figure 18: Example of results obtained after application of the Sky-cube deglitching method to ISOCAM data - Leo Metcalfe

`http://www.iso.vilspa.esa.es/science/pub/2000/cosmic_ray.ps.gz`

All these de-glitching tools are available with CIA v4.0 or will soon be made available in CAM v5.0 (expected release in mid 2001).

Concerning OLP, a prototype of the faint source treatment, including improved de-glitching will be implemented in OLP v9.5. Later, it will be decided whether the full package will be implemented in OLP v10.0.

`GL: LWS status: improved de-glitching techniques`

SPD processing has slightly been modified in OLP 8.7, leading to a better glitch detection. Regarding LIA and OLP 10.0, no further efforts are foreseen to improve de-glitching. The recognition of glitches in the pipeline can be considered to be in its final form.

`GL: Low-energy proton propagation in the mirrors of the XMM-Newton telescope and effects on the onboard CCD detectors`

As part of the contribution made by members of this WG to other space projects, efforts have been made by Petteri Nieminen in the context of the XMM-Newton mission to simulate the processes involved in the transport of protons through the telescope mirrors and generation of non-ionising doses in CCDs. This process can potentially produce severe damages to X-ray CCDs as it apparently happened on Chandra's detectors. Estimates of the flux of damaging protons that each instrument is exposed to were obtained for different environments using Monte-Carlo simulation techniques and the GEANT code.

The investigations carried out show that protons can propagate through the grazing-incidence mirrors on XMM-Newton and Chandra and reach the focal plane detectors, causing NIEL (Non-Ionising Energy Loss) damage. The effect is at least a factor 2 more important in the case of Chandra.

Protection measures implemented on XMM-Newton prevent against this type of damage occurring (shield closure to protect the EPIC measurements during radiation belt passages and on ocassion of strong solar events which can be detected through the monitoring of the background noise on the RGS instruments). Fortunately, the CCDs on the RGS instruments, for which no protective measures can be taken, are not expected to be significantly affected by radiation damage.

Another important conclusion from this study for future missions is that protons with this low energy, not normally seen as a problem, should be seriously considered. So far, they are poorly described in models of solar particle events and in radiation belt models.

`GL: PACS/FIRST radiation effects simulations`

Helmut Feuchtgruber reports that no further experiments/simulations with PACS/FIRST detectors have been performed since the previous meeting. PACS consortium has decided to use bolometer arrays instead of photoconductor arrays for the photometric channels which are supposed to be somewhat less sensitive to radiation effects. Photoconductors will be used only for the spectrometers.

2.2.3 Line profiles:

`LP: Determination of the SWS spectral resolution and instrumental line profiles.`

The analysis of the SWS AOT01 spectral resolution as a function of the scanning speed and the instrumental line profiles has been completed. Summary tables with the most relevant numbers concerning spectral resolution of this mode are provided in Section 3.3.4 of the *"ISO SWS Handbook"*, available at:

`http://www.iso.vilspa.esa.es/manuals/HANDBOOK/VI/sws_hb`

The speed 4 resolutions vary between 800 and 1700 increasing with wavelength. This is approximately half of the AOT 2 resolution, matching expectations, and slightly better than expected for extended sources. The FWHM remains nearly constant.

Additional information on the grating instrumental profile and resolution can be found in Section 6.11 of the ISO SWS Handbook above refered and in van den Ancker et al. (1997), accesible at:

`http://www.iso.vilspa.esa.es/users/expl_lib/SWS/doc/sws_ip/`

where possible instrumental effects on emission line profiles observed with SWS are discussed.

Ground-based tests showed that the SWS01 Instrumental Profiles have a gaussian shape up to accuracies of a few percent and this is confirmed by the analysis of in-flight data, with the exception of a slight 'shoulder' on the blue side of the base of the profile and a depression on the red side, possibly dependent on the position of the source in the slit.

The last version of the document *ISO-SWS grating resolution and instrumental line profile as measured by the full resolution modes SWS02 and SWS06* by D. Lutz, H. Feuchtgruber and J. Morffin can be found at:

`http://www.iso.vilspa.esa.es/users/expl_lib/SWS/SWS02-06.ps.gz`

It includes a description of the database used and existing models for the determination of SWS spectral resolution in these two observing modes. In addition, an analysis of the effect of rebinning and extension of the source observed on the spectral resolution is presented. The reproducibility, observed trends with time and the possible dependence of resolution on detector, line flux or continuum flux are also investigated.

For most practical purposes, it is completely adequate to assume that an SWS instrumental profile is intrinsically a gaussian. The document gives a formula to estimate the expected line width as a function of source extent.

Other effects like mispointing, ghosts and transients are also discussed in the document.

Future plans include the extension of the analysis to other sources increasing the database and the implementation of a cross-talk correction which might explain the broad wings observed at a few per thousands level.

Resulting FWHM values have already been implemented in SWS IA, via an update in the 'resolution' module.

With respect to SWS Fabry-Pérot modes, the FWHM as measured with the internal calibrators can be found in Section 6.3.1 of the *"ISO SWS Handbook"*. Esentially, the spectral resolution decreases towards the short wavelength ends of the wavelength ranges covered by the two Fabry-Pérots, where the wavelengths corresponding to the resonances of the reflective meshes are approached. The Fabry-Pérot spectral resolution depends on precisely parallel F-P plates.

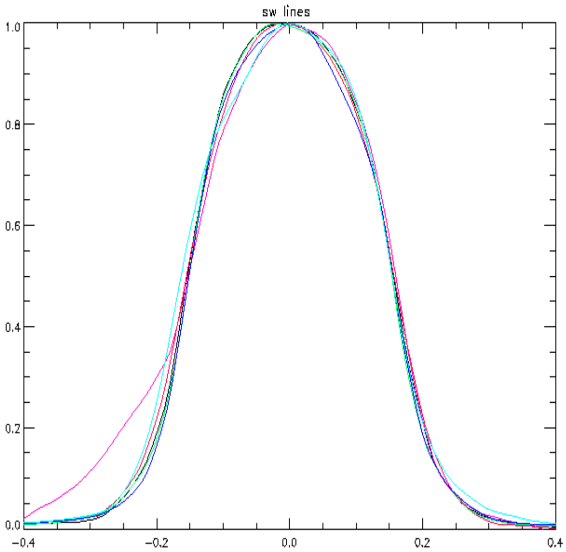

Figure 19: LWS line profiles observed in NGC 6543, NGC7027 and NGC 6826. The plot includes the mean profiles observed at 52 μm (as observed on the SW2 and SW3 detectors), 57 μm (on SW2 and SW3), 63 μm (on SW3) and 88 μm (on SW5). The only discrepant assymetric profile corresponds to the 57 μm line detected on the SW2 detector - Rosario Lorente

Measurements of the Fabry-Pérot spectral resolution in-orbit suffered from the lack of bright, narrow lines. Three lines were measured and lower limits found to the spectral resolution that were very close to expectations. This is reported in Valentijn et al. (1996, A&A 315, L60.)

`LP: Progress on the analysis of LWS line profiles`

The study of the LWS grating profile was completed for point sources and short wavelength detectors by Rosario Lorente. The result is a single profile valid for all SW detectors (Figure 19). Unlike SWS, LWS line profiles deviate slightly ($\sim$4%) from a gaussian shape, as expected. The error made on the flux determination by using a gaussian fit is only of the order of 2%, however.

The asymmetry found in the 57 μm line in the SW2 detector is still being studied in relation to the presence of an unidentified line (or feature) in the Fabry-Pérot spectra.

The line profile analysis was later extended to the long wavelength (LW) detectors and completed by Cecile Gry, resulting also in one single mean profile for all the detectors.

The line profile analysis has also been applied to extended sources, with the result that there is no profile distorsion coming from the off-centering of the

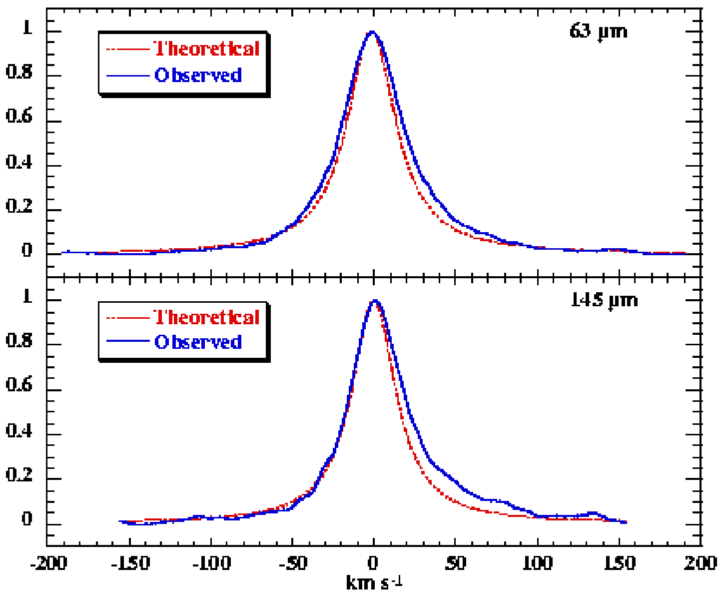

Figure 20: Theoretical and observed Fabry-Pérot line profiles at 63 and 145 μm. Note the asymmetries probably due to memory effects. - Emmanuel Caux

source or from their spatial extension. A final report on LWS grating profile is being prepared at these moments.

Meanwhile, the mean profiles are available in numerical form. The intention exists to find an analytical function (e.g. a combination of a lorentzian and a gaussian function) to fit the numerical values. This function will eventually be implemented in LIA or as part of the 'multi-fit' module in OSIA.

The LWS grating profiles have also been compared to pre-launch ray-tracing results at 45 μm by Anna di Giorgio. The agreement found is very good at the top of the line although the base of the line is wider than predicted.

Concerning the LWS Fabry-Pérot profiles, they have been derived by Emmanuel Caux for several lines (52 μm, 57 μm, 63 μm, 88 μm, 122 μm, 145 μm and 158 μm) on three objects (G0.6−0.6, NGC 7023 and NGC 7027), observed with the standard AOT LWS04. They compare very well with the theoretical profiles apart from an asymmetrical widening probably due to memory effects, although a misalignment (if the tilt has been changing during the scan) could also produce a similar effect (see Figure 20).

The origin of this asymmetry is currently being studied by Anna di Giorgio using special calibration observations performed with both forward and backward scans which will be compared with standard LWS04 observations (for which only one scan direction was used) of the same object.

It is confirmed that the resolution at short wavelengths seems significantly lower than expected from ground-based measurements. Definitive results, however, will have to await for the results of the memory effects analysis which is still pending due to a lack of manpower.

It is foreseen that a tool will be provided in LIA to fit the Fabry-Pérot spectra with the derived profiles.

2.2.4 Photometric calibration:

```
PH: ISO Calibration web pages available as part of the ISO Data
      Archive
```

The old *Calibration Liaison* web pages, used during the mission for posting cross-calibration information originally intended for internal use only by the ISO Calibration Team have been updated by Pedro García-Lario. The intention is to make the information there contained available to the ISO users community as part of the ISO Data Archive.

Very soon (release expected early July) these new *ISO Calibration* web pages (see Figure 21) will become public, now that a few pending proprietary issues have been solved.

These pages will contain detailed information on the calibration standards on which the absolute flux calibration of ISO is based. This includes a description of the ISO Ground Based Preparatory Programme (GBPP) and the Cohen, Walker, Witteborn et al. (CWW) absolute calibration programme, as well as information on the asteroids and planets that were used for the calibration at longer wavelengths as well as the specific list of astronomical sources used in the calibration of each ISO observing mode. Photometric and spectral data are provided together with model spectra of the different ISO calibrators and the definition of the system zero-points.

These pages will regularly be updated with additional information and improved data as it becomes available.

```
PH: Organisation of the Workshop: "ISO Beyond the Peaks", held
      at VILSPA (February 2-4, 2000)
```

The 2nd ISO Workshop on analytical spectroscopy with SWS, LWS, PHT-S and CAM-CVF was held in Villanueva de la Cañada, very close to the ISO Data Centre (VILSPA, Madrid) on February 2−4, 2000.

This Workshop was aimed at highlighting theoretical and empirical methods impacting the detailed analysis and interpretation of ISO spectra, assessing the data quality and calibrations. More than 130 astronomers gathered at VILSPA to discuss ISO observations and associated scientific interpretation, two years after the end of the ISO mission.

A broad range of observational and theoretical branches relevant to ISO were covered through specific topic-oriented sessions including Solar System Observations, Interstellar Medium and Star Formation, Stars and Galaxies, as

ISO Calibration

The calibration of ISO data

Definition of ISO calibration standards

Stars

The absolute flux calibration of three of the four ISO instruments (CAM, PHT and SWS) is based primarily on results obtained on stars selected from the ISO Ground-Based Preparatory Programme (GBPP) and from the Cohen, Walker, Witeborn et al. (CWW) absolute calibration programme. The confidence in the absolute flux level of the calibration stars is about 3% in the 2.5 to 35 microns wavelength range and better than 10% at longer wavelengths up to 300 microns.

Asteroids

Asteroids are used to cover the 35 to 200 microns wavelength range in ISO calibration since stars are usually too faint to be used in this wavelength range. An extensive ground and airborne based calibration programme was carried out to quantify the fluxes and to monitor the light curves of the prime asteroids 1 Ceres, 2 Pallas, 4 Vesta, and 10 Hygiea, and other asteroids that have been observed with ISO. For the current calibration the absolute fluxes of the asteroids were derived using a thermophysical model (Mueller and Lagerros 1998). The accuracy of the predicted asteroid fluxes is in general 10% in the wavelength range from 24 to 500 microns.

Planets

The outer planets Neptune and Uranus were used for calibration at the longer wavelengths in the high flux density range up to 1000 Jy. The model SED's for a given time in the mission were provided by M. Abbas. Currently, the absolute flux calibration of LWS is based on Uranus as primary source. Comparison with independent model predictions for Uranus showed a consistency of better than 20% in the wavelength range between 30 and 240 microns. At shorter wavelengths the models become less certa

Photometric and spectral data

Results from the ISO Ground-Based Preparatory Programme (GBPP). They consist of near and mid-IR photometry of a wide sample of stars observed from La Palma (P. Hammersley) and ESO-La Silla (N. van der Bliek, J. Manfroid and P. Bouchet) observatories.

Results from M. Cohen et al., including calibrated spectra and extrapolations to 300 microns for a few stars.

Models

Models of Uranus and Neptune

Model spectra of stars in the Ground Based Preparatory Program. The visible magnitudes and near-infrared photometry observed in the GBPP have been fitted with a Kurucz model to provide the flux densities at longer wavelengths. The overall spectral energy distribution is believed to be correct within 5% .

Model spectra assembled from ground-based and KAO observations from M Cohen et al.

Definition of the system zero-points

The model spectra of Vega (1-300 microns, R = 4000 throughout, 400 kB) provides the definition of the system zero points (by adoption of the ideal [i.e. model] Vega as zero magnitude in every passband) so that long wave measurements can be quoted in magnitudes or at least with reference to a common context as measurements at other shorter wavelengths. See also explanatory note for details.

The model spectral energy distribution of Sirius (1-300 mic, R = 4000 up to 35 microns) is also available. This star was also considered a primary reference star for calibration purposes.

Other documents

Cross-calibration

- ISO Post-Operations Cross-Calibration Status Report, SAI/1999-060/Rp, (07-Jun-1999)
- ISO Cross Calibration Plan (June 1999)
- "Reference wavelengths for ISO CAM and PHOT filters" by A. Moneti, L. Metcalfe and B. Schulz, SAI/97-002/Dc (15-Sep-1997)

Please send corrections, comments and suggestions to Pedro Garcia-Lario
(Last update: 08-06-2000)

Figure 21: The introductory new ISO Calibration web page

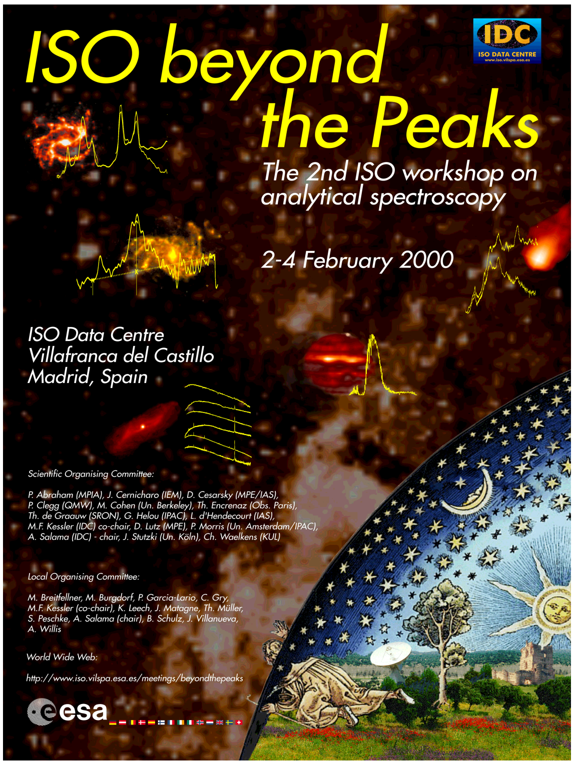

Figure 22: Poster announcing the Workshop "ISO Beyond the Peaks", held at VILSPA on February 2−4, 2000

well as specific sessions devoted to the latest data analysis techniques, theoretical models and laboratory experiments. Finally, the impact of these results in the design of future missions and instruments was also briefly addressed.

The abstracts of the (more than 80) contributions presented at the Workshop are available at:

`http://www.iso.vilspa.esa.es/meetings/beyondthepeaks/`

As for its predecessor, the proceedings will be published in volume 456 of ESA Special Publications series.

`PH: Organisation of the "ISO Legacy Conference", to be held at VILSPA (February 5-9, 2001)`

As a continuation of the series of Workshops and Conferences organised by the ISO Data Centre we are planning the celebration of a new conference in the week 5−9 February 2001 on *"The Calibration Legacy of the ISO Mission"*.

The programme of the conference will reflect the wide range of astronomical and instrumental calibration issues which have been tackled during the history of the ISO project to-date. Topics range through:

- the establishment of major databases of reference astronomical calibration sources;
- lessons learned relevant to the design of future instruments;
- actual techniques developed, and problems encountered, in the ground-based and in-flight calibration of the ISO instruments.

Particular emphasis will be placed upon the relevance of the ISO experience to calibration of future space missions.

The Proceedings of this Conference, as usual, will also be published as an independent volume of the ESA Special Publications series.

```
PH: Evaluation  of calibration improvements recently achieved
     and investigation on cross-calibration problems reported
     in the last Status  Report affecting OLP and/or  IA data.
```

Following the new *statistical* Cross-calibration strategy described in the First Cross-Calibration Status Report, every six months we present an analysis of the calibration improvements achieved either in the OLP pipeline or in IA, based on the evaluation of the effects observed in the spectrum of a few hundred sources which had been observed in at least two of the following AOTs: SWS01 (low resolution spectroscopy), PHT40 (PHT-S staring or chopped measurements), or CAM04 (CAM-CVF spectrophotometry).

The goal is to evaluate the internal consistency of ISO calibration for sources observed with these three instruments in the overlapping region from 2 to 15 μm. The sample includes a variety of blue and red objects, faint and bright, and of course point-like and extended sources, which makes it ideal for studying the various calibration problems affecting each type of observation made with ISO as a function of the characteristics of the astronomical source observed.

In this Third Status Report we present (see Section 3) an updated analysis of the most recent calibration improvements implemented in the pipeline by comparing the new OLP v9 data products with the previous OLP v8.

Future plans include the extension of the same kind of analysis to longer wavelengths. In this sense, objects observed with both PHT-C filters (photometry beyond 60 μm) and LWS01 containing a few hundred different pointings have already been selected from the ISO Data Archive. The main problem is, in this case, that cross-calibration comparisons are difficult in many cases because the dynamic range of PHT and LWS is very different. Thus, there is a minimum overlapping region in flux level at which both PHT and LWS are of enough quality to derive reliable cross-calibration comparisons. In spite of this, we estimate that a minimum number of 50 cases will probably remain as useful. The results from this comparison will be presented in the next Status Report.

```
PH: Cross-Calibration comparison of ISO Data with other ground-
     based and space facilities
```

One of the goals of this WG is to assess the validity of ISO calibration by comparing ISO data products with data obtained with other ground-based and space facilities using the same or completely different calibrators.

Work has concentrated in the last few months on the cross-calibration of ISO SWS and LWS with IRAS data photometry. The preliminary results are presented in Section 3 of this Status Report.

In addition, we also present in Section 3 some examples of cross-calibration checks made against ground-based UKIRT observations and other space facilities like KAO or COBE/DIRBE, as well as examples of scientific results derived from ISO cross-calibration results.

2.2.5 Polarisation:

`PO: Proceedings of the Workshop on "ISO Polarisation Observations" held at VILSPA (May 25-28, 1999)`

The aim of the meeting was to support the finalization of data reduction and analysis of observing programmes based on polarisation measurements carried out with ISO since the analysis of polarisation measurements requires expertise in advanced data reduction techniques and a deep instrument knowledge.

The workshop was an excelent opportunity for astronomers working on this particular field to access the latest calibration updates with the support of the IDC staff during *hands-on* sessions and at the same time exchange scientific results with other colleagues.

The Proceedings of this Workshop are published in volume 435 of the ESA Special Publications series (Figure 23) and they are electronically available at:

`http://www.iso.vilspa.esa.es/meetings/polarisation/paper/web/`

As an outcome of the ample discussions held during the Workshop, conclusions were reached on the orientation of the CAM polariser which, as it is now defined, looks convincing and provides consistent results on polarisation angles. However, the general feeling was that still a better de-glitching strategy is needed to improve the results obtained and that downward transients are insufficiently corrected in the data with the available detector models.

Following the meeting, a new de-glitching strategy on CAM05 data has been tested by Ralf Siebenmorgen which looks very promising. Additional improvements are obtained when using fine-tuned polarisation flat-fields and new polarisation weight factors with the help of this new de-glitcher.

Concerning PHT, extended sources observed with C200 2x2 raster polarisation maps were shown to give still inconsistent polarisation angles for the central pixel of the resulting 3x3 pixel maps, which is covered by all four C200 pixels.

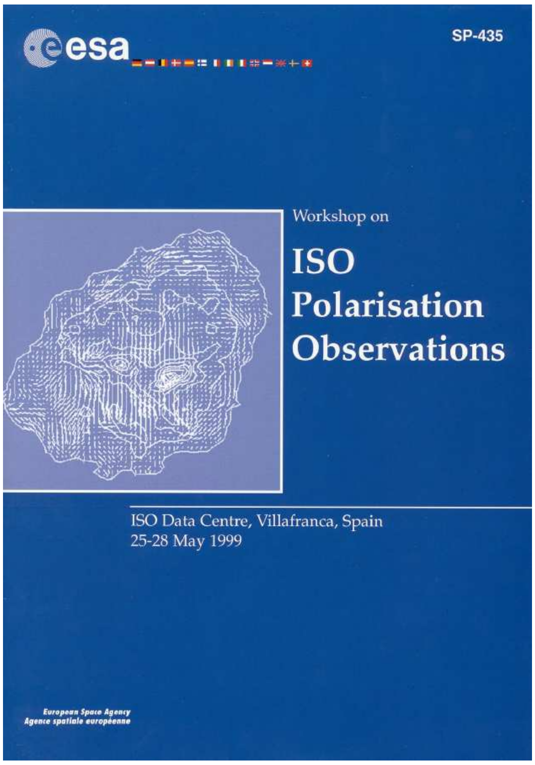

Figure 23: Front cover of the Proceedings of the Workshop on "ISO Polarisation Observations" held at VILSPA on May 25-28, 1999

`PO: Analysis of the PHT polarisation inconsistencies among the C200 pixels`

Re-calibration of PHT instrumental polarisation by including the new linearity correction seems to give better results for discrepant pixels.

A detailed description of the structure and performance of the ISOPHOT observing mode PHT51, which was used to measure the polarisation of astronomical targets in the far-infrared at 170 μm is given in the document *"Processing steps and signal analysis of ISOPHOT Polarisation Observations at 170 micron"* by Rene Laureijs and Ulrich Klaas, available at:

`http://www.iso.vilspa.esa.es/users/expl_lib/PHT/laureijsr_EL.ps.gz`

Special attention is given in this document to the assessment of the instrumental stability and consistency. All background observations taken with PHT51 are evaluated in order to derive the instrumental polarisation.

Although the polarisation angles of the four C200 pixels seem well determined, still the polarisation degrees of all pixels except pixel 4 show significant discrepancies with previous determinations made by Ulrich Klaas et al. which also included point sources in their analysis. The differences between the two sets of instrumental polarisation vectors could be due to uncertainties in the beam profile for each pixel-polariser combination.

`PO: Polarisation observations with ISOCAM`

An overview of the ISOCAM polarisation capabilities can be found in the document *"Polarisation observations with ISOCAM"* by Ralf Siebenmorgen, available at:

`http://www.iso.vilspa.esa.es/meetings/polarisation/paper/web/siebenmr.ps.gz`

The different polarisation modes, necessary steps in the data reduction and the calibration strategy are described. The instrumental polarisation was derived first from observations of the (assumed unpolarised) Zodiacal light for which a mean fractional polarisation of p$\sim$1.0$\pm$0.3% was found. In addition, measurements of unpolarised standard stars were also performed from which an instrumental polarisation of p = 1.5$\pm$0.3% for the LW2, $3''$ p.f.o.v. lens configuration was derived, consistent with the zodiacal light results. These results indicate that with present processing techniques it is possible to achieve a 1 σ = 0.5% accuracy limit of linear polarisation for moderately bright targets using ISOCAM polarisation data.

`PO: ISO Polarisation Observations: Lessons Learned and Plans for the Future`

A review on *"Polarimetry with ISO: Lessons Learned, Enabled Science"* was presented by Rene Laureijs and Bernhard Schulz at the last M4 Meeting held at CfA (Harvard University) in October 1999, where the many different problems that this observing mode had to face during the mission were addressed from a historical perspective.

In summary, it was concluded that, although ISOPHOT and ISOCAM polarisation observations were always considered as 'desirable' before and during the mission, the reality was that there was at the end a minimal support in terms of manpower (only one person per instrument in charge of the preparations and planning of these observations). Moreover, because of the special characteristics of polarisation observations, they always had to be made using the Calibration Uplink System (CUS) mode with the advantage of a full flexibility in the design of the observing strategy but the disadvantage of needing a strong expertise in the preparation and planning of the observations as well as on the reduction of the data so obtained (of course, this has to be made always using Interactive Analysis)

Moreover, it took quite some additional time to determine the best observing strategy because of the 'unexpected' in-orbit performance of the detectors (higher noise for C100 and P3 detectors made of Ge:Ga material; detector transients rendering measurement times less than 32 s unfeasible and difficult to model/predict with sufficient accuracy) and the need of long and stable integrations.

With all the restrictions above mentioned, the best detectors and most suitable filters were chosen to perform polarisation observations both for ISOPHOT and ISOCAM during the mission, according to the detectors characteristics.

In the case of ISOPHOT, the detectors selected were P2 (Si:B) with the 25 μm filter and C200 (stressed Ge:Ga) with the 170 μm filter, both used with a long integration time per polariser cycle imposing redundancy in the observing strategy.

For ISOCAM, where it was found that the polariser change caused source displacement on the array, it was decided to do this change only after completion of small raster maps and perform repointing after each polariser change. In addition, observers had to live with the detector transients (note that a differential signal might be induced if the sensitivity to drifts is different for each individual polariser) and a dead column (2 x 2 raster maps required).

With all these limitations, it was still possible to perform some polarisation observations with ISO thanks to the longer lifetime of ISO.

Considering the small amount of polarisation data finally contained in the ISO Data Archive and the difficulties involved in data reduction, it was recently decided to consider further improvements of the polarisation calibration as a low priority task.

Instead, the possibility is now being considered of providing these data to the users fully calibrated by experts through the ingestion of the calibrated data sets in the Legacy Archive.

Additional information regarding this possibility will be provided in the next Status Report.

2.2.6 Spectral Matching and RSRF:

`SM: Progress on the definition of a new RSRF for LWS based on Uranus`

The validity of the new Uranus model provided by Griffin and Orton in October 1996 which is being used for the absolute flux calibration of LWS is now well established after several cross-calibration comparisons have been made against other solar system targets like Mars, Neptune, Ceres and Callisto also observed with LWS and for which models are available.

- Comparison of Uranus vs. Mars LWS observations:

  A comparison between the spectrum of Uranus and Mars observed at nominal bias was carried out by Bruce Swinyard using both the old (March 1996) and the new (October 1996) Griffin and Orton's Uranus models,

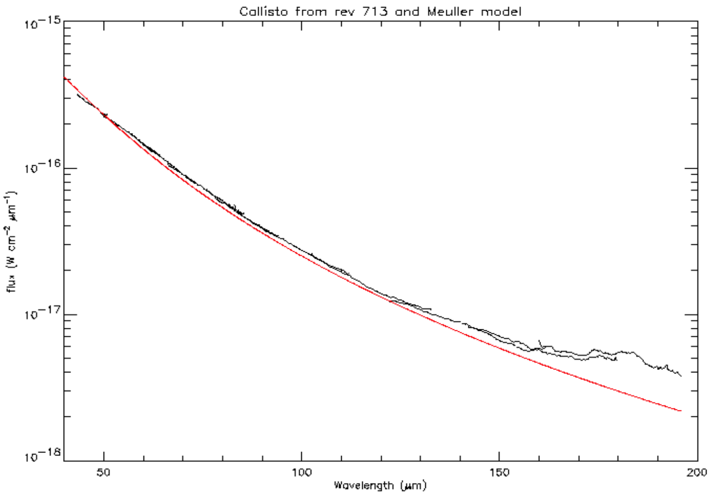

Figure 24: Thermophysical model of Callisto (red line) compared with LWS observations of Callisto made in revolution 713 (black line). The agreement is always within the 15% level except beyond 150 μm due to straylight from Jupiter - Thomas Müller

which were compared to Rudy's model of Mars (run with two different values of the emissivity of 0.79 and 0.93, considered to be uniform over the entire LWS wavelength range). The results obtained suggest a good agreement (within 10%) of the new Uranus model with the Mars model which assumes an emissivity of Mars of 0.93 (similar values for the surface emissivity of Mars have also been derived from other independent methods).

- Comparison of LWS vs SWS observations of Mars:

  In addition, LWS observations of Mars were compared with SWS observations of the same target. Once the SWS data is corrected for de-biasing effects (not needed for LWS band SW1) the agreement with LWS data is within the 10% level.

- Comparison of LWS observations with thermophysical model of Callisto:

  LWS observations of Callisto processed by Bruce Swinyard with pipeline v8.7 in which the background contribution from Jupiter's straylight has been subtracted and for which a new method has been used to remove for memory effects have been compared with the thermophysical model of Callisto produced by Thomas Müller (see Figure 25).

  Although the absolute flux level derived is a 10-15 % factor smaller than the model predictions, the overall shape is in excellent agreement with the thermophysical model (to the 5% level).

  The only exception is a possible feature around 130 μm which might be

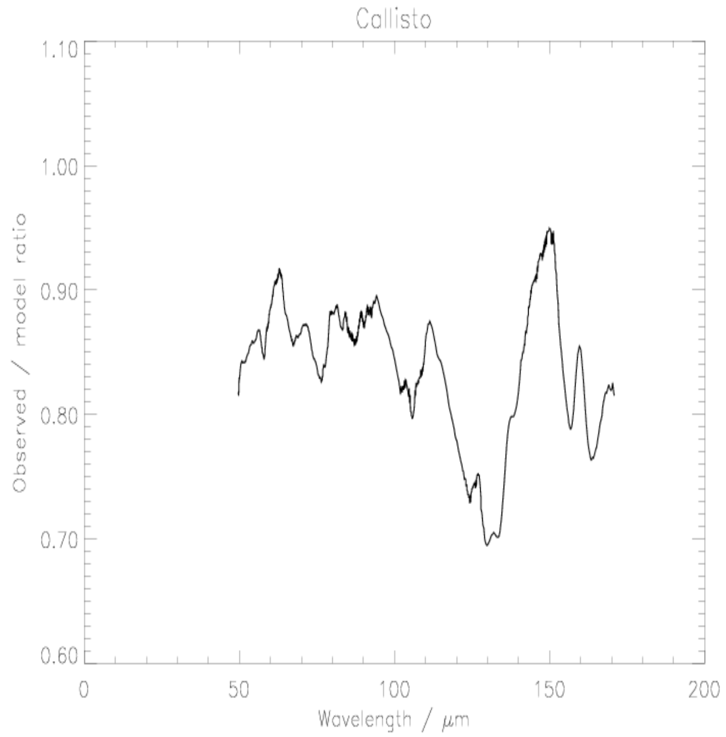

Figure 25: Ratio between the LWS observations of Callisto corrected for straylight from Jupiter and the thermophysical model of Callisto produced by Thomas Müller.

a residual of Jupiter's straylight contribution, although this still needs to be checked.

The use of the new model of Uranus has an effect only at the short wavelength end of the spectrum. The new OLP v8.7 data products, calibrated using this new Uranus model should have now the right flux level at this band (In OLP v7 the photometric level of SW1 was set too high by about 10%).

After re-checking all observations of Uranus, there are indications in SW1 and SW2 that the RSRF might have changed during the period when LWS was switched off (this was in revolutions 380−442). Investigations are still on-going on this subject.

`SM: Progress in the definition of the RSRF for SWS`

A full report on this topic can be found in *"The ISO-SWS Relative Spectral Response Calibration"* by Bart Vandenbussche at:

`http://www.iso.vilspa.esa.es/users/expl_lib/SWS/rsrf_v1.1.ps.gz`

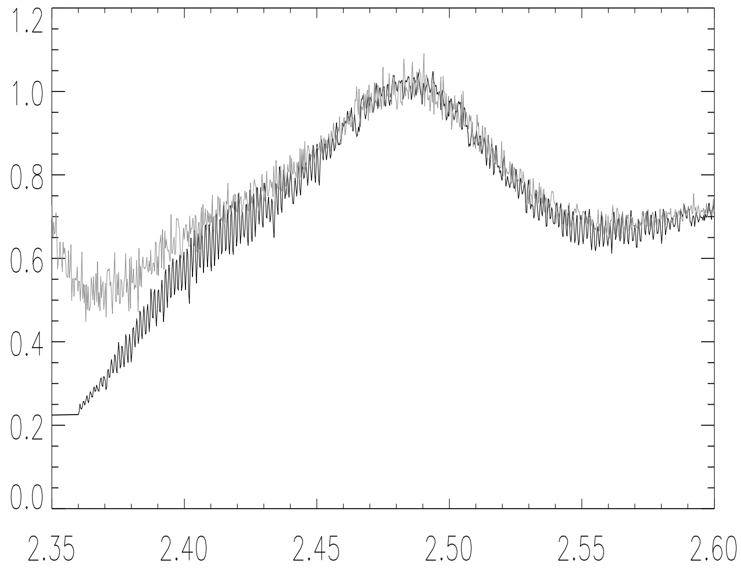

Figure 26: The difference between the RSRF before (black) and after (grey) the first in-orbit correction for SWS band 1A - Bart Vandenbussche

This document describes the different corrections that were applied in different versions of the pipeline to the SWS RSRF and indicates where further improvements can be expected.

Before launch, the SWS RSRF was derived from black-body scans during ILT tests. Uncertainties in black-body temperatures, diffraction losses and leaks in test set-up filters made corrections in the RSRF necessary, based on what it was observed in-orbit on external calibrators.

The impact of the use of an incorrect RSRF on a spectrum after a slightly wrong dark current subtraction is discussed and methods to recognize and cure the problem are provided.

A sudden fall-off at the blue edge of bands 1A and 2A systematically observed in all observations was identified in the past as produced by a leak in ILT set-up filters. The effect was corrected in May 1996 in the corresponding RSRFs (see Figure 26) by comparing the spectrum of Alpha Lyrae (a representative case) with a model spectrum provided by Martin Cohen.

Additional corrections were needed to correct for diffraction losses effects derived from the fact that the black-body sources observed on ground were extended with respect to the SWS slit and not point sources.

In March 1997 new Cal-G files were obtained by applying polynomial corrections to the existing files, based on the differences between SWS spectra of standard stars and reference spectral energy distributions, mostly synthetic spectra and composites (i.e. pieces of synthetic spectra and real data spliced to accurate photometry available).

In the fall of 1997 a new set of RSRF calibration files were derived using more data of known calibration stars with a better sampling of different spectral types. Cross-talk correction was this time considered, as well as a better wavelength calibration and dark current subtraction. Unfortunately, because of the lack of calibration targets with a well known energy distribution in the region 30–45 μm, no correction was applied on the RSRF for band 4. Thus, band 4 absolute flux calibration is still based on ground-based data.

Several features are identified in the document provided by Bart Vandenbussche which might be instrumental effects produced by residuals in the RSRF.

- Band 2C: 9-9.3 μm : possible residue of the correction for an instrumental absorption feature.

- Band 2C: 10.1 μm : possible residue of the correction for an instrumental emission feature.

- Band 2C: 11.0 μm : possible residue of the correction for an instrumental emission feature.

- Band 3A: 12.3 μm : possible residue of the correction for an instrumental emission feature.

- Band 3A, 3C, 3D, 3E : fringes in band 3 were already observed during the instrument level tests, so they are also present in the RSRF and divided out. However, the fringes in the RSRF are less resolved than in real observations of point sources since the blackbody used in the laboratory was extended to the SWS slit. Slight pointing errors also result in a wavelength shift of the spectrum observed, so that the fringes can be slightly shifted with respect to to the fringes in the RSRF, and this results in fringe residues in the spectra.

- Band 3D: the red side of band 3D shows leakage from the wavelength region around 14 μm. Since the RSRF was corrected based on observations of stars that have a relatively high flux at 14 um, no proper correction of the RSRF in the leakage region was applied. In spectra of cold sources a false drop at the end of band 3D can be seen.

- Band 4 : no in-orbit correction has been applied due to lack of suitable observations/sources. It is now known that the laboratory measurements show a strong de-biasing effect, and it can thus be expected that the shape of the current band 4 RSRF has a global inaccuracy of about 10%.

The steep slopes shown by the SWS RSRFs in some spectral regions can induce false shapes in the calibrated spectra. Poor matches between different AOT bands can often be understood (and corrected for) from a combination of a wrong dark current subtraction and a steep slope in the RSRF at a given

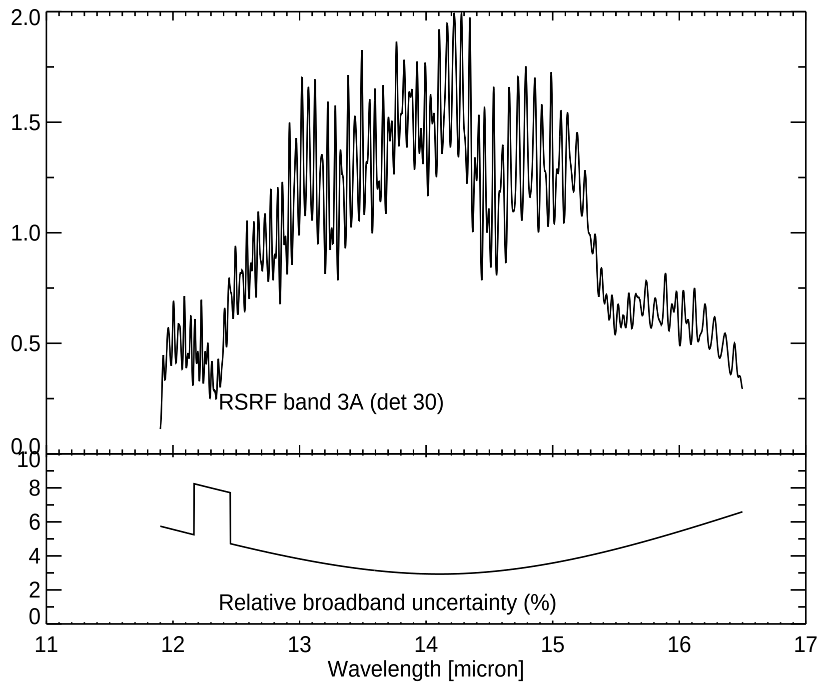

Figure 27: The RSRF for SWS band 3A (top) and relative broad band uncertainty (bottom) - Bart Vandenbussche

wavelength. Note that 10% is typically the difference between two dark current mesurements in an observation. Thus, it is reasonable to expect mismatching problems of this order specially where the signal level of a scan is of similar strength than the dark currents for that band.

Improvements in the RSRF calibration of SWS are expected in the following areas:

- Use of new and improved synthetic spectra.
- Extrapolation of the correction in the leakage region at the red side of band 3D, since verification on cold sources has shown that an extrapolation of the correction factors is better than no correction.
- Re-derivation of the RSRF for band 4 with proper de-biasing correction of the ILT data. De-biasing has shown to be important at the signal levels of these data.
- Re-derivation of the RSRF band 2 with proper memory effects correction of the ILT data.
- Re-derivation of the RSRF for all bands with improvements in the calibration at the slope level.

2.2.7 Transients:

`TR: Applicability of Fouks-Schubert transient correction to the various types of detectors on-board ISO`

The applicability of the Fouks-Schubert method to the various types of detectors on-board ISO can be discussed in terms of the E_j parameter which basically measures the quality of the contacts in the detectors under study.

It is found that for the Si:Ga (∼4−15 μm) detectors on-board ISO (PHT-S, CAM, SWS) we have $E_0/E_j >> 1$ while for the Ge:Ga (∼40−150 μm) detectors (PHT-C, LWS) we have $E_0/E_j \sim 1$ or $<< 1$. Fouks-Schubert model can be used only when $E_0/E_j >> 1$.

The consequence is that for Ge:Ga detectors the Fouks-Schubert model does not seem appropriate. No accurate analytical models can be derived from the set of equations which describe the problem. Numerical models (Haegel et al. 1999 Appl. Optics, 38, 1910) exist but need big computing resources and are very difficult to compare with data, and they cannot be used like analytical models to do transient corrections.

`TR: Implementation of pulse shape corrections in the SWS pipeline`

The so-called SWS 'pulse shapes' are small detector voltage jumps visible at SPD level which affect the calibration of SWS spectra leading to flux shifts of up to 10 Jy in the worst cases.

They occur in only one detector at a time and can be generally described as a sudden decrease or increase of the signal, which then remains constant or has a long recovering time (>> 10 s) after the jump. These jumps are normally seen at low signal levels and there are typically a few of them per hour randomly distributed in time (see Figure 28).

There are indications of a relation between the signal jumps and a residual after reset pulse effect.

A tool has been developed by Fred Lahuis which corrects for these voltage jumps by adjusting a baseline to the affected portion of data which remove almost completely the effect on the calibrated spectra. As a byproduct, the tool also corrects for glitches since they have a similar effect on the signal. This way most of the detector jumps are removed with very high efficiency (although not all and not always up to the 100% level).

The correction tool will be implemented in next OLP v9.5, to be released in September 2000.

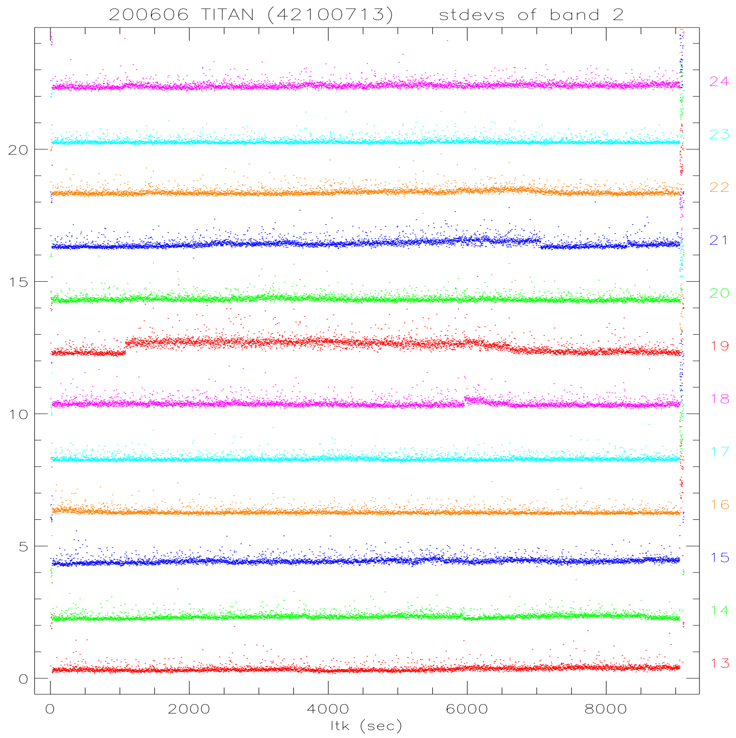

Figure 28: Example of pulse shapes detected in the SWS spectrum of Titan at SPD level - Fred Lahuis

`TR: Transient corrections in band 2 SWS data: implementation plans`

The application of the adapted Fouks-Schubert method to correct band 2 (Si:Ga) detectors for memory effects developed by Do Kester works very well and it will be implemented before the summer in the SWS IA and in OLP v9.5. Later it will be incorporated into OSIA. The recently improved version of the so-called 'dynadark' IDL module is, in addition, now much faster (a factor of 4).

In Figures 29 and 30 we show an example of the application of this method to observations made with SWS on the star γ Draconis. As we can see in Figure 29 the transient effects can be very strong in bands 2A and 2C for bright sources like this (up to 20%), especially if they are observed in the high speed scanning mode. In figure 30 we show how the current tool is able to bring the backward and forward scans into an almost perfect agreement in bands 2A, 2B and 2C (Si:Ga detectors), but fails for band 4 (Ge:Be).

Unfortunately, for SWS band 4 there is no working model yet. Fouks-Schubert method simply does not work in this type of detectors, as we have already mentioned. Efforts are, however, still on-going trying to find an alternative method, although it seems that it will be not possible to implement any solution for this problem in time for its inclusion in OLP v10.0.

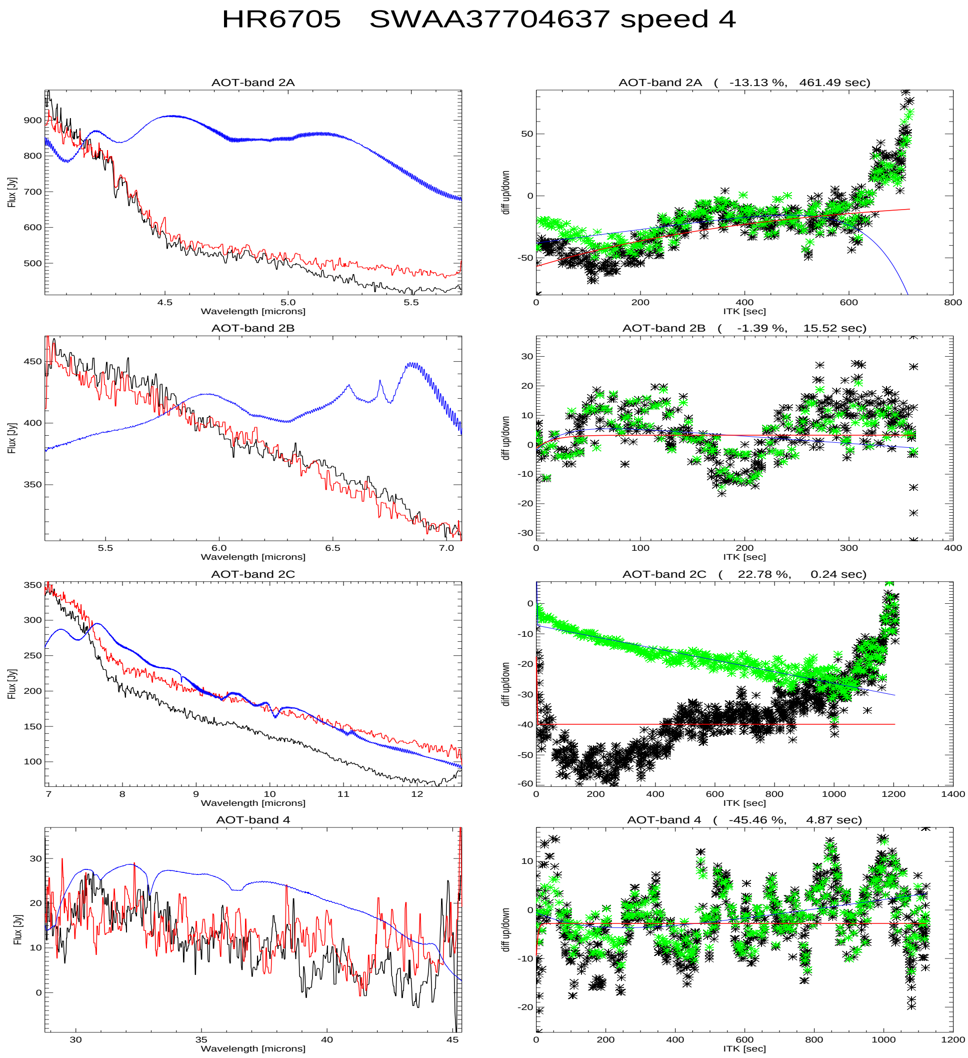

Figure 29: Standard OLP pipeline product corresponding to an observation of γ Draconis. Black shows the up scan and red the down scan in the left panels. The RSRF for each band is the blue line. The transient effects are evident at the start (long wavelength ends) of the scans. They are particularly noticeable in bands 2A and 2C. In the right panels, the differences between the up and the down scans are plotted. The red and blue lines are exponential fits to the differences in respectively the AAR and SPD. This gives an impression of the magnitude of the transient effect - Fred Lahuis

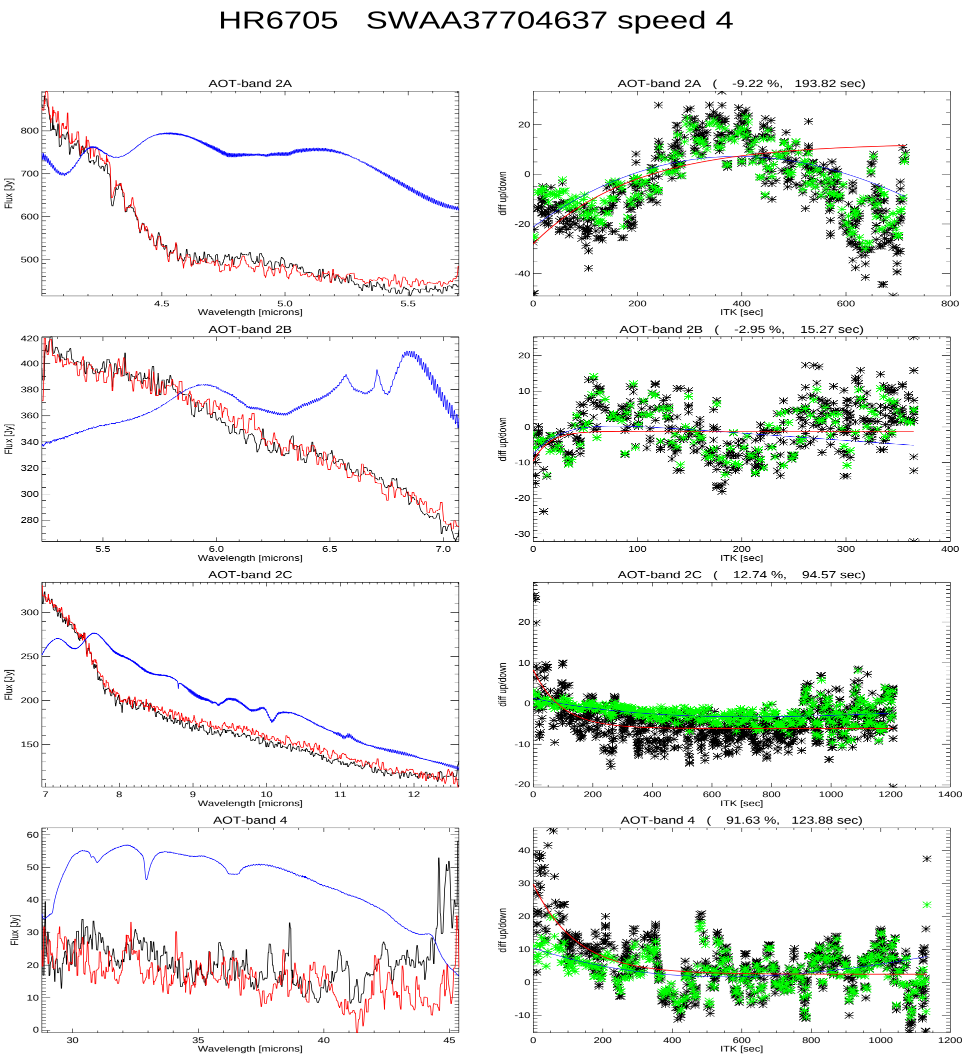

Figure 30: Same as Figure 29, but this time for the observations corrected with the adapted Fouks-Schubert method. The transients are corrected to a high degree only for band 2. Residual offsets remain, but it is likely that other non-transient effects (e.g. a dependency of the dark-current with temperature) play a role here - Fred Lahuis

`TR: Transient effects in ISOCAM: progress status and plans`

A general description of transients in ISOCAM LW detectors can be found in *"Transient correction of the LW-ISOCAM data for low contrasted illumination"* by Alain Coulais and Alain Abergel (A&AS, 141, 533)

available at:

`http://www.iso.vilspa.esa.es/science/pub/2000/ds8869.ps.gz`

This document shows that, for uniform (low gradient) illumination, the Fouks-Schubert model allows us to describe the LW response to upward and downward steps of flux with an accuracy of better than 1%. For each pixel, only two parameters have to be used, which are found to be constant over the whole life of ISO. However, the approach is not valid any more for non-uniform (high gradient) illumination, which is typically the case of point sources.

Alain Coulais is still trying to find a possible solution to the problem of describing the transient behaviour of point sources in ISOCAM data.

Efforts are concentrated on in-flight data taken with CAM with the 1.5″ lens and filters LW10 and LW3 (largest PSF) where the lowest spatial gradients on individual pixels are expected.

Unfortunately, none of the empirical models tested so far give correct responses (closer than 10% for each pixel and each readout).

Recently, an innovative 3-D approach is being tried which looks promising. First attempts were based on an inaccurate knowledge of some important parameters of the detectors (both geometrical and electrical). Part of these missing parameters were unknown, others were not published because they were not considered useful in the past. The new model takes into account the true geometry and good parameters of the detectors in order to derive an adapted semi-analytical model.

Additional tuning of the model is still on-going (taking into account the reflecting plane, for instance, or the rectangular geometry of the pixels, so far considered circular). This is needed in order to obtain satisfactory quantitative results (may be up to the 5-10% level of accuracy). Still there are problems not solved, like how to deal with the different behaviour in the transient response as a function of the precise part of the pixel which is illuminated by a given point source (the behaviour is not the same if the point source falls at the centre of the pixel or at the edges).

The new 3D equations have been obtained with the current conservation condition (1D) replaced by the continuity equation (3D) and some new boundary conditions. The kernel so created is the 3D equivalent to the 1D description of the problem and shows how the charge created under a flux change in one point of the (x,y) plane forms the near-contact field in other points of the plane. This effect is strong because of negligible non-stationary screening in the detector bulk and creates high cross-talkings (current spreading). A pixel is illuminated, but the charge from it creates currents in neighbouring pixels.

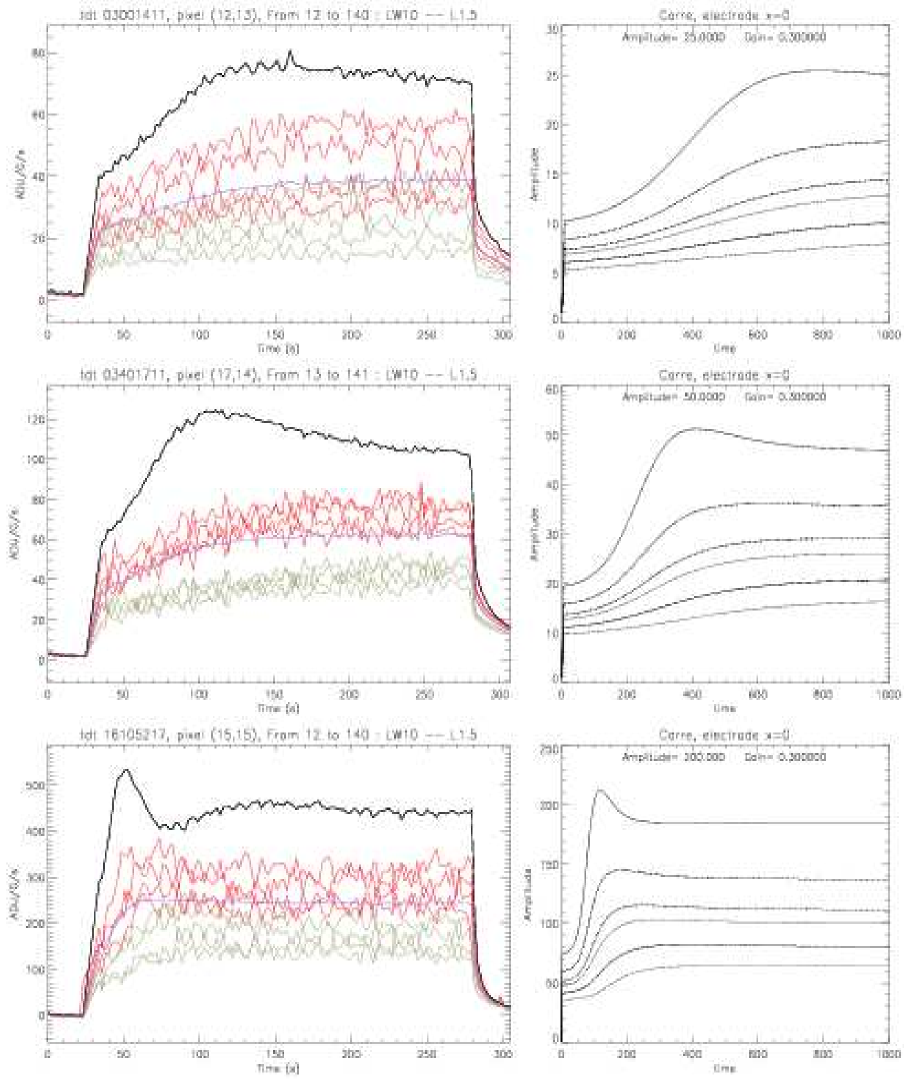

Figure 31: Signals coming from the 3x3 pixels around point sources detected with CAM are shown in the left panels for three different flux levels. The central pixel is plotted in dark; in red, the four closest neighbour pixels; in yellow the four pixels in the corner; the blue line is the mean of the 9 pixels. In the right panels they are compared with the model results - Alain Coulais

So far, the model is able to reproduce qualitatively the overall temporal behaviour of the central pixel and the 8 neighbouring pixels, which is found to be closely correlated with the brightness of the point source (Figure 31).

The description of transients in the case of point sources is a second order model if we consider the description of uniform illumination cases as the first order.

Unfortunately, the amount of work pending is considerable and it seems clear that it seems unlikely to include any tool to correct point source fluxes for transients in the ISOCAM pipeline.

Some lessons have been learned for the future. Many problems found for the description of the transient effects in CAM for point sources could have been avoided with a better knowledge of the detectors (full geometrical, electrical and electronic description) at the time of ground-based testing.

Ideally, in order to develop a valid theoretical model, ground-based experiments (not done for ISOCAM) should be designed to evaluate the effects produced by:

- change of the profile size and shape of the source;
- variable amplitude of the source;
- stabilized prehistory at different backgrounds;
- source on high background (small signal approximation);
- source on well known low background (non-linearity problem);
- on and off-centred source

`TR: Transient effects in ISOPHOT: status and plans`

Full transient correction methods are, in the case of ISOPHOT, restricted to PIA in most cases, where several corrections are available. The main reason for this is that, because the quality of the fit must be checked, these methods are usually highly interactive.

The corrections available in PIA include an empirical solution based on exponential functions for the Ge:Ga type detectors (P3, C100 and C200); or a Fouks-Schubert correction that can be applied to P1 and P2 filters (Si-based) and PHT-S measurements. However, the detector specific constants of P1 and P2 filters have not been fully determined and the model cannot reproduce the often appearing hook responses in the signals of these detectors while the model seems to work well with the chopped PHT-S mode. In OLP v8.4, however, an empirical model is prefered to correct PHT-S chopped data for transients which is based on the comparison of behaviour with respect to reference stars. A similar method to be applied both to PHT-P and PHT-C chopped data also based on pattern recognition is currently under development in Heidelberg. while for PHT-S staring observations the so-called 'dynamic calibration' method is prefered.

This method has recently been implemented both in PIA (since version 7.3) and in OLP v9.0. The correction method is based on the high reproducibility of behaviour of every PHT-S pixel (same time constants) for a given illumination

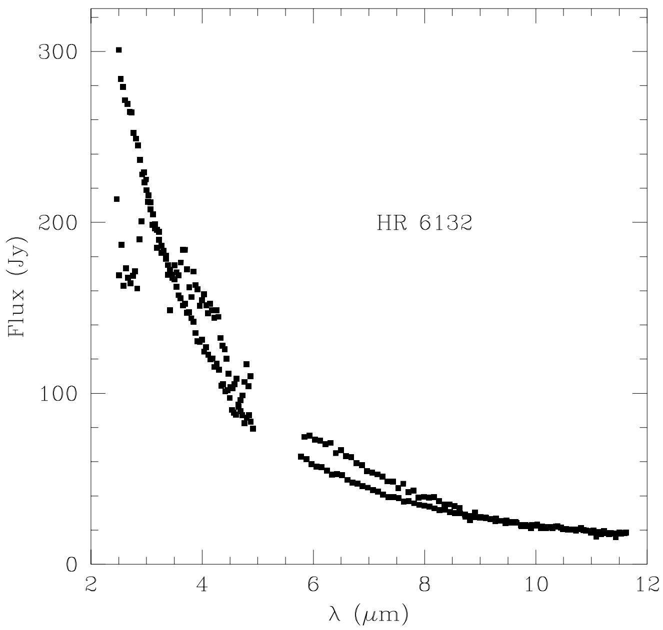

Figure 32: PHT-S (staring) spectrum of the star HR 6132 before (black squares) and after (red squares) the dynamic calibration method to correct for transient effects is applied to the spectrum

level. The calibration is performed by comparing the signal time evolution of the target star with a that of a set of standard stars at similar flux levels.

In PIA the signal time evolution for each pixel is fitted with a Chebyshev polynomial and stored in a database, together with the equivalent flux assigned by comparing the behaviour observed with that of the best matching calibrator. This way an accuracy in general better than 10% can be achieved and the spectral shape is well preserved.

In OLP the method has been automated by creating surfaces which describe the temporal behaviour of each PHT-S detector pixel under different illumination conditions which are just the result of the interpolation of all different calibration observations.

An example showing the extraordinary improvements that can be achieved with this method is shown in Figure 32.

Future work is now mainly concentrated in the correction of transient effects in PHT32 (chopped raster maps). They are mainly caused by fast chopping which produced never-stabilized signals. The effect is a decrease in the source flux measured (up to a factor of 3, depending on the flux contrast between source and background), problems with the determination of PSFs for point vs extended sources and the presence of ghosts (90 arcsec away in the y-axis direction).

The transient behaviour observed cannot be modelled (over- and undershooting effects are usually observed). Richard Tuffs is trying to approach the problem by making use of the redundancy given in PHT32 mode. First results obtained so far look promising. The goal is to include an interactive correction tool soon in PIA (no hope of including this correction in OLP v10.0). Work is still on-going.

`TR: Transient effects in LWS: status and plans`

Emmanuel Caux is working on the correction of memory effects in LWS data applying a correction based on the Fouks-Schubert model adapted for LWS data.

Although the Fouks-Schubert model, as we have already mentioned, is in principle not applicable to Ge-based detectors (with the exception may be of LWS parallel mode observations), memory effects can be at least partially removed for LW detectors which are based on Ge:Ga (note that the stronger memory effects are observed in the stressed Ge:Ga detectors LW2 to LW5) by the application of this correction (see Figure 33)

Satisfactory results are obtained in all cases where the modified Fouks-Schubert method was applied. The method also consider overshooting effects for big flux jumps.

The situation is worse for Ge:Be detectors (the case of SW1) where Fouks-Schubert model simply does not work.

At the last LWS OLP 10 Review Meeting held at RAL in March this year it was decided to support the generation of transient corrected RSRFs (at least for LW detectors) using the adapted Fouks-Schubert model, which should be produced at CESR by Emmanuel Caux. The impact on the whole LWS calibration will be investigated by Tanya Lim at RAL and data sets for this analysis have already been agreed. The improved RSRF so obtained, however, should be implemented only in LIA, but never in OLP v10.

`TR: IFSI activities on LWS transient corrections`

Stefano Pezzuto presented at the Transients WG Meeting held in February this year an update on the status of the activities developed at IFSI concerning correction of transient effects in LWS data.

A simple approach is being tried at IFSI which describes the problem as an autoregressive first-order process where:

$$\mathrm{y(i)} = \alpha_1 \ \mathrm{y(i{-}1)} + \mathrm{x(i)}$$

is the discrete description of a physycal system with 'memory'

$$\mathrm{T}\ [\mathrm{dy/dt}] + \mathrm{y(t)} = \mathrm{x(t)}$$

where T is the time constant.

The intention is to derive the asymptotic ('true') value of the photocurrent rather than describing the temporal behaviour of the detectors.

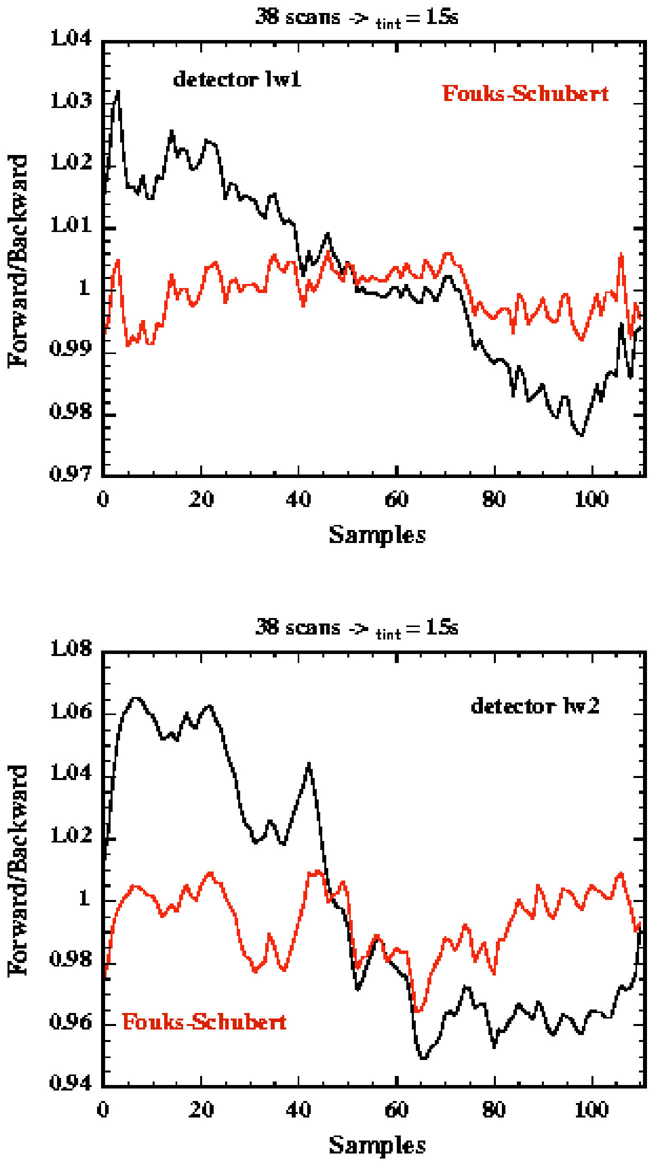

Figure 33: Ratio of LWS forward/backward scans before and after the application of the transient correction based on the Fouks-Schubert model - Emmanuel Caux

In order to derive the time constant of the system, first, signals detected by inactive detectors during LWS04 Fabry-Pérot observations were analysed as test cases, for which values of $\alpha_1 = 0$ were derived as expected. Secondly, LWS02 observations of (moderately) strong sources with the grating at a fixed position are going to be used. In this case, the signal will be assumed to be intrinsically stable and the fluctuations will be dominated by the noise of the detector. Work is still on-going.

`TR: IPAC activities on transients`

A summary of the current activities carried out at IPAC on the understanding of transients in ISOCAM data and the on-going efforts to provide algorithms for correcting the effects of these transients on the ISOCAM flux calibration was also presented by Babar Ali at the Transients WG Meeting held at VILSPA last February.

Rather than modelling the transient itself, the approach adopted is towards understanding how the transient *scale* with source flux. Furthermore, it is assumed that the transient induced by the background flux and the transient induced by a source (if any) can be added separately to approximate the total transient. The observed CAM signal is then compared to a library of known transient shapes (taken from the Fouks-Schubert model and assuming several flux levels) via a χ^2 fitting procedure. In addition to correcting source transients and removing background, this procedure also provides a method to deglitch the data.

First results using this technique have already been obtained, but still additional analysis work is on-going.

A report on the CAM calibration of a sample of point-sources observed with the LW1 filter over a wide dynamic range from 1.5 to 4400 mJy to investigate linearity and stability of the detectors and determine whether the fast response can be used to calibrate the data is in preparation.

`TR: The transient response of Ge:Ga detectors on board ASTRO-F`

Issei Yamamura and Hirohide Kaneda, from the japanese ASTRO-F project, presented at the last Transients WG Meeting held in April this year the results obtained during recent ground-based experiments carried out with the Ge:Ga detectors that will go onboard ASTRO-F. The goal of these experiments is to understand and model the transient properties of these detectors over a wide range of background and signal incident fluxes (10^4 to 10^9 photons/sec).

The slow transient response was analysed by the use of two internal blackbody sources illuminating the detectors and opening and closing a cold shutter at constant intervals of 5 minutes. This way a very slow transient response was found with a long time τ_1 constant of a few 10 s, longer for smaller fluxes. For the downward step, the contribution of the transient component was found to be very small.

In order to model the transient response of the upward step, additional time constants were needed: τ_2 for the fast transient response; and τ_3 which describes a decreasing exponential in order to reprodude overshoot cases (they appear for strong signal fluxes).

In the case of the downward step, only one component with an instantaneous drop was needed for the fitting and a time constant τ_c.

Contour maps of τ_1, τ_2 and τ_3 have been produced for a wide range of background and signal fluxes. All these time constants are strongly dependent on the incident signal/background fluxes showing a negative correlation.

The contribution of each of these components as a function of the incident flux to the total transient effect observed has also been determined.

In addition, the dependence of time constants on detector bias (longer time constants for smaller bias) and detector size (time constants are 2 times longer for $1\times1\times1$ mm^3 detectors than for $0.5\times0.5\times0.5$ mm^3 detectors) was also investigated. Note that a small detector size is prefered to avoid cosmic ray hitting.

In the near future, additional experiments are programmed including:

(1) the measurement of the transient response under chopping conditions (mirror movement with a speed of 2 mm s^{-1} covering wavelengths from 50 to 200 μm using a cryogenic motor);

(2) simulation of space weather conditions of irradiation due to high-energy electron hitting of ambient materials using gamma-ray isotopes such as ^{60}Co and ^{241}Am;

(3) SAA passage simulation irradiating the detectors with a 100 MeV proton beam using a nearby synchrotron facility.

A brief description of how the memory effects will affect the ASTRO-F Far Infrared Survey was also presented. Reduced peak intensity, delay of peak position and persistance of the memory effects after passing bright sources are the main problems foreseen.

The simplified inversion model proposed at the WG Meeting to deal with these problems both for the survey and the spectroscopic data was found to be not convincing because of the non-linearity of the equations involved in the description of Ge-based detectors. Discussions during and after the meeting were hold to try to find a solution. Boris Fouks suggested a number of additional experiments that should help to better describe the characteristics of the detectors. They should help to try to construct a theoretical model able to describe their behaviour.

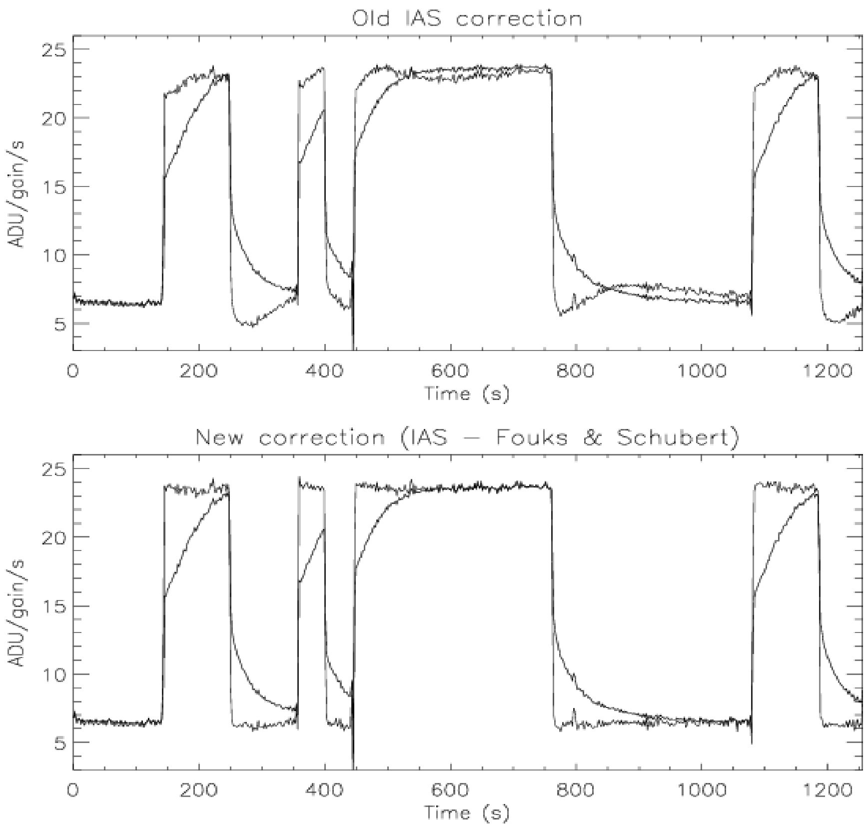

Figure 34: Correction of ISOCAM transients with the old IAS inversion method (upper panel) and with the Fouks-Schubert method (lower panel) - Alain Coulais

`TR: Problems of operation of space IR detectors, their physics, possible solutions and/or ways around the problems`

Boris Fouks, who was invited to participate at the last Transients WG Meeting, presented an overview of the many different problems which are known to affect the operation of space IR detectors.

Non-stationary processes in high resistivity semiconductors show a lot of peculiarities which are hard for comprehension and explanation (non-stationary screening, non-stationary injection,..). The principles are known but there are a lot of problems to describe their behaviour with an exact theory described by analytical formulae.

The problems are more pronounced in space IR detectors, which are difficult to design and have additional manufacturing problems, appart from being affected by other effects like high-energy irradiation from cosmic particles.

Only in the case of the low-background Si:Ga detectors ('high-field' detectors) it is possible to obtain the analytical solution of the equations which describe the transient behaviour, but still there are problems to describe real detectors (3D-effects, like field and current spreading).

2.2.8 Interactive Analysis

`IA: Distribution of questionnaires on IAs`

In order to improve the communication flow with the users, the decision was taken by SWS, PHT and LWS members of the WG to follow the initiative of CAM and send an e-mail questionnaire out to users soliciting thoughts on their IAs. PHT has already sent out its own questionnaire to PIA users (over 100 identified) last February while SWS will soon do the same with a similar questionnaire adapted to the specific characteristics of this instrument to be sent to OSIA users.

`IA: Recent IA releases: major improvements and future plans`

A summary of the implementation status and plans per IA can be found below together with a list of major improvements contained in the more recent versions released with respect to previous versions.

- **PIA v8.2:** (released April 7, 2000)

  - following requests from many users the entire source code is distributed with PIA v8.2. This should help the users to develop own routines to be used by the PIA system.

  - PIA v8.2 is a pre-PIA 9.0 version; as such, it contains all the elements of the OLP 9.0 pipeline (and will be used for validating it).

  - a mapping simulation system is released with PIA v8.2 which allows the user to simulate sky (background + point/extended sources) and what the detectors PHT-C100 or PHT-C200 should have seen from it in any of the different observation modes (PHT22 or PHT32), including glitches and transient effects. The data derived can be ingested as normal measurements into PIA.

  - the 'dynamic calibration' method for processing PHT-S staring observations is included.

  - IMAP, a special tool developed at IPAC for cleaning PHT32 type data is integrated into PIA.

  - An extension of the AAP level of reduction incorporates as further variables RA and DEC for every single point, including the chopper deflection and the pixel offset to the central position of the array. This includes a recognition of 'old' saved AAP internal files and their proper conversion by reading in.

  - Photometry tables from AAP level quoting the apertures in arcseconds are now available.

- Since this version is almost parallel to the OLP 9.0 release, it only reads OLP9.0 final AAR products, for their display. To access earlier final pipeline products, an earlier version of PIA is needed.

- **CIA v4.0:** (released April 11, 2000)

  - CIA v4.0 includes an improved implementation of the Fouks-Schubert transient correction leading to better results and to a reduction in processing time up to a factor of 20. Obsolete algorithms used for transient correction and de-glitching were removed.

  - an improved dark correction using a second-order time-dependent correction which reduces the dark uncertainty by up to 30% is included.

  - access to long-term transient correction and variable flat-field algorithms routines via the SLICE package (see previous Status Report for a description) is now possible.

  - 'back_project' module allows the possibility to back project a raster mosaic to a set of exposures to verify stability and de-glitching.

  - 'raster_scan' module offers now the option '/weight' to use the weighted mean to create a mosaic.

  - CIA v4.0 allows the handling of Solar System Object and polarisation observations.

  - 'ximage' provides improved functionality for astronomical image display, especially for the analysis of data from raster observations.

  - 'xcvf' provides an interface to the spectral analysis package ISAP.

  - users are warned of saturations in the data. The position of the saturated pixels can be obtained and masked out.

  - new algorithms to treat faint sources in CAM-CVF observations are included

  - v5.0 of CIA is expected in June 2001 (will include error propagation)

- **OSIA v2.0:** (to be released in September 2000)

  - still the details are to be defined but OSIA v2.0 will basically contain the same routines that will be used in the SWS 9.5 version of the pipeline.

  - the 'dynadark' module to correct band 2 SWS data for transient effects and the 'pulse shape' correction are among the major improvements expected.

- a pointing correction module applicable to off-centred SWS observations will also be incorporated in OSIA v2.0.

- improved glitch detection algorithms are expected

- OSIA v3.0 will only be released after OLP v10.0 (expected in February 2001).

- **LIA v8.0:** (released May 4, 2000)

  - A new tool has been written for Interactive Fabry-Pérot Multi-Gaussian Fitting of blended lines. The input data should be averaged LWS spectra produced by the ISAP 'average'.

  - Another tool has been made available with LIA v8.0 which can be used for interactive defringing of LWS data (LWS01, LWS03 and LWS04 modes).

  - An option has been added in the 'short_aal' module to include data following glitches in the output LSAN file.

  - LIA v8.0 is valid for LWS OLP v8.7 data products only

- **ISAP v2.0:** (released May 3, 2000)

  - ISAP v2.0 is now able to cope with standard ISO LWS, SWS, PHT-S and CAM-CVF spectra.

  - the transmission profiles for the SIRTF instruments: IRAC (InfraRed Array Camera) and MIPS (Multiband Imaging Photometer for SIRTF) are now available in their preliminary versions in the 'Synthetic Photometry' package.

  - now it is possible to read in simple ASCII spectra, and many routines have been modified to operate in such spectra which require few or no keywords.

  - the internal 'Feeder-merger' routine is now used for the advanced routines: 'Average', 'Clip', 'Smooth', 'Norm', 'Rebin'. 'Feeder-merger' strips away the YAAAR data structure before processing arrays, and reassembles the structure afterward. Thus, these advanced routines now process simple arrays, and in principle, may be used independently of ISAP.

  - for LWS data, the user may now apply a 'Small source to Large source Correction' which consider the shape of the LWS beam profile.

  - also for LWS data only, the user may now apply an aperture vs. wavelength correction, as a refined correction to the standard pipeline processing.

- the Zodiacal light predictor (based on J. Good's IRAS model) has been generalized to handle spectra from ISO or any other mission, as long as FITS keywords for RA, DEC and DATE are present in the headers and it can re-introduce the FIR offsets found in the IRAS data set, as a function of wavelength.

- Lorentzian fitting is now supported (useful for PAH's in CAM)

- the enhanced line list in 'line-fit' now includes many mid-IR Unidentified Bands (PAHs) and some FIR Unidentified Lines.

- multiple lines can now be fit freeing one λ and constraining a fixed $\Delta\lambda$ to exist between fitted components.

- Flux per steradian (Intensity) is now allowed as a unit and is carried through routines.

- the user can now convert between intensity and flux, by specifying aperture.

- there is an enhanced 'shift' routine that handles lines and scans as desired (to obtain mean values, overlap values, etc.) - a convenience for SWS and LWS processing.

- the user may clip many sigma data points without averaging using the standalone graphical Clip routine.

- there is now convenient merging of groups of spectra.

- improved reduction recipes for LWS and SWS have been delivered in the /isap/doc/recipes area.

- no further updates of ISAP are foreseen in the future.

2.3 Updated overall schedule

Below is the updated schedule for cross-calibration activities in the framework of the important events (impacting instrument calibration) during the remaining POPS. It contains all on-going actions previously identified and reported in the Cross-calibration Plan which are still pending as well as new actions activated during the last six months not previously included in previous versions of the Cross-calibration Plan.

Note that a major change in the new schedule below is the new delivery dates for future OLP releases (versions 9.0, 9.5 and 10.0) recently agreed by all the parties involved.

A graphic version of this schedule can be found at:

`http://www.iso.vilspa.esa.es/users/expl_lib/ISO/schedule_plan_3.ps`

CROSS-CALIBRATION PLAN
(as of June 8, 2000)

```
==============================================================================
  * Third Post-ops X-Cal. Status Report                            08 Jun. 2000
==============================================================================
  * OLP v9.0 (CAM+PHT) IDC --> NDCs                                30 Jun. 2000
==============================================================================
PH: The ISO Calibration Web pages go public (July 2000)
IA: PIA v9.0 release (July 2000)
TR: Implementation of Fouks-Schubert transient correction in CAM OLPv9.5
     (July 2000)
TR: Implementation of Faint Source Treatment  in CAM OLP v9.5 (July 2000)
BP: Beam profile calibration files for SWS data ready for distribution
     with SWS OLP v9.5 (July 2000)
TR: Implementation of  pulse shape correction in SWS OLP v9.5 (July 2000)
GL: Implementation of improved glitch detection algorithms in SWS OLPv9.5
     (July  2000)
TR: Implementation of the adapted  Fouks-Schubert method  to correct SWS
     band 2 data for transients in OLP v9.5 (July 2000)
==============================================================================
  * Delivery of Cal-G files for OLPv9.5 (CAM+SWS)                  05 Jul. 2000
==============================================================================
SM: Cross-calibration analysis of SWS, PHT-S and CAM-CVF observations of
     Neptune (September 2000)
SM: Cross-calibration analysis of SWS, PHT-S and CAM-CVF observations of
     Titan (September 2000)
SM: Statistical cross-calibration analysis of sources in the ISO Data
     Archive observed with CAM-CVF, PHT-S and SWS: results for OLPv9.0
     (September 2000)
SM: Investigation on discontinuities found between SW1 and SW2 bands in
     LWS and possible trends with source properties (September 2000)
SM: Analysis of spectral line fluxes; cross-calibration comparison with
     external - KAO - data (September 2000)
TR: Applicability of transient corrections to ISOCAM point sources:
     revision of status (September 2000)
TR: Transient effects in SWS band 4 data: revision of status (September
     2000)
TR: LWS RSRFs corrected for memory effects: revision of status
     (September 2000)
TR: Characterization of memory effects affecting Fabry-Perot LWS line
     profiles  (September 2000)
TR: Progress report on IFSI activities on LWS transient corrections
      (September 2000)
BP: Implementation of pointing correction tool in OSIA v2.0 (September
     2000)
GL: Implementation of improved glitch detection algorithms in OSIA
      v2.0 (September 2000)
TR: Implementation of pulse shape correction in OSIA v2.0 (September 2000)
```

```
TR: Implementation of the adapted Fouks-Schubert method to correct SWS
     band 2 data for transients in OSIA v2.0 (September 2000)
IA: OSIA v2.0 release (September 2000)
===============================================================================
  * OLP 9.5 (CAM+SWS) IDC --> NDCs                                03 Oct. 2000
===============================================================================
BP: Field distortion correction: revision of status (October 2000)
BP: Ghosts in ISOCAM: revision of status (October 2000)
BP: Straylight in CAM parallel and PHT raster maps (October 2000)
GL: Implementation of a two-threshold de-glitching method in PHT
     OLP v10.0 (October 2000)
PH: Correction for inhomogeneous illumination of PHT-P apertures
      by FCS implemented in OLP v10.0 (October 2000)
BP: Beam profile corrections for PHT-P data implemented in OLP v10.0
     (October 2000)
PH: Surface brightness calibration in PHT raster maps available in
      OLP v10.0 (October 2000)
PH: Implementation of refined flat-field corrections in raster maps
     taken through PHT-C filters in OLPv10.0 (October 2000)
TR: Implementation of non-linear long-term drift corrections in PHT
      raster maps in OLP v10.0 (October 2000)
PH: Implementation in OLP v10.0 of a new dark subtraction method in
     SWS band 2 data (October 2000)
GL: Implementation of new glitch detection methods and de-glitching
     algorithms in CAM pipeline v10.0 (October 2000)
BP: Beam profile calibration files for LWS data ready for distribution
     with OLP v10.0 data products (October 2000)
GL: Implementation in OLP v10.0 of an improved glitch detection algorithm
     in LWS data (October 2000)
PH: Improved correction of fringes in LWS data implemented in OLP v10.0
     (October 2000)
PH: Implementation in OLP v10.0 of the 'intelligent' dark current
      subtraction method in LWS data for faint sources (October 2000)
IA: Report on recent improvements implemented in the four ISO instruments'
     IAs (October 2000)
SM: Statistical cross-calibration analysis of sources in the ISO Data
     Archive observed with CAM-CVF, PHT-S and SWS: results for OLPv9.5
     (October 2000)
PH: Evaluation  of calibration improvements recently achieved and
     investigation on cross-calibration problems reported in the
     last Status  Report affecting OLP and/or  IA data with  special
     emphasis on  OLPv9  data products (October 2000)
===============================================================================
  # Working Group Final Reports - drafts -                        15 Nov. 2000
===============================================================================
GL: Report on latest results on PACS radiation effects simulations
     (November 2000)
TR: Improvement in LWS RSRFs after correction for transient
     effects: evaluation of results (November 2000)
PH: Statistical cross-calibration analysis of sources observed with SWS and
```

```
     LWS and comparison with IRAS data: final results (November 2000)
PH: Statistical cross-calibration analysis of sources in the ISO Data Archive
     observed with LWS and PHT-C filters (November 2000)
==============================================================================
  * Fourth Post-ops X-Cal. Status Report                         28 Nov. 2000
==============================================================================
  $ Delivery of CAL_G files for OLPv10 (all)                     11 Dec. 2000
==============================================================================
SM: Analysis of spectral line fluxes: cross-calibration comparison of
     measurements on the same line obtained by different ISO instruments
     (December 2000).
PO: Internal cross-calibration of ISO Polarisation measurements
     (December 2000)
PH: "ISO Calibration Legacy" Workshop to be held at VILSPA
      (5-9 February  2001)
==============================================================================
  * OLP 10.0 final OLP IDC --> NDCs                              12 Mar. 2001
==============================================================================
IA: OSIA v3.0 release (March 2001)
PO: External  cross-calibration of ISO Polarisation measurements
     (March 2001)
IA: Report on recent improvements implemented in the four ISO instruments'
     IAs (March 2001)
PH: Evaluation  of  calibration  improvements recently achieved and
    investigation on cross-calibration  problems reported in the last
    Status  Report affecting  OLP and/or  IA data with special emphasis
    on OLPv10 data products (April 2001)
==============================================================================
  # Working Group Final Reports                                  12 Apr. 2001
==============================================================================
  * Final Post-ops X-Cal. Status Report                           15 May 2001
==============================================================================
PH: Description of photometric data reduction in IA's that could not be
     implemented into OLP processing due to being appropriate to only a
     subset of data or to limited OLP implementation resources (May 2001)
==============================================================================
  * ISO Data Archive final delivery                              01 Jun. 2001
==============================================================================
IA: CIA v5.0 release (June 2001)
PH: Document on 'Lessons learned from the ISO experience and
      Engineering/Design problems we had to fight' (July 2001)
==============================================================================
  * Legacy (final) archive available to community                31 Aug. 2001
==============================================================================
  * ISO Explanatory Supplement final issue                       01 Nov. 2001
==============================================================================
  * End of Post-operations Phase                                 31 Dec. 2001
==============================================================================
```

3 Internal and external cross-calibration

3.1 The concept of cross-calibration

Cross-calibrations can be used (i) as consistency checks, and (ii) as true calibrations. In the first instance observations of a source by a pair of instruments are compared to evaluate internal consistency: if the results do not agree (to within the stated uncertainties) then the calibration procedure of one of the instruments (though possibly both) is incorrect. In the second instance, results from the less accurate instrument(s) can be calibrated against data from the more accurate one(s).

In the case of ISO, the above concept can be applied both to pairs of ISO instruments that overlap in wavelength range and also to ISO instruments vs other non-ISO instruments.

3.2 Definition of standard and cross-calibration sources

The absolute flux calibration of three of the four ISO instruments (CAM, PHT - at short wavelengths - and SWS) is based primarily on results of the Ground-Based Preparatory Programme (GBPP, Jourdain de Muizon and Habing, 1992 Les Houches Series: Infrared Astronomy with ISO, p. 129) and of the Cohen, Walker, Witeborn et al. (CWW) absolute calibration programme (Cohen et al. 1992a AJ 104, 1650, 1992b AJ 104, 2030 and 1995 AJ 110, 275), though the long wavelength filters of PHT also use planets and asteroids to cover the bright and intermediate part of their dynamic range. The absolute flux calibration of LWS is currently based on Uranus as primary source.

For cross-calibration purposes a small set of astronomical sources was used in the past, composed by a few bright stars (like HR 7310, HR 7341, HR 6436, γ Dra or α Boo), planetary nebulae (NGC 7027 and NGC 6543), galaxies (Mrk 279), asteroids (Cybele, Hygiea) and planets (Neptune) on which most of the cross-calibration comparisons carried out so far have concentrated. For most of them, observations exist taken throughout the whole ISO mission with more than one instrument and in many cases covering a wide range of wavelengths.

Note that, because of the limited common dynamic range between the ISO instruments, not all kind of inter-comparisons are possible. Stars are too faint in the long wavelength range of ISO to be used for cross-calibration analysis in the spectral region beyond 100 μm and asteroids and planets have to be used instead. While the results of the CWW and the GBPP programmes, based on stars, are believed to be accurate to $\pm 5\%$ or better and are consistent with one other, the uncertainties in asteroid and planet model spectral energy distributions are larger ($10-15\%$ level). In the case of asteroids their characterization is additionally complicated by their variability. Thus, the cross-calibration of LWS in the long wavelength range is especially difficult, since the comparison has to be made against PHT measurements, and the dynamic range overlap between

PHT and LWS is limited.

Another important limitation is imposed by the fact that calibration problems do not necessarily affect all the cross-calibration sources in the same way. Thus, some comparisons do not shed any light on the understanding of a given problem if we restrict our analysis to the small sample of objects listed above.

3.3 A new cross-calibration strategy

In order to take into account all the limitations and caveats considered above a new cross-calibration strategy was activated in Post-Operations based on the statistical analysis of large data sets of sources.

The following aspects need to be considered:

- cross-calibration data sets must be able to ensure proper handling of differences in beam sizes, filter profiles and spectral resolution, as well as the use of differing absolute calibration systems and of different sets of astronomical standard sources.
- the detailed investigation of specific calibration problems may require the selection of dedicated subsamples of targets. Thus, cross-calibration data sets should contain a combination of bright/faint, red/blue, point/extended sources. This way it will always be possible to draw a complete picture of the impact on ISO data of an existing problem or evaluate recent achievements in ISO calibration properly.
- calibration data sets should satisfy at least one of the following conditions:

  - they have been observed with more than one instrument/configuration at least once during the ISO mission (for internal cross-calibration purposes)

  - infrared data from non-ISO instruments exists (for external cross-calibration)

  - accurate models exist against which ISO data can be compared (for absolute flux calibration).

3.4 Selection of cross-calibration data sets

3.4.1 The short wavelength range ($\lambda < 45\ \mu$m)

Internal cross-calibration:

A total number of 277 different positions in the sky have been identified using the ISO Data Archive where spectra were taken during the mission with at least two of the following AOTs: SWS01, CAM04 (CAM-CVF) and PHT40 (PHT-S staring or chopped).

Unfortunately, not all the observations are suitable for a direct cross-calibration comparison. In some cases there are slight pointing offsets which, as we have already mentioned in this document, can account for strong variations in flux. For this reason, pointings which differ by less than $3''$ from each other have been considered appart. Note that the subsample of bad pointed observations so defined is not useless at all, since it constitutes an excellent database of test cases for checking the pointing correction tools now available in PIA and soon in OSIA for PHT and SWS data, respectively.

In addition, some of the sources in this large cross-calibration sample are known to be extended. They were also identified and considered as a different subgroup. Again, the subsample of extended sources observed with various instruments so defined constitutes an excellent database to be used for the analysis and comparison of beam profile models, the test of aperture size corrections, or to study the effects induced by the extension of the sources on line profile resolution, fringes, etc.

Last, but not least, there is a further aspect to consider in the massive cross-calibration analysis we propose to perform here and this is variability. We know that many of the stars observed by ISO are characterised by their strong variability. They are in many cases pulsating stars in the Asymptotic Giant Branch (AGB) phase evolving into planetary nebulae (young stellar objects are also variable but usually the amplitude of the variations in the ISO spectral range is not that large). These variable sources were also removed from the initial sample (note that we only need to remove those observations that were not taken simultaneously).

After all, if we restrict our analysis to the subsample of non-variable point sources not affected by pointing problems and bright enough to provide reliable data, we end up with a much smaller database compared to the initial one, but which still includes around 10 to 20 different sources observed with CAM04, and between 100 and 150 different positions of the sky observed either with SWS or with PHT-S.

Note that the smaller number of CAM-CVF observations available for cross-calibration is just the natural consequence of the predominant use of this observing mode to observe faint extended sources which otherwise cannot be detected and/or spatially resolved by SWS or PHT. Thus, there is only a small overlap of observations between CAM-CVF and SWS or PHT-S.

External cross-calibration:

For external cross-calibration, specific observations in the ISO database have been compared with observations of the same sources made with ground-based facilities like UKIRT, as we will show later, or with other space facilities, like IRAS, COBE/DIRBE, KAO or MSX.

A special effort has recently been spent in the generation of a large cross-calibration database of sources selected from the ISO Data Archive to be statistically compared with IRAS in the SWS range. The idea is to compare the ISO observations made with SWS with IRAS photometry at 12 and 25 μm. The preliminary results from this analysis are presented in Section 3.5. Other comparisons have also been performed between IRAS and PHT photometry at 25 μm or between PHT-S and COBE/DIRBE photometry at 4.9 and 12 μm and the results will also be presented in Section 3.5.

3.4.2 The long wavelength range ($\lambda > 45$ μm)

Internal cross-calibration:

With respect to the internal cross-calibration of the long wavelength spectral range covered by ISO, a similar exercise was performed as for the short wavelength range. This way, it has been possible to select a few hundred different positions in the sky from the ISO Data Archive where ISO observations taken both with PHT-C filters (photometry beyond 60 μm) and LWS01 are available.

The main problem again is that cross-calibration comparisons between PHT and LWS are difficult because of the very different dynamic range of the two instruments. Thus, there is a minimum overlapping region in flux level at which both PHT and LWS observations are of enough quality to derive reliable cross-calibration comparisons. In spite of this, we estimate that a minimum number of 50 cases will probably remain as useful. The results from this cross-calibration comparison will be presented in the next Status Report.

External cross-calibration:

Concerning external cross-calibration, efforts are concentrated in the generation of a specific cross-calibration data set of observations selected from the ISO Data Archive to be compared with IRAS photometry at 60 and 100 μm. This work is being carried out by Josephine Chan at RAL and the preliminary results will also be presented in Section 3.5.

In addition, we also present in Section 3.5 the results obtained from a cross-calibration comparison of LWS raster scans performed on two different fields showing complex extended emission at 100 μm with IRAS maps obtained at the same wavelength, between ISOPHOT and IRAS photometry at 60 μm and a cross-calibration analysis of ISOPHOT C100 and C200 maps with COBE/DIRBE data.

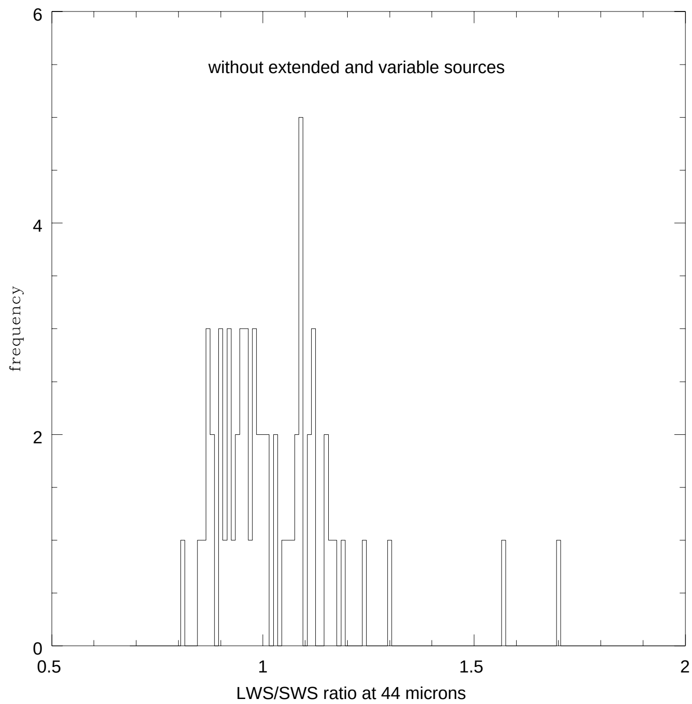

Figure 35: Distribution of LWS/SWS ratios at 44 μm when variable and extended sources are removed from the sample - Pedro García-Lario

3.4.3 Connecting the short and the long wavelength range

In order to give consistency to the results obtained in the short and the long wavelength range, an internal cross-calibration analysis was also performed between SWS and LWS observations, whose results were already presented in the previous Status Report.

LWS/SWS ratios at 44 μm (this is in the overlapping region between SWS and LWS) were determined for all the sources in the ISO Data Archive for which both SWS01 and LWS01 observations were available. A total number of 122 different positions in the sky were identified with flux $>$ 100 Jy at 44 μm. When all the known variable and extended sources in the sample are omitted, the level of agreement found between SWS and LWS is within 20% for 95% of the sources of the sample (see Figure 35).

An important point to consider is that the mean value of the LWS/SWS ratios so obtained was $<$LWS/SWS$>$ = 1.02, very close to unity. This is remarkable, if we consider that LWS and SWS were calibrated in a totally different way (LWS calibration is based on Uranus as primary calibrator while SWS band 4 calibration is mainly based on ground-based ILT experiments using blackbody sources).

3.5 Cross-calibration comparisons

3.5.1 Cross-calibration of sources observed with SWS, CAM-CVF and PHT-S

A summary of the first results derived from the analysis of the sample of astronomical sources observed at the short wavelength range of ISO (between 2 and 15 μm with SWS01, CAM04 (CAM-CVF) or PHT40 (PHT-S) was already presented in the previous Status Report. At that time, the analysis made was based on OLP v8 data products and compared to OLP v7.

In this issue we review again the same data set of CAM-CVF SWS and PHT-S observations in order to evaluate the latest improvements achieved in the calibration of ISO data as for OLP v9.

Changes are mainly expected as a consequence of: (i) the application of the dynamic calibration method in PHT-S staring observations to correct for transient effects; (ii) the use of the Fouks-Schubert model in ISOCAM data to correct for transient effects; and (iii) the new transient correction based on the Fouks-Schubert model applied to SWS band 2 data (in OLP v9.5).

Unfortunately, it was not possible at the time of writing this Report to use 'real' PHT and CAM OLP v9.0 data products directly retrieved from the ISO Data Archive because the distribution of this new version of the pipeline has been delayed a few weeks, nor the SWS v9.5 data products are yet available (release scheduled for September 2000).

For that reason, in the cross-calibration analysis below, we will be comparing pipeline data products generated with OLP v8, as they are directly retrieved from the ISO Data Archive, with 'manually' upgraded versions of these data products (using the tools available in the different instruments' IAs) which in principle should be equivalent to future OLP v9 data products. Although minor differences with real OLP v9 pipeline might exist, we are confident that the conclusions derived from our analysis will be esentially correct.

<u>SWS versus PHT-S</u>

Starting with the objects in the sample observed both with SWS and PHT-S, we would like here to evaluate first the improvements represented by the future availability in OLP v9.0 of the dynamic calibration method to correct PHT-S staring observations for transient effects.

Figure 36 shows a number of examples of OLP v8.4 data products corresponding to a few sources in the working sample as they are retrieved from the

ISO Data Archive. The examples shown include representative cases of 'red' sources [AFGL 2999 and S Per] (upper panel), 'blue' sources [HR 6132 and HR 7310] (middle panel) and 'faint' sources [PV Cep and IRAS 21434+4936] (lower panel), all of them observed with PHT-S in staring mode, with the exception of IRAS 21434+4936, for which the triangular chopping mode was used, and it is here included for comparison.

As we can see, there is a general good agreement in the overall shape of the spectra. However, strong discrepancies of the order of 20% to 40% are observed in some cases which are far from acceptable.

Some of the problems that might be affecting the data in the most discrepant cases are well known. They are in a high percentage related with transient effects in PHT-S data taken in staring mode (especially at the shortest wavelengths), for which no correction was applied in OLP v8.4. This is clearly reflected in the fact that the only chopped observation shown in Figure 36, that of IRAS 21434+4936, shows an excellent agreement with SWS data even at a very low flux level. Note that chopped PHT-S observations are corrected for transients in OLP v.8.4 using a different, empirical method which gives quite satisfactory results and, thus, they are not affected by this problem.

If this is the case, one should then expect to strongly improve the level of agreement of staring PHT-S data with SWS simply by applying the dynamic calibration method to the OLP v8.4 data products using PIA v8.2, where this method is implemented exactly in the same way as it will be in OLP v9.0.

This is what we did and the results obtained after this correction is applied are shown in Figure 37 where the same sources are again plotted against the SWS OLP v8.4 data.

As we can see in Figure 37, the improvement is significant in all cases and the level of agreement reached is found to be better than 5-10% in some cases, like in HR 6312 and HR 7310, at all wavelengths.

However, there are still significant discrepancies (of the order of ~20%) which especially affect the two red sources selected for display, AFGL 2999 and S Per, coincident with the strong flux jump produced by the silicate emission detected at 10 μm in these two sources. Since this is the spectral region which in SWS is known to be mostly affected by transients we considered the possibility of this discrepancy being originated by memory effects in band 2 SWS data as a potential explanation for the discrepancies observed.

In order to check for this, we applied the 'dynadark' module, as it is currently implemented in the SWS IA, to correct for memory effects the band 2 SWS spectrum of AFGL 2999, as a test case.

The result obtained after correction, which is expected to be very similar to what it will result from the OLP v9.5 pipeline, is shown in Figure 38 (right panel), together with the original OLP v8.4 data products (left panel). As we can see, the improvement is evident and most of the discrepancy is removed, as expected, reaching a level of agreement better than 10% at most wavelengths.

Considerable discrepancies between SWS and PHT-S data of the order of ~20% are also detected around 10 μm in the spectrum of PV Cep, which is a

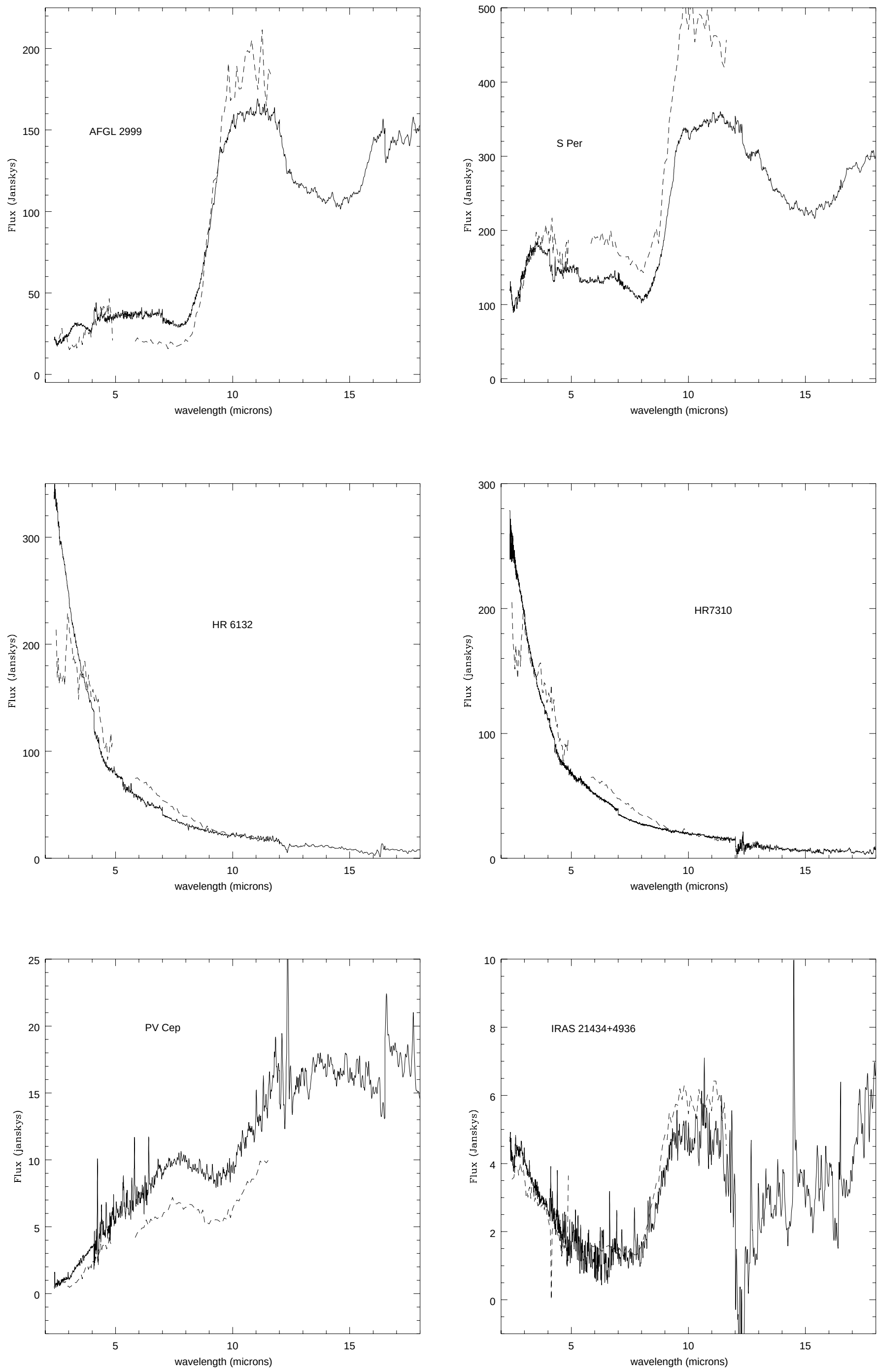

Figure 36: SWS (solid line) versus PHT-S (dashed line) OLP v8.4 spectra of a few sources in the sample retrieved from the ISO Data Archive

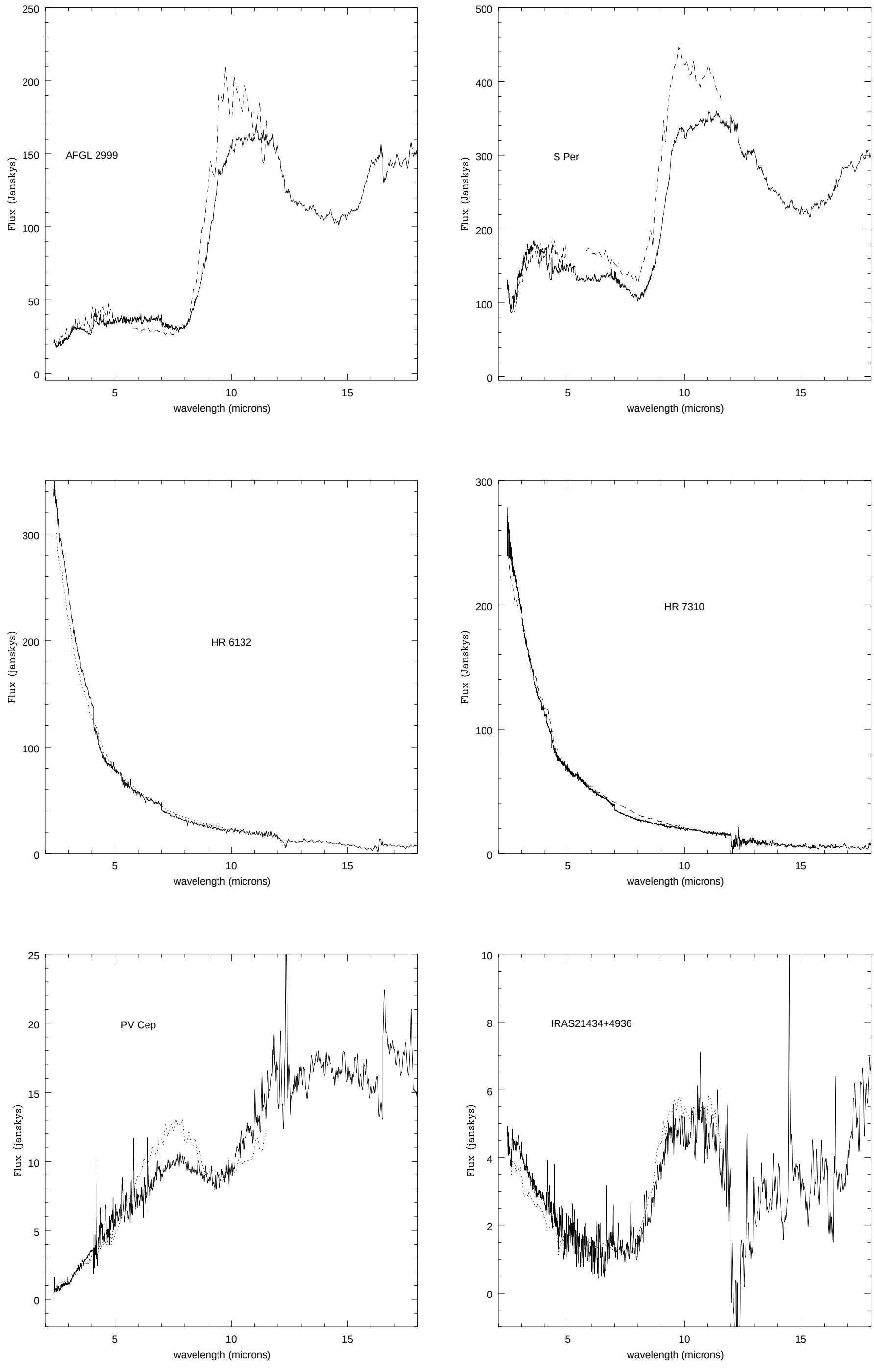

Figure 37: SWS OLP v8.4 data (solid line) versus PHT-S (dashed line) spectra of the same sources once the PHT-S staring spectra have been corrected for transient effects using the dynamic calibration method, as it has been implemented in OLP v9.0

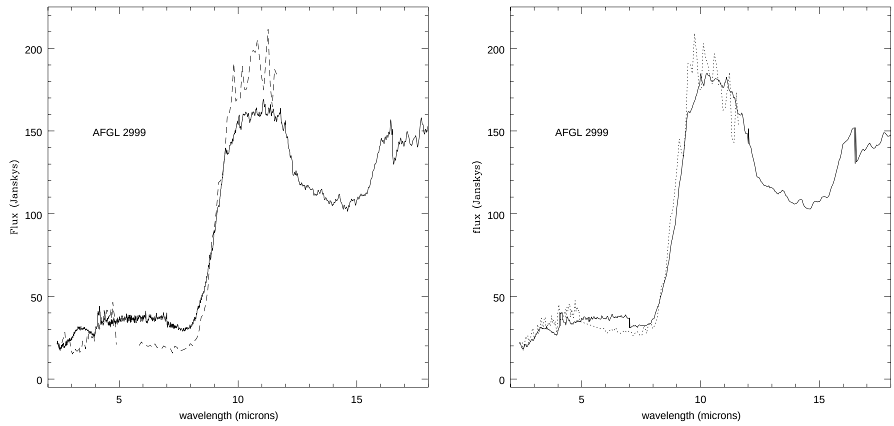

Figure 38: The SWS (solid line) and PHT-S (dashed line) spectra of AFGL 2999 are compared before (left) and after (right) transient corrections are applied both to SWS and PHT-S data (see text for details).

much fainter star, as we can see in Figure 37. This is surprising since for faint sources like PV Cep memory effects are not expected to be strong in SWS band 2 data. For safety, this possibility was checked (and discarded) through the application of the 'dynadark' correction to the SWS spectrum, which did not produce any significant change in its shape (not shown).

In this case, it is possible that the still remaining discrepancies between PHT-S and SWS might be due to the fact that the PHT-S spectrum of PV Cep was slightly overcorrected whith the application of the dynamic calibration method. This is supported by the strong transient correction that was needed, suggesting that the signal was originally far from stabilisation, which always makes the results of the transient correction more uncertain.

Other minor calibration problems are also evident in Figure 37. They consist mainly in small flux jumps observed between bands in some of the SWS spectra there displayed. As we have already mentioned, most of them might be due either to the possibility that the source was observed slightly off-centred or to an incorrect dark current subtraction. In both cases, manual intervention is needed using IA. In the first case, a major improvement has been achieved in the last few months with the availability of the new SWS pointing correction tool which will soon be implemented in OSIA v2.0. With respect to the second problem, it is always possible to try a slightly better dark current subtraction using IA.

The typical effect of an incorrect dark current subtraction appears quite clear in the case of the SWS spectrum of the faint source IRAS 21434+4936, where a strong flux jump is observed between bands 2C and 3A at 12 μm, bringing the flux into negative values at the short wavelength edge of band 3A.

The SWS spectrum of IRAS 21434+4936 was manually processed with IA in order to show how a better dark current subtraction can improve strongly the quality of the data. The resulting SWS spectrum, which has also been corrected for memory effects (with an almost negligible effect) is shown in Figure

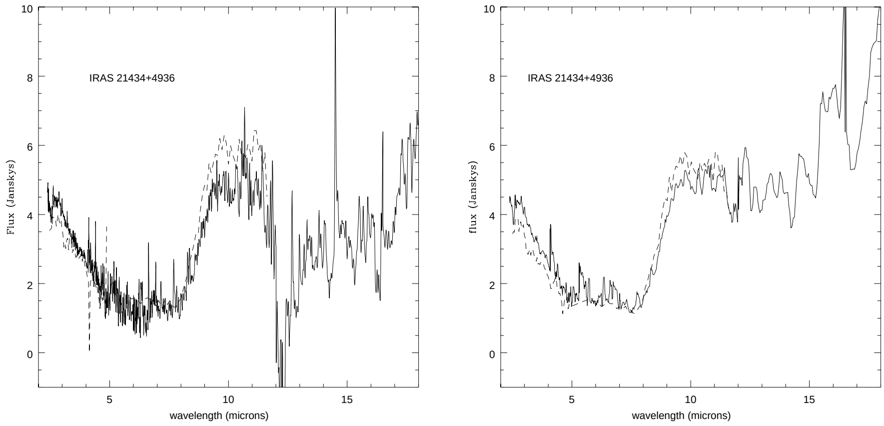

Figure 39: The SWS spectrum (solid line) of IRAS 21434+4936 is compared with the original OLP v8.4 PHT-S spectrum (dashed line) of the same source before (left) and after (right) manual processing of the SWS spectrum with IA, including a better dark current subtraction in band 3A and correction for memory effects in band 2

39 together with the original OLP v8.4 PHT-S spectrum before (left panel) and after manual processing (right panel).

SWS versus CAM-CVF

Figure 40 shows two examples of CAM OLP v8.0 and SWS OLP v8.4 data products as they are retrieved from the ISO Data Archive. They correspond to the bright star HR 7310 and the faint star HD 179218, two sources contained in the cross-calibration sample which are considered to be representative of the general behaviour observed for CAM and SWS OLP v8 data products.

As we can see, there is a general good agreement between SWS and CAM, within the 15% level, both in the overall shape of the spectra and in the absolute flux level, with the exception of the edges of the CAM-CVF scan on HR 7310, which strongly disagree with SWS data, and some small jumps which look like absorption features in the CAM-CVF spectra of both stars. In addition, a small jump between bands 2C and 3A is also observed at 12 μm in the SWS spectrum of HR 7310. It closely resembles the one we have just described in IRAS 21434+4936 and can be attributed to an incorrect dark current subtraction in band 3A by OLP v8.4.

We know that the small jumps observed in the CAM-CVF spectra are quite probably due to the automatic system used by OLP to extract individual CAM-CVF spectra of point sources detected in the field (basically because of an in-

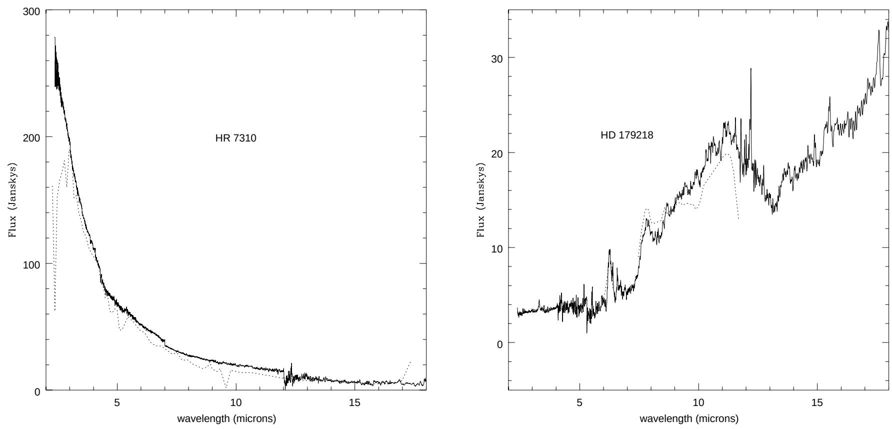

Figure 40: SWS OLP v8.4 (solid line) versus CAM-CVF OLP v8.0 (dotted line) spectra retrieved from the ISO Data Archive of two of the sources in the sample

correct PSF fitting). In order to get rid of these artifacts, for which a solution is planned to be implemented soon with the definition of a new extraction procedure, we performed manual aperture photometry in the CAM-CVF fields with the help of CIA v4.0. This way we were able to obtain a much better agreement with SWS data, as it is shown in Figure 41.

In principle, the SWS spectra are not expected to change significantly in OLP v9.5 with respect to the OLP v8.4 data products plotted in Figure 41 (may be just minor corrections in the spectrum of HR 7310, which is relatively bright, and negligible corrections in HD 179218). Thus, this correction has not been performed.

With respect to the discrepancies still observed at the blue and red ends of the CAM-CVF spectrum of HR 7310, we know that they are probably due to the effect of transients. Unfortunately, there is no transient correction yet implemented in the pipeline, but a correction based on the Fouks-Schubert model is foreseen for implementation in OLP v9.5. This transient correction, however, is in principle only valid for low gradient illumination. Thus, only the photometry of extended sources and of very faint point sources is expected to improve significantly.

In spite of this, and in order to try to simulate the impact that the future implementation of the Fouks-Schubert correction method will have in OLP v9.5 we have used the Fouks-Schubert correction tool available in CIA v4.0, to correct the CAM-CVF spectra of HR 7310 and HD 179218 for transient effects and the results are shown in Figure 42.

As we can see, there is no significant change in the spectrum of HR 7310, which is apparently not affected by this correction, nor even at the edges of the spectrum. This might be just due to the fact that the correction was applied to the data products using CIA and not the pipeline. In CIA the correction is applied to the CVF scan ignoring the previous history of illumination in the detector which will not be the case when the correction will be implemented in

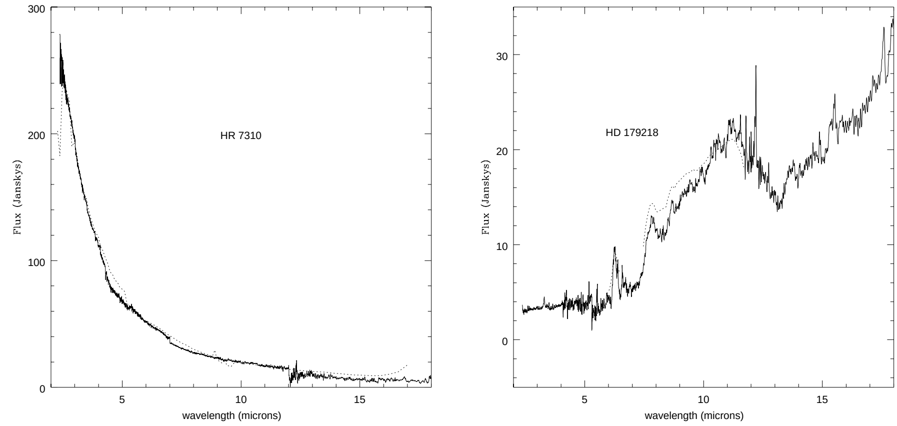

Figure 41: SWS OLP v8.4 (solid line) versus CAM-CVF (dotted line) spectra of the same sources once the CAM-CVF spectra have been extracted using manual aperture photometry with CIA

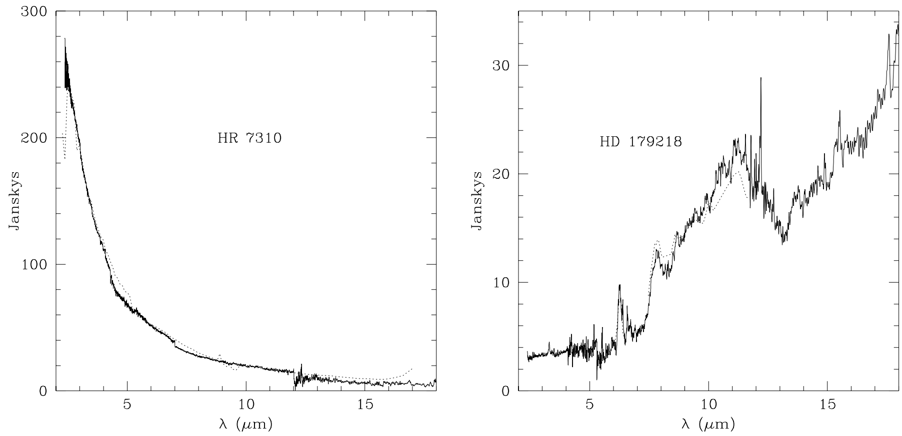

Figure 42: SWS OLP v8.4 (solid line) versus CAM-CVF (dotted line) spectra of the same sources after the CAM-CVF spectra have been corrected for transient effects using the Fouks-Schubert method available in CIA v4.0 (to be implemented in OLP v9.5).

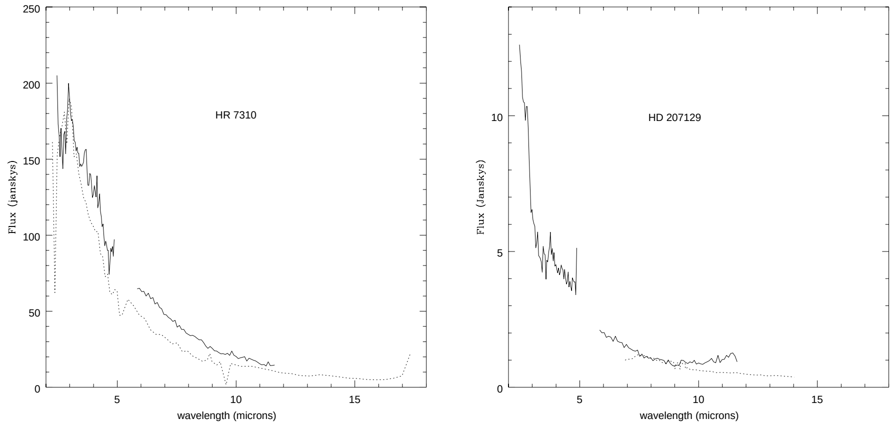

Figure 43: CAM-CVF OLP v8.0 (dotted line) versus PHT-S OLP v8.4 (solid line) OLP v8 spectra of two of the sources in the sample as they were retrieved from the ISO Data Archive

OLP v9.5. In principle, we will need to wait for the real OLP v9.5 data products to check whether our assumption is correct.

However, it is interesting to note the small but significant impact that the Fouks-Schubert correction had on the spectrum of the faint star HD 179218. If we compare the spectrum before and after the correction we can see that the emission features detected at 6.2, 7.7 and 8.6 features appears now sharper and in better agreement with the detections made by SWS. This is a nice example of the kind of improvements that the application of the Fouks-Schubert transient correction might produce in OLP data products.

CAM-CVF versus PHT-S

In Figure 43 we present the OLP v8.0 CAM-CVF and OLP v8.4 PHT-S spectra of two of the sources in the cross-calibration sample as they are retrieved from the ISO Data Archive. They correspond to the bright star HR 7310 and the faint star HD 207129, which have been selected as representative of the general behaviour observed for CAM and PHT data products in OLP v8.

Again, we can see that although a general good agreement in the overall shape exist, there are strong discrepancies in the absolute flux level which can reach more than 20% in some regions of the spectral range.

The discrepancies are partially removed when manual aperture photometry is applied to CAM-CVF data using CIA v4.0 and transients are corrected in PHT-S data using the dynamic calibration method for staring observations in the case of HR7310). Note that the PHT-S observation of HD 207129 was taken in chopping mode and the transient corrections in this case are already included

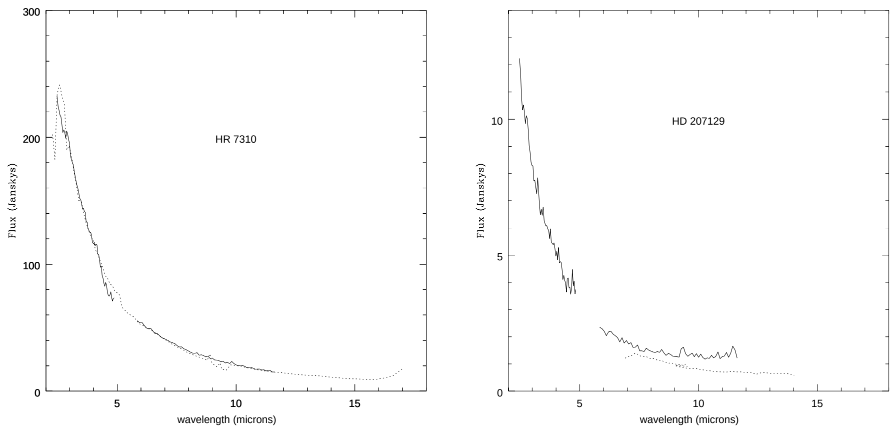

Figure 44: CAM-CVF (dotted line) versus PHT-S (solid line) spectra of the same sources after the Fouks-Schubert correction for transients is applied to the CAM-CVF spectrum, which has been manually extracted and the PHT-S spectrum has been reduced carefully using PIA v8.2

in the OLP v8.4 data products. The CAM-CVF spectra were also corrected for transients using the Fouks-Schubert method as it is implemented in CIA v4.0 but it did not produce any significant change in the spectra.

The results obtained after detailed data reduction (shown in Figure 44) are excellent in the case of HR 7310 in the overlapping region between PHT-S and CAM-CVF, where there is almost a perfect match. Again, however, note the incorrect shape of the CAM-CVF spectrum at the red end due to the transients, which are not removed by the CIA Fouks-Schubert correction.

With respect to HD 207129 the situation is worse. We can see clearly in Figure 43 that the red end of the spectrum looks clearly overcorrected already in OLP v8.4 and the situation does not improve too much in Figure 44 with an alternative data reduction made using PIA v8.2. PHT-S shows a strong discrepancy (more than a 20%) with CAM-CVF in the overlapping spectral region. As for PV Cep, observed in staring mode, the same effect has been detected in other relatively faint sources observed with PHT-S where the stabilization of the signal takes always a longer time and the transient correction needed is very strong.

<u>SWS versus CAM-CVF versus PHT-S</u>

Observations are available from the three instruments for a few sources in the cross-calibration sample. This is the case, for instance, of HR 5999, a star

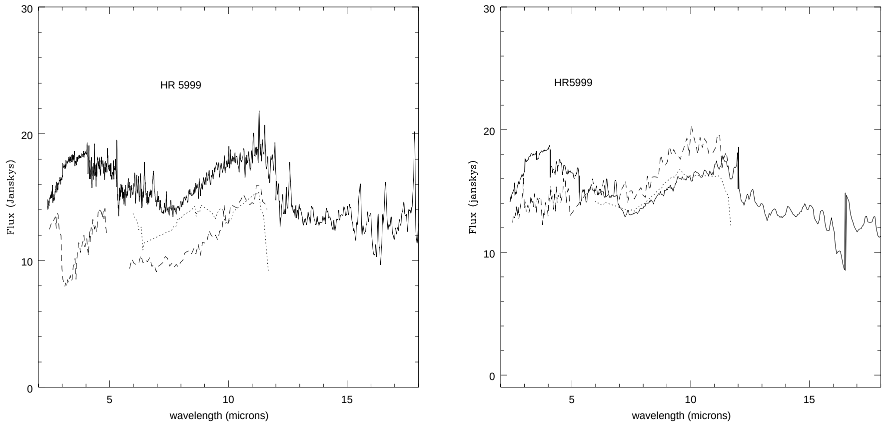

Figure 45: SWS (solid line), CAM-CVF (dotted line) and PHT-S (dashed line) OLP v8 spectra of HR 5999, one of the sources in the cross-calibration sample observed with the three AOTs under analysis, as they are retrieved from the ISO Data Archive (left) and as they will probably look in OLP v9 (right)

which is taken here as a representative case of the improvements expected in future OLP v9 data products with respect to the older OLP v8 version.

Figure 45 shows at the same time the SWS, PHT-S and CAM-CVF OLP v8 spectra of HR 5999 (left) as they are retrieved from the ISO Data Archive together with the results expected in OLP v9. For this we have considered the application of the dynamic calibration method to the PHT-S spectrum (staring), manual extraction and Fouks-Schubert correction for transients in CAM-CVF data and the application of the adapted Fouks-Schubert correction to band2 in the SWS spectrum.

As we can see in Figure 45, the OLP v8 data products showed a strong disagreement. PHT-S shows the usual strong transient effects especially at short wavelengths and they seem to be present also at the edges of the CAM-CVF spectrum. In addition, the SWS spectrum show small mismatches between bands which should be the result either of a bad pointing or an incorrect dark subtraction which significantly affect the shape of the spectrum.

If we now look at the right panel of the same Figure, we can see that a general improvement is observed. It is evident that the dynamic calibration method applied to PHT-S has been able to completely removed the transients and the flux level of CAM-CVF is now in much better agreement with the other instruments. Note that this is basically due to the manual extraction of the spectrum, and not to the Fouks-Schubert correction which has a minor effect on the shape of the spectrum. Unfortunately, the removal of the small jumps observed in the SWS spectrum require a much more detailed data reduction and the effect of the application of the 'dynadark' module in band 2 SWS data at these relatively low flux levels is very small (because the transients are very small).

3.5.2 Cross-calibration of sources observed with IRAS and ISO SWS

In order to make a systematic analysis of the behaviour of SWS data as a function of the characteristics of the objects observed by ISO with this spectrograph, it is useful to compare the results obtained with SWS with those provided by the IRAS satellite.

The use of the IRAS database can be a quite powerful tool for this purpose since a large number of astronomical sources observed with SWS were also detected by IRAS at the 12 and 25 μm bands and included in the IRAS catalogues, either in the Point Source Catalogue, or in the Catalogue of Low Resolution Spectra (LRS, hereafter). The latter contains low resolution spectral information between 8 and 22 μm of an important number (a few thousand) of IRAS sources detected above a certain brightness limit. Note that these LRS spectra were absolutely calibrated in flux by simple scaling the spectrum with the photometric IRAS flux at 12 μm.

With the help of IRAS data we can create a statistically meaningful sample of ISO SWS observations for which there is also spectroscopic and photometric information in the IRAS catalogues. They will be associated to a wide variety of properties ('red' and 'blue' spectra, faint and bright sources, etc.) which constitutes an ideal database for cross-calibration purposes.

In order to compare the absolute flux calibration of IRAS and ISO SWS we took the full list of sources contained in the IRAS LRS Catalogue (5425 sources) and searched the ISO Data Archive for observations made with ISO at the same positions of the sky allowing for a maximum offset of $1.5'$.

This way, we found 556 different pointings in the ISO Data Archive containing SWS01 observations corresponding to around 400 different sources.

Some of them, unfortunately, cannot be used for this cross-calibration analysis, because they are extended sources for which a direct cross-calibration between the SWS flux and the IRAS photometry cannot be made since the SWS calibration is based on point source flux calibration. In addition, many of these extended sources are usually located in areas of the sky with a complex structure at 12 and 25 μm, which complicates even more the problem.

Sources which look extended to SWS are easily recognised because the spectra show strong flux jumps between bands coincident with changes in the aperture size. A good example of this is shown in Figure 46.

Another factor which has to be taken into account in this cross-calibration analysis is the intrinsic variability of many of the sources contained in the sample. As we have already mentioned in this document, we know that many of the stars observed by ISO are characterised by their strong variability. They are known to be pulsating stars in the Asymptotic Giant Branch (AGB) phase evolving into planetary nebulae. In some cases, also some young stellar objects might be found variable but usually the amplitude of the variations in this spectral range is not very large. In principle, we only removed from the working sample variable AGB stars well recognized as such in the literature.

This way, we end up with a list of more than 250 sources. Each of these 250

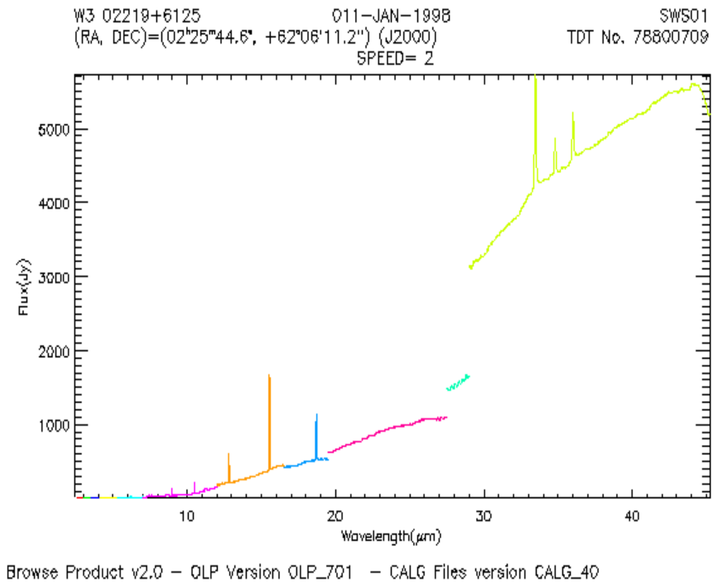

Figure 46: Example of the discontinuities observed in one of the extended sources included in the sample. Jumps between bands in the SWS range are coincident with changes in the aperture size - Pedro García-Lario

individual spectra are now being further processed with ISAPv2.0. Basically, bad data points affected by glitches are identified and removed from the spectra using the available tools in ISAP and what we can call 'ISO SWS photometry' is performed at 12 and 25 μm with the help of the 'syn_phot' application in ISAP, which simply convolves the ISO spectrum with the transmission profile of the IRAS filters at 12 and 25 μm and assigns a monochromatic flux at these two wavelengths under the assumption that the source SED shape is of the form $\nu \times f_\nu$ = constant, or equivalently $\lambda \times f_\lambda$ = constant, in the same way as IRAS did.

In Figure 47 we show the preliminary results obtained from this study at 12 μm for part of the sources in the sample (still work is on-going). Figure 48 shows the results for the same subset of sources at 25 μm.

Although the plots are still preliminary they already give a feeling of the consistency of ISO data with IRAS results.

As we can see in Figure 47, the first conclusion that we can extract from our analysis is that there is a clear systematic underestimation of the ISO fluxes at 12 μm with respect to the IRAS photometry at the same wavelength. ISO synthetic photometry at 12 μm is found to provide fluxes which are typically 14% fainter than IRAS. After correcting for this effect of yet unknown origin there is a very good agreement in the majority of cases between the IRAS photometry and ISO. The agreement is found to be quite good (within the 10-15% level typically) for strong sources (above 50 Jy), although it becomes worse for low flux levels (typically within the 30-40% level for fluxes below 30 Jy).

A similar behaviour is observed at 25 μm in Figure 48. ISO fluxes at 25 μm appear also systematically underestimated with respect to the IRAS photometry at the same wavelength although this time the effect is not so strong. ISO synthetic photometry at 25 μm provides fluxes which are in the mean 9% fainter than IRAS. After this systematic effect is removed, we find a good agreement again between ISO data and IRAS (within the 10-15% level) for strong sources (¿25 Jy) which becomes a bit worse for fainter objects (typically within the 20-30% level).

When comparing ISO data with IRAS photometry one should be aware that the calibration of the two instruments is based on different absolute photometric references. Especially at the shorter IR wavelengths (λ ¡ 25 μm) the ISO system is mainly based on stellar calibrators for which the fluxes are tied to the Walker and Cohen (1992 NASA CR177604, NAS2-13327) system, which does not completely match the IRAS system. After analysis of a set of IRAS calibration stars, as listed in the IRAS Point Source Catalogue, Walker and Cohen found that the ratio between their zero magnitudes and those of IRAS are:

$$\mathrm{R}(12,25,60,100) = (0.978,0.936,0.921,0.896)$$

Consequently, if we use Walker and Cohen calibration at any of the IRAS wavelengths, our values would be expected to be systematically lower than the IRAS values by 2.2, 6.4, 7.9 and 10.4%.

At 25 μm the expected discrepancy (6.4%) is not too different from that derived from our results (around 9%). This would be more or less consistent with Walker and Cohen's predictions. But at 12 μm we only expect an underestimation of about 2% while we clearly detect a much stronger discrepancy.

Note also that some of the strongly discrepant cases observed both at 12 μm and 25 μm have been investigated further finding that they are the result of bad pointed observations and will be removed from the sample.

This can sometimes be checked through the comparison of the SWS spectroscopy with data taken with the same instrument by a different observer with a slightly different pointing or through the comparison with observations taken by other ISO instruments like PHT-S and CAM-CVF.

Usually SWS observations affected by a pointing problem are easy to recognize because the show characteristic flux jumps between bands which are not correlated with the different sizes of the SWS apertures (as it should happen if the reason for the jumps could be attributed to the extended nature of the source). In Figure 49 a typical example of a bad pointed observation is shown.

However, a systematic bad pointing effect would affect in the same way the data obtained at 12 and at 25 μm, something which is not observed. Whatever the origin of the 14% discrepancy observed at 12 μm could be, it is clear that it affects more strongly the ISO data obtained at 12 μm.

A possibility exists that the discrepancies observed at 12 μm could be due to the transient effects in band 2 ISO data which are not yet corrected for in OLP v8.4. This in principle could affect strongly the ISO synthetic photometry at

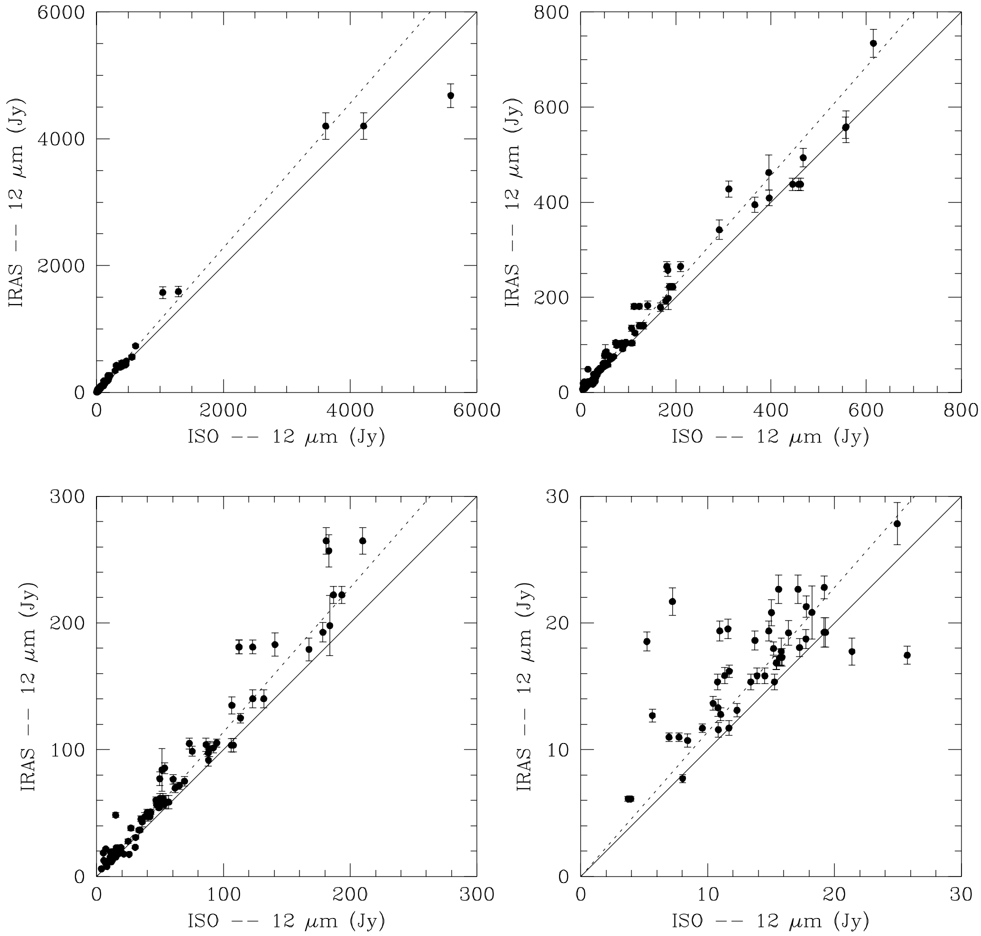

Figure 47: ISO SWS synthetic photometry at 12 μm compared to IRAS photometry at the same wavelength. The dashed red line represents a 14% systematic underestimation of the ISO fluxes with respect to IRAS (see text for details) - Pedro García-Lario

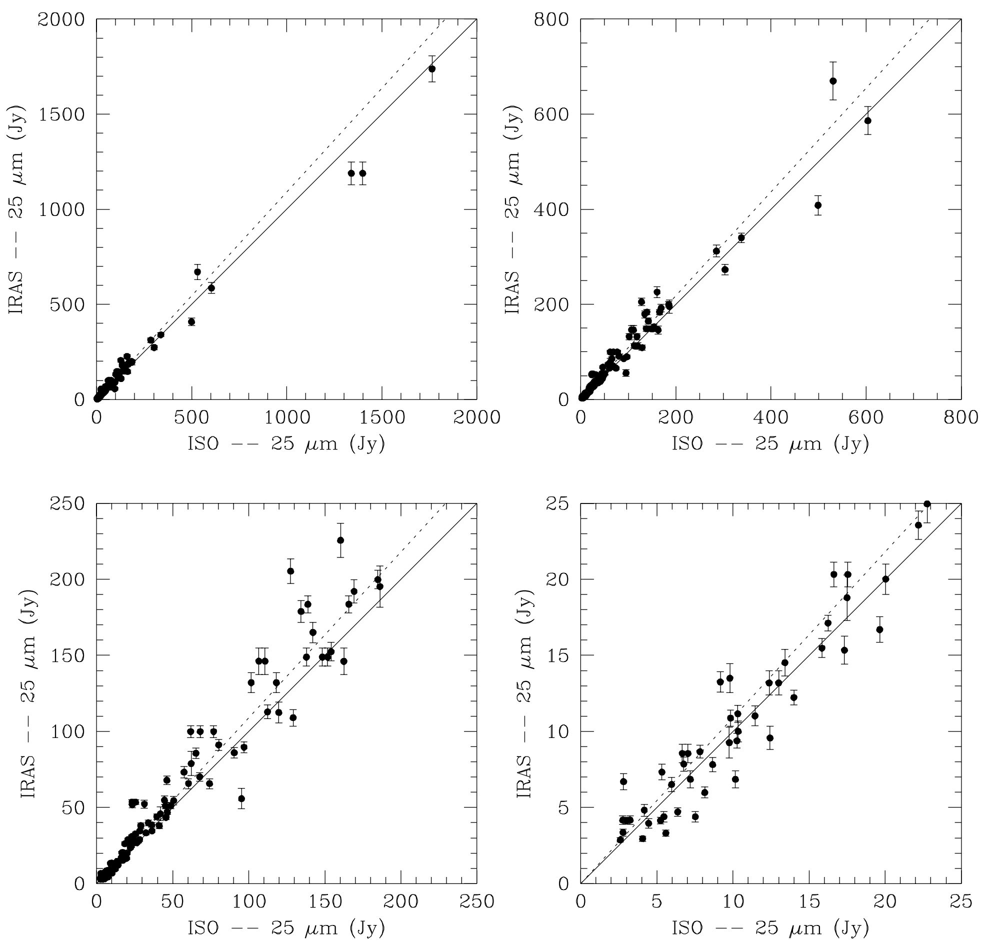

Figure 48: ISO SWS synthetic photometry at 25 μm compared to IRAS photometry at the same wavelength. The dashed red line represents a 9% systematic underestimation of the ISO fluxes with respect to IRAS - Pedro García-Lario

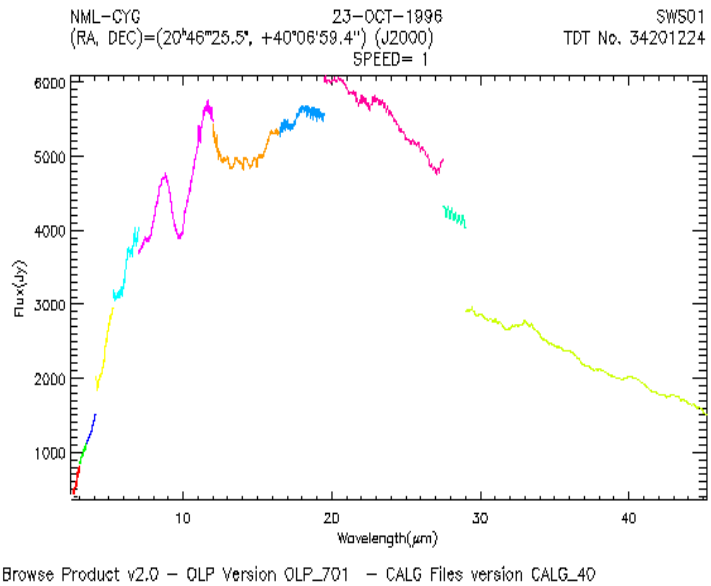

Figure 49: Example of the discontinuities observed in one of the bad pointed sources included in the sample. Jumps between bands are not correlated with the aperture size - Pedro García-Lario

12 μm. Unfortunately, we will have to wait until the new data products (OLP v9.5) are available to check this hypothesis.

A similar cross-calibration work will be started soon using the same database of IRAS LRS spectra for comparison with ISO PHT-S spectra. A preliminary search show that there are 232 PHT-S spectra in the ISO Data Archive which can be identified with sources included in the IRAS LRS Catalogue. The intention is to extend the analysis in the future also to CAM-CVF data.

3.5.3 Cross-calibration of sources observed with IRAS and ISO LWS

Josephine Chan, in collaboration with Bruce Swinyard, is carrying out a similar analysis considering a database of sources observed with ISO LWS for which there is available IRAS photometry at 60 μm and 100 μm.

The goal is also to make a systematic study of the behaviour of ISO-LWS data under different conditions as a function of the type of object observed (bright/faint, blue/red, point/extended,...) by determining the consistency with IRAS data in each case.

Again, the starting point is the construction of a statistically meaningful sample. There are 2322 LWS01 grating observations in the ISO Data Archive corresponding to almost 500 different objects.

In order to compare the absolute flux calibration of IRAS and ISO LWS we took these almost 500 different pointings for which LWS01 spectra are available in the ISO Data Archive and searched the IRAS Point Source Catalogue for counterparts based on the following criteria:

1. Search radius: $2'$;
2. IRAS flux density qualities ≥ 2 in the 60 and 100 μm bands;
3. $F_\nu(100\mu m) < 1000$ Jy
4. $F_c/F_s < 1$ where F_c/F_s is the flux ratio of cirrus and source
5. source is not far-infrared variable

This way a total number of around 170 common pointings between ISO LWS and IRAS were found to be susceptible to be included in this cross-calibration analysis.

As a second step, the ISO Spectral Analysis Package (ISAP) is being used for the spectral analysis of the selected LWS01 spectra. Three main applications 'zip','average' and 'syn_phot' are heavily being used for processing the AAR LWS data. The 'ISO LWS photometry', equivalent to the IRAS photometry at 60 and 100 μm, of these sources is obtained simply by convolving the ISO spectrum with the transmission profile of the IRAS filters at 60 and 100 μm using the 'syn_phot' application again assigning a monochromatic flux at these two wavelengths under the assumption that the source SED shape is of the form $\nu \times f_\nu$ = constant, or equivalently $\lambda \times f_\lambda$ = constant.

In order to compare these results with the IRAS photometry it is important to take into account that at 100 μm the infrared sky is characterized by emission from interstellar dust on all spatial scales which is expected to significantly contribute in many cases to the flux detected at this wavelength. While the IRAS photometric fluxes quoted in the PSC are already corrected for this background 'cirrus' emission, the photometry derived from LWS data contains also this background contribution. Therefore, it is necessary to recover the uncorrected CIRRUS flux at 100 μm from the original information contained in the IRAS PSC and derive the uncorrected IRAS flux at 100 μm if we want to compare ISO with LWS data. This can be estimated from the CIRR2 parameter, which is directly related via an analytical expression to the value of F_c/F_s.

The preliminary results are still under analysis but we can already conclude that the agreement between ISO LWS and IRAS is reasonably good (typically within the 20% level) for a wide range of flux levels.

3.5.4 ISOPHOT-P and -C versus IRAS at 25 and 60 μm

The database of ISO observations generated by the Vega project, intended to search for Vega-like debris disks around nearby main-sequence stars, have also been used to assess the quality of ISOPHOT photometric calibration.

The sample contains more than 80 main sequence stars that were observed with ISOPHOT at 25, 60, 150 and 170 μm, in order to determine whether the star had an infrared excess indicating the presence of a dusty disk. Unfortunately, the number of stars found with disks is very low: only 8 out of 65 stars showed a significant excess at 60 μm.

The positive point, from our cross-calibration perspective, is that the non-detected stars constitute a nice homogeneous sample of observations which can be used to improve our knowledge of the quality of the observations made with ISOPHOT by comparing the observations with models and with previous IRAS photometry of the same sources at 25 μm at 60 μm.

The subsample of observations here analysed were made using the AOT PHT03 (PHT-P detectors) in triangular chopped mode at 25 μm and mini-maps (3$\times$3 with 46$''$ steps) centred at the source location at 60 μm using the AOT PHT22.

In Figures 50 and 51 we show the result of the ISO observations compared to the IRAS photometry (when available) of the same stars at 25 and 60 μm. As we can see, the level of agreement with IRAS photometry at 25 μm is in most cases better than 25%. The brighter targets ($F_{25} > 1$ Jy) appear to have systematically lower ISO flux densities. This underestimate is expected from the usage of the chopped mode where a relatively high source-background contrast causes a signal loss due to transient responsivity in the PHT-P detector. On the other hand, the fainter stars ($F_{25} < 300$ mJy) are overestimated. It is still not clear what the explanation is for this overestimation but it might be the result of (i) the transient behaviour of the P2 detector, (2) a low level signal non-linearity, or (3) peculiarities in the IRAS calibration.

At 60 μm the statistics become poorer. IRAS fluxes are available only for 11 targets. The obvious outlier showing $F_{60,IRAS} >> F_{60,ISO}$ appears to consist of 3 resolved point sources in the ISOPHOT map. For the remaining detections the correlation is high. However, the ISO observations are systematically (to 25%) below the IRAS values. For the brighter sources the discrepancy can be attributed to the fact that we have assumed point source calibration in the conversion from measured flux in an array pixel to the final target flux. In case of small extended sources - like Vega and β-Pictoris which are contained in the sample - the flux is underestimated.

The same data set can be compared to the infrared fluxes predicted at 60 μm by fitting Kurucz models to Geneva photometry previously obtained in the optical for the sources in the sample. The results are shown in Figure 52, where we can see that at the fainter end of the 60 μm data the ISO detections appear to be systematically brighter than the predictions, even for high S/N detections. Taking the result from the comparison with IRAS data into account, we infer that the extrapolation introduces a systematic underestimate of the photospheric flux.

As we have seen with this example, the validation of chopped photometry calibration is not yet succesful over a sufficiently large flux range for all ISOPHOT-P and -C detectors. However, the signal processing could be considerably improved by introducing the chopped pattern, a concept on which further improvements of the photometric calibration will built up. First refinements will be implemented for OLP v9.0; the final calibration method can, however, only

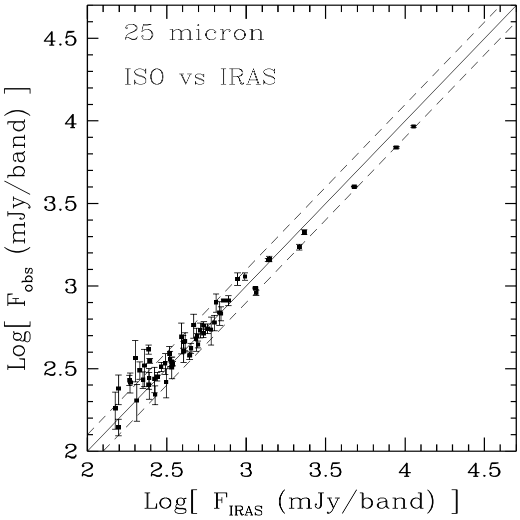

Figure 50: The 25 μm flux densities obtained with ISO chopped PHT-P observations for 80 main sequence stars included in the Vega project are compared to IRAS photometry - Rene Laureijs et al.

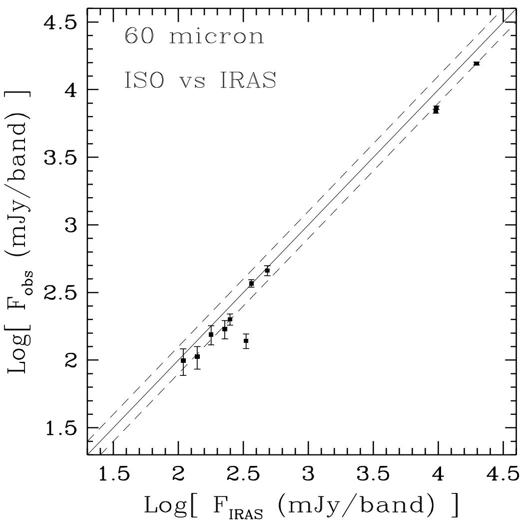

Figure 51: The 60 μm flux densities obtained with ISO chopped PHT-C observations for 80 main sequence stars included in the Vega project are compared to IRAS photometry - Rene Laureijs et al.

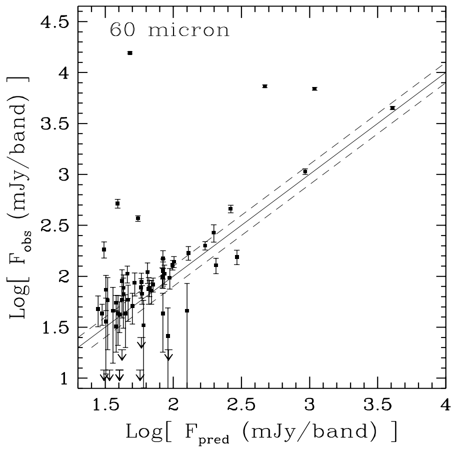

Figure 52: Predicted photospheric flux versus ISO PHT-C observations at 60 μm of the stars in the Vega project - Rene Laureijs et al.

be expected for OLP v10.0 (release expected in February 2001).

The full report on this cross-calibration analysis can be found in the document "A systematic search of Vega-like stars with ISO" by Rene Laureijs et al. (1999, Proc. of 'Astrophysics with Infrared Surveys: A Prelude to SIRTF', Asp. Conf. Series, v. 177),

3.5.5 ISO LWS raster scans versus IRAS photometry at 100 μm

LWS observations have been made at a number of positions in the Trumpler 14 and 16 fields and these have been compared with the IRAS 100μm fluxes at the same positions. Both fields contain a large area of extended emission, which although relatively smooth, does change by a factor of 2 - 3 within each region.

The point source fluxes (Jy) provided by the current LWS calibration have been converted to extended source fluxes (GJy sr^{-1}) using the correction factors recently derived by Chris Lloyd and implemented in ISAP v2.0.

Figure 53 shows the comparison of the converted LWS and IRAS 100 μm fluxes. As we can see, the results indicate that there is an excellent agreement between the fluxes provided by ISO and the IRAS results. From the analysis of the data we obtain a mean ratio, LWS/IRAS = 0.90$\pm$0.2.

Ideally, for this comparison the extended flux should be distributed as evenly as possible, and part of the uncertainty is probably due to unresolved structure within the beam.

These corrections have been derived under the assumption of a smooth and very extended flux distribution. In the real world, structure or embedded sources

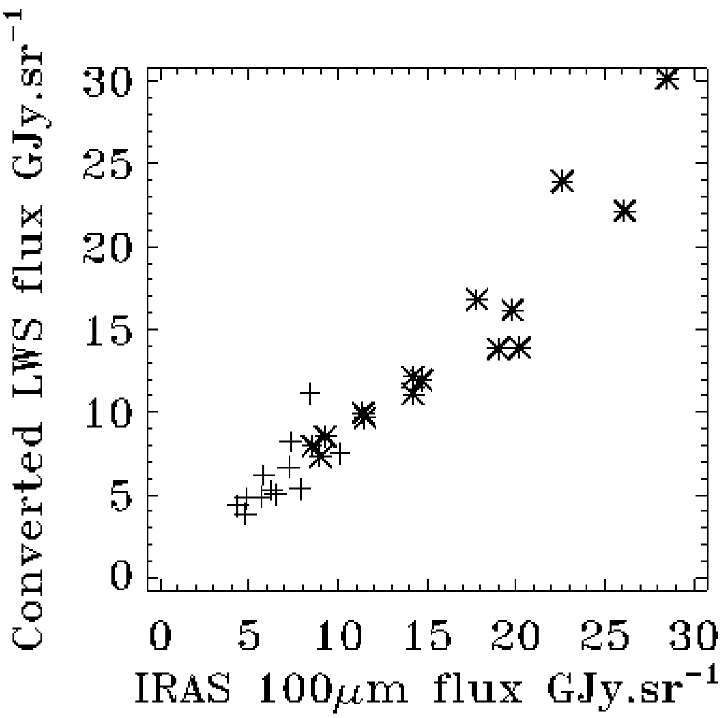

Figure 53: Comparison of converted (GJy sr^{-1}) LWS and IRAS 100 μm extended source fluxes in the Trumpler 14 (+) and 16 (*) fields - Martin Burgdorf

could produce significant discrepancies from the ideal situation and, with it, differences in flux.

Note also that for fields containing multiple sources the observed flux will depend critically on the precise positions of the sources relative to the optical axis. To recover or model the observed flux will require positional information on the sources and a deconvolution with the PSF and instrumental profile. Indeed, for single point sources observed off axis a similar procedure will be required to recover the correct flux.

3.5.6 ISOPHOT versus COBE/DIRBE

The comparison of ISOPHOT data with COBE/DIRBE results is complicated by the vastly different beam sizes (42' FWHM for COBE/DIRBE). As part of the scientific validation of OLP v8.4 ISOPHOT pipeline, several cross-calibration comparisons with COBE/DIRBE were made by Ulrich Klaas. Some of them are described below.

The details of this cross-calibration analysis can be found in te "Report on the PHT Scientific Validation for OLP Vesrion 8.4" by Ulrich Klaas et al., available at:

`http://iso.www.vilspa.esa.es/users/expl_lib/PHT/phtolp84_scivalrep_v2.ps.gz`

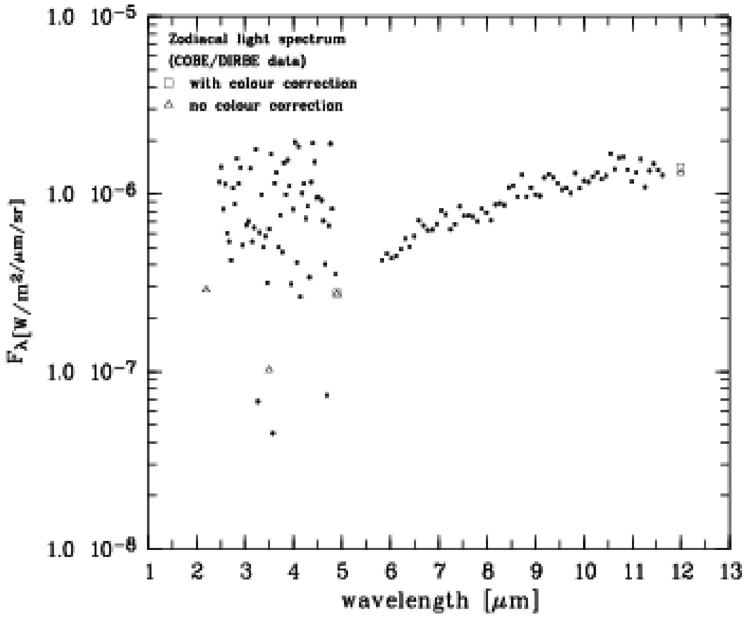

Figure 54: Comparison of the PHT-S spectrum of the Zodiacal light at a position of the ecliptic plane located at a minimum ecliptic longitude of 66 degrees (close to the ISO Sun constraint) with COBE/DIRBE photometry at 4.9 and 12 μm. For colour correction of the COBE/DIRBE data points a 260 K black body has been assumed - K. Wilke + U. Klaas

Absolute Surface Brightness spectrum of the Zodiacal light:

For many types of ISOPHOT observations knowledge of the emission contribution from the Zodiacal dust cloud is necessary. In particular the background in PHT-S was estimated from modelling Zodiacal Light (which is the dominating background at the PHT-S wavelengths) with an emission component (blackbody of T=267 K) plus a reflection component (BB of T=6000K). The relative scaling of the two components was done using COBE/DIRBE weekly averaged measurements at bands matching the PHT-S wavelengths.

In order to check the consistency between the absolute flux calibration of COBE and PHT-S, the extended source spectrum of the plain Zodiacal light background from a position in the ecliptic plane located at an ecliptic longitude of 66 degrees was compared by K. Wilke and U. Klaas against the COBE/DIRBE photometric data at 4.9 and 12 μm, as there should be no impact by the very different beam sizes.

Figure 54 shows this ISOPHOT-S spectrum. For the short wavelength channel the detection limit is reached and the extremely low flux in the cosmological window is not measurable with the comparably small aperture of PHT-S. The long wavelength channel shows a well detected flux over the full wavelength range. This is a measurement of one of the faintest sources (4 10^{-7} W m^{-2} μm^{-1} sr^{-1} at 5.8 μm corresponds to 4.5 MJy sr^{-1}) performed with PHT-S. We see that the PHT-S spectrum fits nicely between the COBE/DIRBE photometric data points at 4.9 and 12 μm.

Unfortunately, COBE did not cover wavelengths in between 5 and 12 μm, in the range where the brightness of the zodiacal light rises very steeply. The results obtained with PHT-S, PHT-P and ISOCAM suggest that the zodiacal emission spectrum can be well approximated by a blackbody of 267 K. ISOCAM CVF and ISOPHOT-S measurements suggest that the spectrum is featureless between 5 and 16 μm.

Absolute Surface Brightness values of C100 maps:

As part of the scientific validation of staring raster maps the consistency of the absolute sky brightness derived from ISO C100 maps with COBE/DIRBE was also verified by Ulrich Klaas covering a wide range in flux.

The mean surface brightness was derived from the full C100 maps used for the flat-field assessment and compared with the surface brightness values in the corresponding filters or adjacent filters of COBE/DIRBE. The use of the full area of the ISOPHOT maps offer the advantage to get a comparable solid angle coverage with the COBE/DIRBE pixels. However, in most cases the solid angles of the ISOPHOT maps are still considerably smaller than one pixel in COBE/DIRBE. The COBE/DIRBE annual maps were considered (since at the wavelengths considered the contribution from the zodiacal light is very small) to determine the fluxes for the DIRBE pixel coincident with the map area centroid. For a check of the large scale variations of the sky background average fluxes of a 1.5 deg circular area were as well determined. ISOPHOT maps containing bright sources were not considered (they would give a considerably higher average surface brightness due to the smaller area considered).

In Table 1 we present the results obtained. Except for the different beam sizes a comparison of the ISOPHOT/DIRBE 60 and 100 μm filters is relatively straightforward. In general a good agreement better than 25%, in particular for those maps with comparable sizes to the COBE/DIRBE beam, is found. All larger deviations can be explained by the source structure which is extended over the ISOPHOT map area, but compact inside the COBE/DIRBE beam. The largest outlier shows a similar excess in the C200 ranges.

Without any correction, the ISOPHOT 90 μm filter maps seem to show a systematic positive surface brightness excess with regard to the DIRBE 100 μm photometry. However, inspection of the COBE/DIRBE SEDs indicates a steep decline in flux between 60 and 100 μm. In fact, the 90 μm ISOPHOT values are practically always in between the 60 and 100 μm DIRBE values. Very often, the surface brightness ration 60/100 is about 2, i.e. with a linear interpolation between 60 and 100 μm, the 90 μm flux is by 25% higher than the 100 μm flux due to the shape of the SED. Then, also the 90 μm map surface brightnesses are consistent with COBE/DIRBE within better than 25%. If the discrepancy between the ISOPHOT 90 μm surface brightness and the DIRBE 100 μm surface brightness is small, usually the source SED is reasonably flat between 60 and 100 μm. Whether there is still a positive excess at 90 μm cannot be solved by this kind of study, but needs better matching area and a proper colour correction of the background SEDs.

From the consistency found in the three filters at 60, 90 and 100 μm and the relative photometric accuracies of all ISOPHOT C100 filters, we conclude that the consistency should also hold for the remaining ISOPHOT filters at 65, 80 and 105 μm. The good correspondance holds for the flux range 4.5 to 400 MJy sr^{-1}.

Absolute Surface Brightness values of C200 maps:

A similar analysis was also performed by Ulrich Klaas for C200 maps. Since the longest COBE/DIRBE filters (140 and 240 μm) have an internal uncertainty of 20 to 30%, for a subsample of maps with low dynamic range the average fluxes of a 1.5 deg circular area were used, which gives a more robust photometry (this means averaging over 70 COBE/DIRBE pixels).

In Table 2 we present the results of the comparison. No colour correction with regard to a modified blackbody describing the background spectral energy distribution nor a wavelength correction to better match the COBE/DIRBE filter central wavelength with the ISOPHOT filter central wavelength were performed. Again we have to remark that nearly all the ISOPHOT maps are considerably smaller in area than the solid angle of one COBE/DIRBE pixel. Therefore, structures in the source or background can affect the resulting absolute flux. In case of a flat field, the flux of the centred COBE/DIRBE pixel as well as the 3 deg circular area average is listed to give an impression of the variation of the background (and also the stability of the COBE/DIRBE measurement in one pixel). If the map contains a bright target and is smaller than the COBE/DIRBE pixel, then only the flux of the centred COBE/DIRBE pixel is given.

Taking into account the discrepancies in beam size and the non-correction for different wavelengths of filters and background SEDs, the general agreement is in the order of 20 to 30% at all four filters considered (150, 170, 180 and 200 μm). Restricting the comparison to ISOPHOT maps with comparable solid angles with the COBE/DIRBE measurement, the consistency is confirmed to be better than 25%. This holds for all filters and a surface brightness range between 2.5 and 600 MJy sr^{-1}.

Larger deviations between the average ISOPHOT map flux and the COBE/ DIRBE flux only occur for bright central sources which are compact in comparison with the COBE/DIRBE beam. In these cases, the COBE/DIRBE fluxes are always less than the ISOPHOT fluxes, as expected.

Table 1: Consistency check of C100 map absolute surface brightness with COBE/DIRBE annual map photometry. The solid angle of one COBE/DIRBE pixel is 19.5 10^{-5} sr. No correction for the wavelength shift between ISOPHOT 90 μm and DIRBE 100 μm filters has been performed which causes for most sky backgrounds a systematic positive excess of the 90 μm flux (see text for details).

OLP product name	filter (μm)	surface brightness (MJysr^{-1})	solid angle (10^{-5}sr)	DIRBE flux (MJysr^{-1})	DIRBE filter (μm)	solid angle (10^{-5}sr)	consistency (%)
19002101	60	6.8	0.81	6.6	60	19.5	+2.2
08900102	60	9.5	1.60	6.5	60	19.5	+47
85001219	60	22.8	0.21	22.3	60	19.5	+2.2
13400214	60	39.8	0.22	39.6	60	19.5	+0.6
68300807	60	21.3	6.77	27.2	60	19.5	−22
84403913	60	23.9	1.04	24.5	60	19.5	−2.5
69801101	60	107.4	1.16	122.3	60	19.5	−12
35100809	90	5.1	5.49	3.3	100	19.5	+55
58200903	90	11.8	3.06	12.9	100	19.5	−7.9
19201091	90	4.8	7.30	3.1	100	19.5	+52
86901244	90	5.2	2.75	3.6	100	19.5	+44
41502788	90	8.1	5.10	5.7	100	19.5	+44
09000606	90	11.8	0.77	11.3	100	19.5	+4.4
08901904	90	15.1	0.23	13.6	100	19.5	+11
40100614	90	14.7	6.80	13.3	100	19.5	+10
87001338	90	5.3	2.93	3.6	100	19.5	+47
57501902	90	12.1	1.15	9.7	100	19.5	+25
53700514	90	4.4	0.85	3.7	100	19.5	+21
60002009	90	7.1	4.24	5.2	100	19.5	+37
50000124	90	4.8	8.87	3.3	100	19.5	+43
50100273	90	5.8	8.68	3.5	100	19.5	+68
20701079	90	25.6	0.33	22.8	100	19.5	+12
20800709	90	5.8	3.49	4.0	100	19.5	+46
86800640	90	5.7	2.96	3.6	100	19.5	+60
10101158	100	30.7	1.71	21.0	100	19.5	+46
79401149	100	44.2	0.51	40.6	100	19.5	+9.0
44900714	100	387.7	15.2	440.1	100	19.5	−12
15601578	100	17.4	1.82	6.1	100	19.5	+187
27600420	100	15.4	1.74	12.1	100	19.5	+27
71901220	100	18.5	3.66	16.0	100	19.5	+15
33401134	100	96.4	4.06	49.3	100	19.5	+96

Table 2: Consistency check of C200 map absolute surface brightness with COBE/DIRBE annual map photometry. The solid angle of one COBE/DIRBE pixel is 19.5 10^{-5} sr (see text for details).

OLP product name	filter (μm)	surface brightness (MJysr^{-1})	solid angle (10^{-5}sr)	DIRBE flux (MJysr^{-1})	DIRBE filter (μm)	solid angle (10^{-5}sr)	consistency (%)
56200110	150	3.6	2.91	4.1	140	19.5	−13
56201814	150	22.2	0.42	20.9	140	19.5	+6.2
08900103	150	5.5	1.26	7.7	140	19.5	−29
179400434	170	3.2	3.15	2.2	140	19.5	+45
				2.9	140	215.3	+10
59300101	170	3.5	6.53	3.5	140	19.5	−1.4
				3.4	140	215.3	+4.2
19800208	170	3.2	3.41	5.0	140	19.5	−37
				3.3	140	215.3	−3.6
210001305	170	3.6	3.39	4.1	140	19.5	−12
				3.5	140	215.3	+3.4
79900733	170	6.0	0.50	7.0	140	19.5	−14
33600108	180	2.7	2.50	2.7	140	19.5	−2.6
				2.8	140	215.3	−4.0
33600705	180	4.7	2.55	5.7	140	19.5	−17
				5.7	140	215.3	−17
35100907	180	4.1	4.92	4.5	140	19.5	−8.2
16701206	180	15.0	4.11	12.7	140	19.5	+18
152700412	180	3.2	0.87	3.8	140	19.5	−16
				3.2	140	215.3	+0
85001037	180	8.1	3.78	10.1	140	19.5	−19
				9.3	140	215.3	−13
78200101	200	6.3	28.40	5.3	240	34.45	+20
36803005	200	14.8	0.71	15.5	240	19.5	−4.5
				14.9	240	215.3	−0.9
39602213	200	36.2	6.22	29.2	240	19.5	+24
26101401	200	69.8	11.03	85.4	240	19.5	−18
33401133	200	138.6	3.89	87.6	240	19.5	+58
86101801	200	251.9	5.01	287.9	240	19.5	−13
15601577	200	11.4	1.38	5.9	240	19.5	+95
33300559	200	38.0	6.55	55.7	240	19.5	−32
10101157	200	69.7	1.41	45.2	240	19.5	+54
31000625	200	345.4	1.45	207.8	240	19.5	+66
26701013	200	593.3	15.49	494.5	240	19.5	+20
40900802	200	6.9	1.97	5.6	240	19.5	+23
28001303	200	13.0	2.00	12.8	240	19.5	+1.6

3.5.7 ISO SWS versus other ground-based or space facilities

ISO SWS01 and SWS06 observations of a number of proto-planetary nebulae (PPNe) have recently been analysed and compared with results obtained on the same set of targets with IRAS, KAO and UKIRT by Hrivnak et al. (2000, ApJ 535, 275).

The SWS01 observations were carried out in a variety of scan speeds covering the full spectral range from 2.4 to 45 μm. Some of the sources were observed also in the SWS06 mode between 16.5 and 24 μm in order to detect the presence and study in more detail (higher spectral resolution) the still unidentified 21 μm feature usually associated to stars in this short evolutionary stage.

The SWS01 data reduction was carried out using OLP v7 of the standard pipeline processing. Further manual processing was performed also with ISAP v1.6. Basically, bad data points were removed, and the full set of data values was averaged to produce the final spectra with a uniform wavelength spacing in bands 1 to 3D and in bands 3E and 4. Band 4 was found severely affected by glitches, and it was not always possible to remove them in a satisfactory manner (a lower resolution was selected in these cases to plot the data).

In most cases the SWS01 data had strong problems in band 3E (27.5−29.0 μm), which is known to be subject to more noise.

In order to assess the flux calibration carried out this way the ISO spectra were compared to previously existing data on the same sources from IRAS (LRS spectra), ground-based (UKIRT CGS3 observations) and Kuiper Airborne Observatory (KAO) observations.

The IRAS LRS spectra were taken from the IRAS database at Calgary (note that they were flux calibrated against the 12μm flux IRAS photometry) while UKIRT spectra were taken from Justannont et al. 1996 (1996 AA 309, 612) and KAO observations are described in Omont et al. (1995 ApJ 454, 819).

The result of this cross-calibration comparison is shown in Figure 55. The various data sets have not been shifted in any way. As we can see, there is an excellent agreement in most cases. This is usually better than the 10−15% level between all instruments and observing modes with two remarkable exceptions. These are IRAS 19477+2401 and IRAS 18576+0341, which have clearly been observed by ISO with the source off-centre, since the SWS spectra is well below the flux level at which these sources were detected using other facilities and show the characteristic flux jumps already mentioned in this document usually associated to bad pointed observations. Although not so clear, a similar pointing problem might be affecting the spectrum of IRAS 01005+7910.

Appart from these obvious strong effects, the only other remarkable discrepancy is observed between the SWS01 and the SWS06 observation of Z02229+6208 (25% difference), not yet understood. The IRAS 12 μm photometry is in close agreement with the SWS01 spectrum while the 25 μm band is in agreement with the flux level of the SWS06 observation. The observations were taken 4 days apart but we do not expect such a strong flux variation in that small period of time.

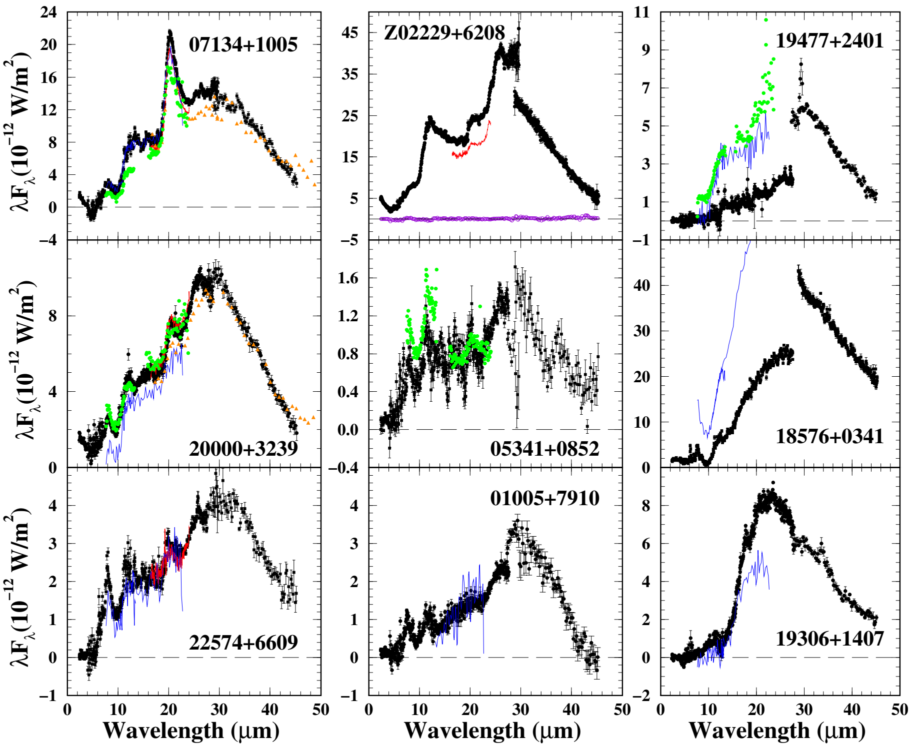

Figure 55: ISO SWS01 spectra (black squares), plotted with error bars. Plotted for comparison are IRAS LRS (blue lines), UKIRT CGS3 (green circles), KAO (orange triangles) and ISO SWS06 (red lines) spectra. No scaling factors have been applied to the ISO data - from Hrivnak et al. (2000, ApJ 535, 275)

The rest are minor differences which appear to reflect the levels of the precision in the calibrations of the various instruments.

Observations of four of the stars in the sample were also taken with PHT-S in the spectral region covering from 2.5 to 11.6 μm. The data were taken in staring mode for IRAS Z02229+6208 and IRAS 20000+3239 and in chopped mode for the two fainter sources, IRAS 01005+7910 and 19306+1409. They were reduced using PIA v7.3.2 at IPAC. The absolute flux calibration was carried out using the dynamic calibration method to correct the PHT-S staring spectra for transient effects and the special chopped mode calibration for the chopped observations.

The results are plotted in Figure 56 together with the rest of available data. Note that in this plot correction factors of 1.50, 2.92 and 1.82 have been applied respectively to the SWS01 spectra of IRAS 01005+7910, IRAS 19477+2401 and IRAS 18576+0341 to remove the effect of flux losses due to bad pointing.

In all cases PHT-S and SWS01 spectra agree well in shape where the source is bright enough to have a good quality SWS01 spectrum. The PHT-S data

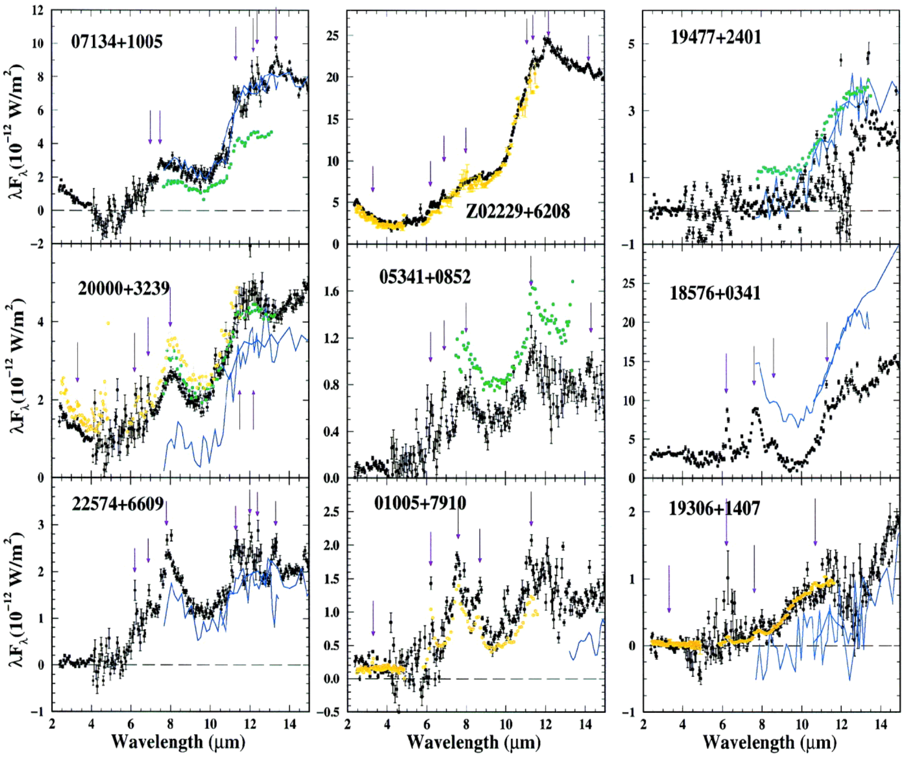

Figure 56: Expanded plot of the ISO SWS01 spectra in the 2−15 μm region, with ISO PHT-S (orange circles) spectra included, and spectral features marked by arrows. Other symbols are the same as in the previous Figure. The SWS flux densities for IRAS 01005+7910, 19477+2401, and 18576+0341 have been scaled by factors of 1.50, 2.92, and 1.82, respectively, while a scale factor of 0.76 was applied to the PHT-S spectrum of IRAS 20000+3239, as discussed in the text - from Hrivnak et al. (2000, ApJ 535, 275)

are shown to be particularly valuable as a supplement to SWS01 band 2 data, especially for detection of faint features in this wavelength range such as the 3.3 μm UIR feature. The agreement in flux level is good for all sources except for IRAS 20000+3239, for which the PHT-S spectrum was found 30% higher than the SWS01 spectrum.

Comparison with broadband photometry showed that the PHT-S observations for IRAS 20000+3239 were too high in flux density for unknown reasons while the SWS01 observations agreed with the photometry. Therefore, a scale factor of 0.76 was applied to the PHT-S data for this object and produced good agreement with the SWS01 data.

3.5.8 Science with ISO cross-calibration

Multi-wavelength observations of the proto-planetary nebula Hen 401

ISO SWS and PHT-S observations of the bipolar proto-planetary nebula

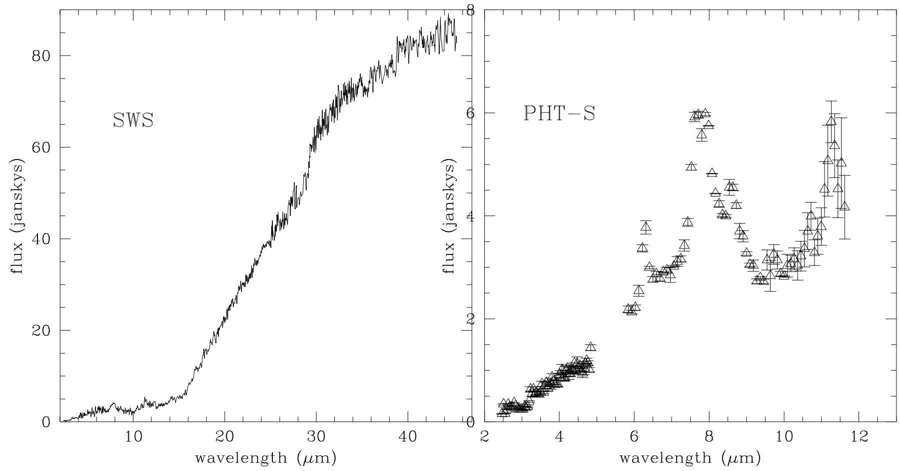

Figure 57: ISO SWS (left) and PHT-S (right) spectrum of the proto-planetary nebula Hen 401 - Parthasarathy et al. (2000 A&A, submitted)

Hen 401 (= IRAS 10178−5958) have been used in combination with ultraviolet (IUE) spectroscopy, optical and near infrared ground-based photometry and IRAS photometry at 12, 25, 60 and 100 μm to reconstruct the overall spectral energy distribution of this source from 1150 Å to 100 μm.

The full range (speed 1) SWS01 spectrum, originally standard pipe-line processed with OLP version 8.4, was reprocessed using OSIA v1.0 All detector signals were inspected for spurious features (small jumps and glitches) which were removed. A flux depression originally observed in band 3E of the SWS spectrum was identified as an artifact and, thus, the emission of this band was manually shifted to match the flux level of the adjacent bands 3D and 4.

The PHT-S spectrum, taken in staring mode and also originally standard processed with OLP version 8.4 was further inspected for residual glitches not detected by the pipeline and corrected for transients using the available dynamic calibration method as it was implemented in PIA v8.1.

Figure 57 shows the ISO SWS spectrum (left) and the ISO PHT-S spectrum (right) of Hen 401. A first inspection reveals the presence of PAH features at 3.3, 6.2, 7.7, 8.6 and 11.3 μm, suggesting a C-rich nature of the circumstellar envelope, overimposed on a cool continuum. A comparison between the two ISO spectra shows a very nice agreement both in the overall shape and in the absolute flux level (within 10%).

In Figure 58 we show the ISO results plotted together with IRAS photometry at 12, 25, 60 and 100 μm, the IUE spectrum, ground-based optical BVRI photometry and near infrared photometry taken in the J, H, K, L' and M filters.

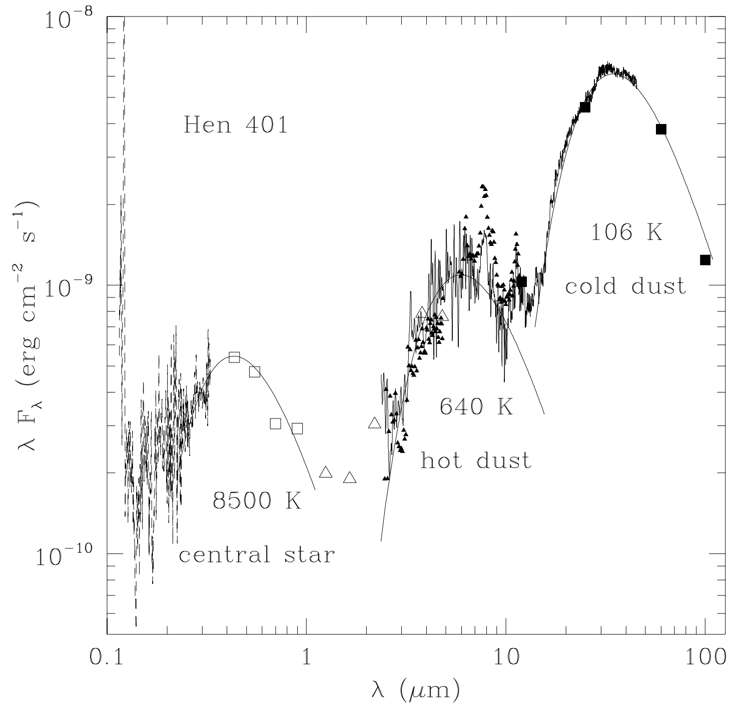

Figure 58: The flux distribution of Hen 401 from the UV to the infrared. ISO SWS (solid line), PHT-S (filled triangles) and IUE data (dashed line) are plotted together with ground-based optical BVRI (open squares), near infrared JHKL'M (open triangles) and the IRAS photometry at 12, 25, 60 and 100 μm (filled squares).

As we can see, there is a nice consistency also with the results coming from the various other sources of information.

From the analysis of the results obtained, it can be concluded that the overall spectral distribution of Hen 401 can be well reproduced by a very simple model composed of three different black-bodies emitting at 106, 640 and 8500 K. The cool dust component is interpreted as thermal emission from the dust present in the circumstellar envelope of Hen 401, the remnant of the previous strong mass loss AGB phase, while the hot dust component is attributed to emission from dust grains recently formed in the outflow close to the central star as a result of on-going post-AGB mass loss; the third, stellar component is the result of the contribution from the A8-B0 type central star detected in the optical and in the UV.

The full multi-wavelength analysis of this source can be found in the paper *"IUE and ISO observations of the bipolar proto-planetary nebula Hen 401"* by Parthasarathy et al. (submitted to A&A).

4 Calibration accuracies and 'Error Budget'

In the following, we will try to summarize the 'state-of-the-art' of the calibration of each of the instruments on board ISO as of June 8, 2000. Note that this cross-calibration report may not reflect the latest up-to-date information on a specific instrument/observing mode.

For a revision of the latest information available we suggest to check the general ISO documentation available in the Web at:

http://www.iso.vilspa.esa.es/users/expl_lib/expl_lib.html

4.1 PHT

4.1.1 Improvements in OLPv8.4 for PHT

In August 1999, version 8.4 of the PHT OLP pipeline for automatic data processing was released. This version represented a major upgrade in the calibration of PHT data.

This is a summary of the main improvements implemented in version 8.4 of the pipeline:

- **Flux dependent signal linearization:** calibration measurements on celestial standards demonstrate that the detector has a non-linear response. Data used to calibrate the internal radiation sources (FCS) with celestial standards become now more consistent after linearization. Since it is applied early in the signal processing chain, it required the redetermination of several Cal-G files. Considerable changes of photometric results are expected in cases where the FCS measurement is not taken at an adequate power level, like in multi-filter AOTs on targets with a steep spectrum, extended sources - when moving from a small aperture to a large one can easily give a factor of 10 increase in power on the detector (note that the FCS is always tuned according to the brightest flux) - or maps with a high dynamic range.

- **PSF factors for PHT-C arrays**: the upgraded PSF factors for the PHT-C arrays provide consistent photometric results, in particular for all filters in C200

- **Multi-filter staring modes:** The OLP processing of the PHT staring modes PHT03 and PHT22 were successfully re-validated. This includes extended source photometry with PHT-C (PHT22). In general, both the absolute and relative calibration are improved by this OLP version.

- **Absolute photometric modes:** The OLP processing of the PHT absolute photometric modes PHT05 and PHT25 were also successfully re-validated. Spectral shapes and features are maintained. Good matches in absolute level and relative shape with reference spectra and photometry are found.

Table 3: Covered wavelength range and typical aperture sizes of ISOPHOT subinstruments. Note that for PHT–C the first aperture number denotes the pixel size, the second one the array size.

subinstrument	**detector**	**dimension**	**wavelength range** [μm]	**typical aperture size** [“]
PHT–P	P1	1	3 – 17	5 – 180
	P2	1	15 – 29	23 – 180
	P3	1	40 – 130	52 – 180
PHT–C	C100	3x3	40 – 130	43.5 / 138
	C200	2x2	100 – 240	89.4 / 182
PHT–S	SS	1x64	2.5 – 4.8	24
	SL	1x64	5.8 – 11.8	24

- **Spectroscopy in staring mode on extended sources:** The OLP processing of the spectroscopic mode PHT40 (PHT-S) staring on extended sources was successfully re-validated. It now contains the updated solid angle determination, including the extension of the beam beyond the physical PHT-S aperture size.
- **Chopped modes:** a new calibration method developed at MPIA was implemented in the pipeline which provides better robustness against glitches and a better correction for the signal losses. The new products were, however, still not validated pending a critical assessment. It makes use of the periodicity of the measurements and constructs a characteristic pattern, representing both signal levels - on source and off source - by 8 data points. Three classes of patterns were already distinguished: a linear case, a curved case and an overshooting case.

4.1.2 Current calibration accuracies and 'Error Budget' for PHT

The latest report available concerning updated PHT calibration status still refers to OLP v8.4 and it is contained in the document *Release Note for ISOPHOT OLP Version 8.4* by Ulrich Klaas and Phil Richards available at:

`http://www.iso.vilspa.esa.es/users/expl_lib/PHT/olp_84release.ps.gz`

Soon a new document corresponding to OLP v9.0 data will be posted in the web and announced conveniently.

More general information on the calibration status of PHT can be found in the document *ISOPHOT Calibration Accuracies* by U. Klaas et al. available at:

`http://www.iso.vilspa.esa.es/users/expl_lib/PHT/calacc_v3.ps.gz`

Again, an updated version of this document is expected soon.

Table 4: ISOPHOT Photometric Calibration Accuracy Overview (as of OLP v8.4).

detector	**source type** point / extended	**source brightness**	**typical on-source integration** [s]	**absolute accuracy** [%]	**multi-filter accuracy** [%]
P1	p	30 – 6000 Jy	32	10	20
P1	p	0.1 – 30 Jy	$\leq$ 256	40	TBD
P2	p	10 – 200 Jy	32	$<$ 15	5
P2	p	0.5 – 10 Jy	$\leq$ 256	$<$ 15	5
P3	p	0.5 – 25 Jy	32	15	10
P3	p	$<$ 0.5 Jy	$\leq$ 256	30	TBD
C100	p	5 – 25 Jy	32	15	25
C100	p	$<$ 1 Jy	$\leq$ 360	40	TBD
C100	e	5 – 15 $\mathrm{MJy\,sr^{-1}}$	32	20	$<$ 30
C200	p	0.5 – 900 Jy	128	10	30
C200	p	0.2 – 1 Jy	$\leq$ 240	30	TBD
C200	e	4 – 10 $\mathrm{MJy\,sr^{-1}}$	64	20	$<$ 30
SS staring	p	2 – 5000 Jy	256	$<$ 30	$<$ 30
SS staring	e	50 – 10^5 $\mathrm{MJy\,sr^{-1}}$	256	$<$ 30	$<$ 30
SL staring	p	1 – 5000 Jy	256	$<$ 30	$<$ 30
SL staring	e	50 – 10^5 $\mathrm{MJy\,sr^{-1}}$	256	$<$ 30	$<$ 30
SS chopped	p	2 – 5000 Jy	256	10	10
SS chopped	e	50 – 10^5 $\mathrm{MJy\,sr^{-1}}$	256	10	10
SL chopped	p	1 – 5000 Jy	256	10	10
SL chopped	e	50 – 10^5 $\mathrm{MJy\,sr^{-1}}$	256	10	10

Table 4 gives a summary overview of the currently achieved photometric accuracies. Absolute and relative accuracies are still based on the analysis made with OLPv8.4 data products.

Note that a number of AOTs are not yet scientifically validated (see Table 5) and, thus, no global accuracies can be provided. In addition, the two polarisation modes PHT50 (PHT-P) and PHT51 (PHT-C) are processed by the pipeline only to raw data level and are not here considered. It is the goal of ISO Post Operations to scientifically validate the OLP processing of all standard AOTs in Table 5 for which this is pending.

Most of the problems above listed are among the list of currently known limitations and caveats which are discussed in Chapter 2 of the *Release Note for ISOPHOT OLP Version 8.4* above cited. The reader is refered to this document for a more detailed description of each of these individual problems.

Note that a careful interactive analysis using PIA may significantly improve the calibration accuracy numbers given in Table 4. Unfortunately, it is not possible here to give numbers as a function of the AOT and/or the characteristics of the source observed since so far no comprehensive systematic investigation was performed. But one can expect to achieve a higher accuracy using PIA in the following cases:

1) measurements with signal transients which do not stabilise during the measurement time, but which are long enough to perform a reasonable transient fit.
2) flat-fielding of maps, depending on the sampling mode and the dynamic range.
3) correction of non-linear signal drifts in maps.
4) detection of faint sources by refined deglitching and filtering.
5) photometry from mini-maps, through visual determination of sky background

4.1.3 Improvements expected in PHT OLP v9.0

In late June 2000 the new version 9.0 of the PHT OLP pipeline for automatic data reduction will be released. Note that this means that, after this release, PHT data retrieved from the ISO Data Archive using the *'Latest Processing'* option will be processed with OLPv9.0.

This is a summary of the main improvements expected in this new version 9.0 of the pipeline:

- **PHT-S dynamic calibration:** probably the most relevant improvement in OLP v9.0. Used to correct staring observations for transient effects, it will bring down the errors associated to this observing mode (sometimes as high as 30%) to just a few percent. For a short description of the method see the *'Transients WG'* Section of this document. Unfortunately, it cannot be applied to raster maps, since there is no dark measurement preceding the spectra at each raster pointing (needed for the reproducibility of the transient behaviour as a function of flux). In any case, PHT-S raster maps represent only a minor fraction of the PHT data.
- **Non-linearity corrections:** refinements of the flux-dependent signal linearisation have been incorporated in OLP v9.0.
- **Chopped mode observations:** Some improvements have been implemented in PHT-P and PHT-C chopped calibration.
- **Provision of Source Flux density and Surface Brightness in Products:** For point source photometry, in addition to the PSF corrected (for aperture size or array size) source flux per pixel and source + background flux per pixel in units of Jy/pixel, the equivalent surface brightness in MJy/sr will also be written to the AA product. For extended source photometry, in addition to the source surface brightness and the source +

background surface brightness in units of MJy/sr, the equivalent flux in Jy/pixel will also be written to the AA product.

4.1.4 Future plans in PHT calibration

In the next (and last) version of the OLP pipeline v10.0 other calibration problems will be addressed. The main pending calibration issues concern:

1) validation of chopped photometry calibration
2) PHT-P aperture calibration, both for external (sky) and internal (FCS) beams
3) PHT32 (chopped raster maps) calibration

While issue 1) is in good track with good confidence to be finalized for OLP v10.0, the other two issues are still open with regard to what results can be finally achieved. The likelihood of implementation in OLP v10.0 is not high, due to the complexity of the tasks and manpower limitations.

Concerning assessment of chopped observations with P2 filters, a report has recently been prepared by R. Laureijs and M. Jourdain de Muizon on *Processing of ISOPHOT chopped photometry at 25 μm* available at:

`http://www.iso.vilspa.esa.es/users/expl_lib/PHT/report_25chop.ps.gz`

This document presents the results derived from a refined analysis of a homogeneous sample of more than 80 main sequence stars which were observed with PHT03 at 25 μm in chopped mode. After comparison of the ISOPHOT photometry with estimates of the stellar fluxes at 25 μm derived from photometric data in the optical from Hipparcos it is found that the ISOPHOT calibration currently implemented in OLP v8.4 can be strongly improved by assuming a default responsivity for the P2 detector corrected for orbital dependence. In addition, a relationship is derived which corrects for the effect that in chopped mode the fluxes of bright objects ($>$ 1 Jy) are undererstimated whereas the fluxes of fainter stars ($<$ 3000 mJy) are overestimated. The large deviations from the predictions found using OLP v8.4 processing justify the conclusion that these results cannot yet be scientifically validated.

With respect to the problem of the determination of aperture profiles in PHT-P detectors, aperture calibration will be focused on the 180$''$ aperture in order to safe the wide beam absolute sky measurements for the Legacy Archive. The status is the same for both OLP and PIA, since the implementation limitation is due to the still lacking calibration assessment.

This means that the following modes remain non-validated:

- point source photometry in non-standard apertures
- extended source photometric calibration with PHT-P

Table 5: Status of scientific validation of PHT OLP AOT processing

AOT	submode	scientifically valid since	next upgrades	foreseen in OLP Vx.y
PHT03	staring point source	V6	non-lin R	9.0
			FCS aper	10.0
	staring extended source	no	non-lin R	9.0
	nodding	V6	non-lin R	9.0
			FCS aper	10.0
	chopped point source	no	chop & non-lin R	9.0
	raster map	no	map cal	10.0
			drift	10.0
PHT04	staring point source	no	non-lin R	9.0
			beam & FCS aper	10.0
	staring ext. source	no	non-lin R	9.0
			beam	9.0
	chopped point source	no	chop & non-lin R	9.0
			beam	10.0
PHT05	staring point source	V6	non-lin R	9.0
			FCS aper	10.0
	staring extended source	no	non-lin R	9.0
			beam	10.0
PHT17/9	staring point source	V6	non-lin R	9.0
			FCS aper	10.0
	staring extended source	no	non-lin R	9.0
			beam	10.0
PHT22	staring point source	V7	non-lin R	9.0
	staring extended source	V7	non-lin R	9.0
	nodding	V7	non-lin R	9.0
	chopped point source	no	chop & non-lin R	9.0
	raster map	V8.4	flat-field	10.0
PHT 25	staring point source	V7	non-lin R	9.0
	staring extended source	V7	non-lin R	9.0
PHT32	chopped mapping	no	chop & map cal	10.0
PHT37/9	staring point source	V7	non-lin R	9.0
	staring extended source	V7	non-lin R	9.0
PHT40	staring point source	V5	dyn cal	9.0
	staring extended source	V6	dyn cal	9.0
	chopped point source	V6		
	raster map	V6	TBD	

meaning of calibration upgrades:

FCS aper : correction for inhomogeneous illumination of PHT-P apertures by FCS
non-lin R : refinements of flux dependent signal linearisation
beam : beam profile corrections
chop : chopped photometry corrections
map cal : surface brightness calibration in maps
drift : correction of non-linear long-term drifts
flat-field : refined flat-field corrections
dyn cal :dymamic calibration method to correct for signal transients

- multi-aperture photometry in both cases

Note that the first of these items, point source photometry in non-standard apertures, may only be critical for the largest apertures. It is unlikely that for P1 and P2 point source photometry these large apertures were used (for P3, $180''$ is the standard aperture and hence calibrated).

With respect to the second item listed above, there are plans to perform an assessment of PHT-P extended source calibration vs COBE/DIRBE during the coming months as part of the extended OLP 9 scientific validation. For most PHT-P filters the background should be dominated by the smooth Zodiacal light (hence the beam size effects should not have such a big impact).

Finally, concerning point 3) in the list of pending items for OLP v10.0, a PHT32 processing prototype including full transient modelling is currently being developed by Richard Tuffs within PIA. It is still too early to conclude on possible final calibration accuracies for point sources and slightly extended sources. For OLP v10.0 at least a calibration accuracy assessment will be performed. Some feedback on PHT32 signal losses and transients may also come from the chopped photometry calibration assessment by understanding the commonality in time constants and the crucial parameters behind the chopped patterns.

Other general calibration areas to be improved for all modes in OLP v10.0 are:

- de-glitching: the two-threshold de-glitching method already implemented in PIA will be implemented in OLP v10.0. Chopped photometry de-glitching uses already the robust bi-weight mean method for individual signals derived from read-out pairs in order to construct the 'chopped pattern'.

- transient corrections: handling of transients inside OLP is currently restricted to drift recognition, using the Mann algorithm (also available within PIA); the software recognizes whether a measurement stabilizes within the available time or not; it tries to optimize the resulting signal by using the stable part or the last most evolved signal fraction. Detailed investigations on interactive transient correction methods are currently on hold due to lack of manpower. The evaluation of the FCS calibration data sets using empirical transient fits based on exponential functions including atomatic criteria for acceptance or rejection of the fit done has been suggested for implementation in OLP v10.0. This is, however, somewhat risky without extensive testing to apply a method usually used for relatively long calibration measurements to the majority of shorter FCS measurements in normal observations.

Another big issue which will probably be addressed in OLP v10.0 is a consistent error propagation handling and display in the products. In the current pipeline version the uncertainty information is restricted to statistical errors which are minimal errors.

Other calibration improvements, some of them flagged in Table 5, to reduce limitations on data quality are:

- FCS straylight contamination for C200 measurements (this is a byproduct of FCS calibration)

- correction for flat-field residuals in maps (PIA already offers several methods for improved flat-fielding)

- baseline drift corrections in nodding and raster map observations (PIA already offers median methods to flatten baselines).

- calibration of multi-aperture measurements of slightly extended sources following the method described by Thomas Müller (see *Beam Profiles WG* subsection) in order to provide the users with a method to distinguish between a pure point source and a possible contribution by a slightly extended component.

Of course, ISOPHOT polarisation observations are not processed by OLP. The current scheme to process up to signal level (intensities) per polarizer and derive polarization parameters within a dedicated FORTRAN routine may be upgraded to have the full processing within PIA. There is one open calibration and processing item, namely that for extended sources (can be compact) the four C200 pixels give discrepant polarization parameters.

From the above calibration status overview it is clear that some tasks can only be performed in a period of time which extends beyond the end of the Post-Operations Phase. The goal in any case, as we have already mentioned, will be to increase the amount of validated data products as much as possible in order to avoid a fair amount of unvalidated products in the ISO Legacy Archive.

With OLP 10, we envisage that about 80% of the ISOPHOT OLP data will be scientifically valid and milder caveats will apply. By the end of the Post Operations Phase 90% of the ISOPHOT data should be sufficiently reducible within PIA with regard to available calibration schemes. The remainders need ongoing efforts into an Active Archive Phase to achieve further completion and improved data quality for inclusion into the ISO Legacy Archive.

4.2 SWS

4.2.1 Improvements in OLPv8.4 for SWS

In August 1999 version 8.4 of the SWS OLP pipeline for automatic data reduction was released. This means that, at the present time, when SWS data is retrieved from the ISO Data Archive and the *'Latest Processing'* button is selected the user gets the data processed with OLPv8.4.

Improvements in the data reduction over OLP 7 were:

- **Wavelength accuracy improved:** During the mission it was discovered that the relation between the measured position of the grating (called

LVDT) and the wavelength was shifting steadily at a rate of about 1 LVDT per 6 months at most. This was corrected by re-deriving the relation every so often. As the shift itself was steady, this procedure resulted in a very low amplitude sawtooth-like behaviour of the wavelength calibration in time. In OLP 8.4 a linear interpolation was implemented to remove this sawtooth. The wavelengths are now steady to well within one LVDT, which corresponds to a fraction of a resolution element. The main source of error in the wavelength is (as it was before) the pointing error, corresponding to a few LVDTs.

- **Error information:** Two spare bytes in the AAR product (file swaa*.fits) are used to code the errors on the flux values, which are now used such that byte 0 contains the error in the offset of the slope, in Jy, (from dark current subtraction) whereas byte 1 contains the gain error as a percentage (from the fitting of the ramps themselves). These can be used to generate the 1σ error limits on the spectrum.

- **SPDs and off-band data:** The SPD and AAR products of OLP 7 only contained data from a wavelength within one of the several SWS bands, each band defined by a detector/aperture/order combination - for a list of these bands see Table 3.1 of the *SWS Instrument and Data Manual*. The calibration of data taken outside these bands was not guaranteed. In OLP 8.4, off-band data (i.e. data coming from outside these bands) was made present in the SPD product. This is because it is sometimes useful to have an overlap region between bands when comparing data. This off band data is not propagated through to the AAR product. Note that the next release of OSIA, version 2.0, will support off band data analysis.

- **Post-Helium observations:** S95, S96 and S97 were processed to SPD level and ingested in the ISO Data Archive. The wavelength calibration for these observations, however, is not done correctly and care should be taken if they are retrieved.

4.2.2 Current calibration accuracies and 'Error Budget' for SWS

A document describing the *SWS Calibration Status* as of March 1999, still esentially valid for OLP v8.4 data products is available at:

`http://www.iso.vilspa.esa.es/users/expl_lib/SWS/SWS_Cal_Accuracy.html`

For SWS the goals originally set before the mission (an accuracy of 30% or better) have, in general, been achieved for well-behaved data sets. By well-behaved data sets we understand point sources in the several hundred to several thousand Jansky flux density range that were observed with correct pointing and suffered no instrumental or operational problems.

In Table 6 an overview of flux calibration accuracies of SWS OLP products as of OLP v8.4 is given as a function of the SWS band considered. The quoted

Table 6: Overview of the SWS bands and flux calibration accuracy as of OLP v8.4

	Band	Key wavel. μm	Grating order	Aperture number/area $''$	Detector type	Wavelength range μm	Accuracy key - worst
SW	1A	2.48	SW4	1 / 14x20	InSb	2.38 - 2.60	5% - 7%
	1B	2.87	SW3	1 / 14x20	InSb	2.60 - 3.02	5% - 7%
	1D	3.08	SW3	2 / 14x20	InSb	3.02 - 3.52	5% - 7%
	1E	3.80	SW2	2 / 14x20	InSb	3.52 - 4.08	5% - 7%
	2A	4.50	SW2	2 / 14x20	Si:Ga	4.08 - 5.30	7% - 12%
	2B	5.90	SW1	2 / 14x20	Si:Ga	5.30 - 7.0	7% - 15%
	2C	7.70	SW1	3 / 14x20	Si:Ga	7.0 - 12.0	11% - 25%
LW	3A	14.0	LW2	1 / 14x27	Si:Ga	12.0 - 16.5	11% - 25%
	3C	17.0	LW2	2 / 14x27	Si:Ga	16.5 - 19.5	11% - 20%
	3D	24.0	LW1	2 / 14x27	Si:Ga	19.5 - 27.5	12% - 20%
	3E	28.5	LW1	3 / 20x27	Si:Ga	27.5 - 29.0	20% - 30%
	4	32.0	LW1	3 / 20x33	Ge:Be	29.0 - 45.2	30% - 35%
	5A	11.8	LW3	1 / 10x39	Si:Sb	11.4 - 12.2	11% - 25%
	5B	14.8	LW2	1 / 10x39	Si:Sb	12.2 - 16.0	11% - 20%
	5C	17.0	LW2	2 / 10x39	Si:Sb	16.0 - 19.0	11% - 20%
	5D	24.0	LW1	2 / 10x39	Si:Sb	19.0 - 26.0	12% - 30%
	6	27.0	LW1	3 / 17x40	Ge:Be	26.0 - 44.5	30% - 35%

'worst' uncertainties are primarily valid for the edges of the bands, representing the maximum product of the absolute and relative spectral responsivity uncertainties.

The flux reproducibility was checked during the mission by regular observations of the calibration star HR 6705. The various measurements agreed to within 6% for band 1 and 2 to 15% for bands 2 to 4.

Unfortunately, an 'error-recipe' for the combination of all the known individual error contributions to a useful overall error estimate for SWS data products does not exist yet.

The problem is that the relevance of the various error contributions depends strongly on the properties of the observed source as well as on the type of scientific analysis that is aimed for.

Thus, no 'error budget' in the true sense can be given, although it is possible to provide the user with an indication of the currently known error contributors.

Some of the known sources of error are:

Detector memory effects: Band 2 (Si:Ga) and band 4 (Ge:Be) are specially affected. Strong sources are more seriously affected (up to the 20% level). A transient correction based on the Fouks-Schubert model applicable to band 2 data will be implemented in OLP v9.5 and OSIA v2.0 (both to be released by September 2000) which will bring the errors (sometimes up to 20%) down to the few percent level. The signature of memory effects is that the up- and down-scans are different in flux level. The down-scan normally succeeds the up-scan in the AOT and appears to be already 'accustomed' to the flux level. No working solution has been found yet for SWS band 4 memory effects.

Pulse shapes: these are small detector voltage jumps visible at SPD level which affect the calibration of SWS spectra leading to flux shifts of up to 10 Jy in the worst cases. They might have an important effect in faint sources. A correction tool will be implemented in OLP v9.5 (September 2000). As a byproduct, it will also improve the detectability of glitches.

Dark current problems: dark currents corrupted by memory effects or glitches usually result also in systematic differences between the up- and down-scans. For large errors in the subtracted dark current, the final spectra will resemble the spectral responsivity. Unfortunately, small dark current problems and memory effects have a similar signature in the final spectra.

Fringes: Bands 2 and 3 can be affected. The amplitude and frequency of the fringes depend on the source morphology, brightness and position in the SWS entrance aperture. Fringe amplitudes of about 5% of the continuum level are seen in band 2 and up to 20% in band 3. Fourier filtering or sine fitting can be used to remove the fringes 'manually'.

Pointing Offsets: As a consequence of the non-uniformity of the detector material and small internal misalignments, the signals in the different AOT bands are reduced by band-dependent factors when a point source is observed with a pointing offset with respect to the centre of the SWS aperture. Corrections for this effect is possible now that the detailed beam profiles have been determined and the actual satellite pointing is known with sufficient accuracy. A pointing correction tool will be available in OSIA v2.0. Pointing offsets are recognized by jumps in the continuum level at band edges in AOTs 1 and 6. In AOT 2 data the effect is very difficult to see. In some cases small offsets of just a few arcseconds can lead to 20% flux deviations.

Glitches: All SWS detector data suffer from cosmic ray hits. Some of them are removed automatically, but especially in the long wavelength bands, usually more strongly affected, the removal is far from complete. Tails following a cosmic ray hit are usual in these bands. Currently, they can only be removed manually within OSIA.

Extended sources: SWS calibration is based on point source emission. As a result, the fluxes derived are not appropriate for extended sources (partially) filling the SWS aperture. At the band edges, jumps in the signal level are seen, which are due to changes in the effective size of the detectors. To obtain reliable flux densities for extended sources, the SWS detector beam profiles should be convolved with the source structure at the appropriate wavelength. As a first order correction, the ratio of the aperture sizes can be taken.

Very weak sources: For very weak sources careful inspection of the data is required to be able to filter out data affected by glitches and determine the true dark current level, while fringes are normally insignificant. Proper calibration and analysis of such data is only possible with much manual labour.

Very bright sources: Very bright sources suffer mainly from memory effects and fringes. The data may also be affected by detector saturation which starts to become important at the several 10000 Jy level. Again, manual labour is needed to deal with such observations.

Generally, for well-behaved data sets, the use of OSIA's tools does not lead to strong improvements in the calibration with the exception of data affected by the presence of interference fringes in band 3 and, to a lesser degree, in band 2.

For data sets that are not well-behaved the quoted accuracies are not reached with standard OLP processing. However, often manual processing using OSIA tools allow to reach the same level of accuracy.

4.2.3 Improvements expected in SWS OLP v9.5

In September 2000 a new version 9.5 of the SWS OLP (pipeline) for automatic data reduction will be released. A strong effort has been made to convert the software code from FORTRAN to IDL, so that the same modules are now used in OSIA and in the pipeline (some optimization still needed).

Appart from this S/W change, the new OLP version 9.5 will include among others the following improvements:

1) **Correction for memory effects in band 2:** based on the adapted Fouks-Schubert model, decreasing up to the few percent the error contribution for this effect.

2) **Pulse shape correction:** the tool which correct for these voltage jumps by adjusting a baseline to the affected portion of data is expected to remove almost completely the effect on the calibrated spectra.

3) **Improved glitch detection:** small changes implemented. In general we expect a better detection of glitches after the pulse shape correction is implemented.

4) **Slope fitting:** improved with refined algorithms.

In addition, the new beam profile calibration files will be made available together with the OLP v9.5 data products and in OSIA v2.0. The SWS pointing correction tool will also be implemented as a new module in OSIA v2.0.

4.2.4 Future plans in SWS calibration

There are plans in the future to update or add a large list of modules to the SWS pipeline processing.

They are related to improvementes in: midbit correction, reset cutout length, de-biasing in band 4, AC correction, glitch treatment (including a higher order polynomial fit in the glitch detection algorithm, the extension of the search to the full reset interval and the use of a fit slope+step function) and cross-talk corrections.

Most of these changes will basically lead to a better linearization of SWS integration ramps.

In addition, the wavelenght calibration of post-He observations will be improved. Additional analysis of pre-saturation, improved error calculation and a complete re-derivation of band 2 RSRFs consistent with 'dynadark' are also foreseen, as well as improvements in de-fringing. Finally, a new dark subtraction method in band 2 completely different to the existing one is expected in v10.0 of the pipeline.

It is obvious that the quality of all these improvements can only be judged at the time they are implemented.

In some cases, the corrections, if available, will only be implemented as part of OSIA, but not in the pipeline. This is the case of memory effect corrections in band 4 or the point-to-extended flux conversion.

4.3 CAM

4.3.1 Improvements in OLPv8.0 for CAM

Version 8.0 of the CAM pipeline was released in May 1999. This version contained two minor changes which have implications for the science data provided to the user with respect to version 7.

- Improved LW *"Optical Flats"* in the Cal-G files.
- Improved non-illumination masking (algorithm to detect non-illuminated pixels at the edges of the array, caused by imperfections in instrument wheel positioning).

Appart from these, no other major changes were implemented in this version of the pipeline.

4.3.2 Current calibration accuracies and 'Error Budget' for CAM

The latest report on CAM accuracy is contained in the *ISOCAM Calibration Accuracies Document* by Joris Blommaert and Diego Cesarsky (November 1998) which refers to OLP v7 data products (but it is still esentially valid for OLP v8.0) and it is available at:

`http://www.iso.vilspa.esa.es/manuals/CAM/accuracies/cam_accur/`

An overview of the flux accuracy of the different CAM OLP data products is given in Table 7 for two different brightness levels. The numbers in this Table are based on the analysis of standard stars observed in the central part of the array. Note that although polarisation observations (CAM05) are handled by the off-line software, this mode is not implemented in the standard way (i.e. not via an AOT). Then for this mode the concept of scientific validation does not apply.

A description of the known sources of error affecting CAM calibration and the corresponding 'error budget' is contained in *The ISOCAM Calibration Error Budget Report* by Andrea Biviano (November 1998), available at:

http://www.iso.vilspa.esa.es/users/expl_lib/CAM/errdoc.ps.gz

The following sources of error are identified:

- **Transients:** in general, the dominant error source in CAM images are transients, for which a correction is foreseen in v9.5 of the pipeline based on the Fouks-Schubert model. In general, the photometric fluxes derived in the pipeline are found to be systematically lower than the stellar model fluxes. This is due to the calibration files which assume the data is already stabilized. In particular, most of the CVF observations are usually performed after a discrete filter observation, thus implying a large decrease in the incident flux on the detector. This can introduce important transient effects that last several readouts and hence several wavelength steps. The result is a larger than true flux for the first wavelength steps. We also know that transients are more important for weak sources than for bright sources and this is the most important reason for the differences in the uncertainties quoted in Table 7.

- **Glitches:** the contribution of glitches to the overall noise of CAM images is also important. 'Common' glitches are associated to impacts of cosmic ray electrons while the so-called 'faders' and 'dippers' are linked to impact of protons or α particles. Tipically, 'common' glitches are easy to remove while the rare 'faders', followed by a slow decrease of the signal, and 'dippers', followed by a reduction in the sensitivity of the affected pixel, have a long lasting effect more difficult to remove. Unfortunately, since the detection of glitches in the pipeline is based on simple median filtering algorithms, only a fraction of them are automatically removed and manual processing with CIA is needed.

- **Point Spread Function:** the fluxes for point sources in the CPSL (CAM Point Source List) FITS file are derived by PSF-fitting in the image. This photometry can be affected by larger errors than stated in Table 7 if the fitting is incorrect. The observed PSF is generally quite close to the theoretical one if the ghost contribution is not significant (see below). However, the accuracy of the PSF does not allow deconvolution yet.

Table 7: ISOCAM Photometric Calibration Accuracy Overview.

CAM AOT	$>$ 100 mJy key	$>$ 100 mJy worst	$<$100 mJy
CAM01	10%	20%	30%
CAM03	10%	20%	30%
CAM04	15%	40%	40%
CAM05	n.a.	n.a.	n.a.

- **Ghosts:** CVF observations might be affected by the existence of 'ghosts' generated by multiple reflections between the detector and the CVF surface. Ghosts can appear away from the source image but may as well fall onto (and surround) the sky image, depending on the actual position of the source on the detector. In some cases, the photometric accuracy can be affected up to 35% by the presence of ghosts, and straylight from sources outside the theoretical field of view can also affect CVF images so that sources with a flux below 10% of the background might not be detectable.

- **Flat-field:** because of wheel-jitter the 'library' flat-field may not cover the same detector region as the sky image does. The effect is small in the central region of the array where the uncertainty is less than 1%. The uncertainty becomes, however, very large in the edges (up to a factor of 5 in extreme cases), where vignetting is important (for example in the case of a $6''$ p.f.o.v. measurement). Incomplete stabilization is another issue to consider. A large part of the small residual error in the flat-field observations is probably due to this effect. In any case, the noise levels reached are lower than expected pre-launch (1% in LW and 3% in SW).

Other error contributors like saturation, read-out, gain accuracy, dark current stability are also discussed in the 'error budget' document above refered. A summary of the main conclusions is displayed in Table 8.

Table 8: ISOCAM photometric calibration error budget.

Noise origin	magnitude	after correction
Stabilization (random)	10 x sky noise	2 x sky noise
Stabilization (systematic)	40% of source flux	15% of source flux
Saturation	$\geq$30% decrease in responsivity	
Read-out noise	LW: 0.7 ADU/g SW: 2 ADU/g	
Gain	0.15% output current	
Dark current	LW: 0.5 ADU/g SW: 0.5 ADU/g	0.25 ADU/g
Flat-field	LW: 0.5% (high background) SW: $\leq$ 1%	
Conversion signal$\rightarrow$flux	5%	
Point Spread Function	20%	few%
CVF RSF	3%	
Ghosts	$\leq$35%	
Straylight	10% of sky flux	

Regarding flux reproducibility, repeated photometric observations on HIC 89474 throughout the whole ISO lifetime give a standard deviation of around 2% for both LW and SW detectors. Similar observations on a larger set of absolute flux calibration standards give an r.m.s. of around 5%. It was also found that the LW detector is very linear over a very large range of flux levels from a few mJy up to the saturation level. From CVF observations the derived r.m.s. is 3% for the SW part and 4% for the two LW CVF segments.

Significant improvements in the photometric accuracy of ISOCAM data can be achieved by making use of the software tools implemented in CIA, the Interactive Analysis software package for ISOCAM data reduction.

Deglitching routines are available under CIA although they only mask the frames corresponding to the glitches. Thus, a visual inspection of all pixels histories is needed for a proper masking. The impact of 'faders' and 'dippers' is related to the general problem of the transient behaviour of the CAM detectors and can be corrected using transient correction algorithms implemented in CIA, based on the so-called 'IAS method' (for LW detectors).

Manual elimination of ghost images, which can in some cases lead to errors up to 35% in aperture photometry, is also possible with CIA, as well as the elimination of inaccuracies introduced by inaccurate flat-fields, at least in the case of rasters with sufficient background and redundancy (not possible, however, for staring observations yet).

In summary, the magnitude of all the above effects compared to pre-launch expectations are generally in good agreement. Note that in Table 8 the 5% accuracy quoted as error induced by the conversion factor from ADU/g/s to Jy is worse than the pre-launch value (2%) because the measured photometry is PSF corrected, so this error estimate includes also the uncertainty in the PSF.

The CVF Spectral Response Function (SRF) is very well constrained. Typically the accuracy is at the 3% level on average in the absence of ghosts and straylight.

4.3.3 Improvements expected in CAM OLP v9.0 and v9.5

Very soon (late June 2000), a new version 9.0 of the OLP pipeline for automatic data reduction will be released. In principle, it was intended to contain among others two major changes: the Fouks-Schubert correction for transients and a new proto-type 'faint source treatment'. Unfortunately, due to late hour complications in the validation of the new pipeline, it has been decided to postpone the implementation of these two important improvements a few weeks and release the new version of the CAM pipeline together with the SWS version 9.5 in September 2000.

Note that this means that, as new versions will become available in the next few months, CAM data retrieved from the ISO Data Archive using the *'Latest Processing'* option will be processed either with OLP v8.4, OLP v9.0 or OLP v9.5.

Other improvements which will be implemented in CAM OLP v9.0 concern:

- **pointing:**
- **CSTA generation:**

- **CAM parallel observations:** the new data products have been produced and they have already been been ingested in the ISO Data Archive.

As we have already mentioned, at a later stage, the revised version 9.5 of the pipeline will be released (September 2000) containing:

- **Fouks-Schubert correction for transients:** will increase the accuracy of the photometry by correcting the LW data for transient effects. Note that the correction is very good for low contrast illumination (extended sources and/or faint sources over a high background) but still fails on point sources and strong gradient illumination.

- **Faint Source treatment:** this is a S/W package especially intended to deal with faint sources, which will improve significantly the detection and photometry of sources at very low flux level.

Other algorithms will remain for the time being only available under CIA, like the variable flat-field correction, various sophisticated de-glitchers and the code SLICE to remove long-term transients in CAM redundant data.

4.3.4 Future plans in CAM calibration

The expected accuracies of ISOCAM's final OLP data products will strongly depend on whether ways are found to transfer into the pipeline some of the calibration tools which are currently under development and/or only available under CIA.

In many cases, this will probably not be possible, either because there is no time left for coding the new calibration results (transients in point sources, ghosts model) or because they are tools which require a high degree of interactivity and, thus, it is not easy to make them available in an automated pipeline (mostly those currently available in CIA, such as the various de-glitchers or the SLICE S/W package mentioned above).

Concerning calibration issues which are still under investigation like the transient correction for point sources or the recognition of ghosts and the creation of a ghosts correction matrix, it is assumed that any progress will come too late for its inclusion into OLP v10.0. Should these algorithms become available in time, then their inclusion will become a high priority item but, in principle, they are foreseen only for implementation in CIA at a later stage.

Concerning the tools which are at the present time only available under CIA, it is well known, for instance, that several de-glitching methods under test could also improve significantly the calibration accuracy of CAM maps and point/extended source detection, as well as PSF fitting, which may affect the photometry substantially. And it is also well known that the SLICE S/W package is giving excellent results when applied to extended faint sources in highly redundant CAM raster maps reducing the errors up to the limits imposed by read-out and photon noise equivalent to 100-200 μJy. Again, the problem here basically resides in how to make all these tools available in the CAM pipeline.

There are several areas where improvements are expected in version 10.0 of the CAM pipeline, like: inclusion of final sensitivity Cal-G files, sensitivity errors, a refined version of the 'faint source treatment' package, astrometric correction, flat-field corrections taking the lens-wheel jitter into account, treatment of flat/dark observations and mosaic generation.

4.4 LWS

4.4.1 Improvements in OLPv8.7 for LWS

As of December 1999, a new version (v8.7) of the LWS OLP pipeline for automatic data reduction was released. Currently, when LWS data is retrieved from the ISO Data Archive and the *'Latest Processing'* button is selected, the user gets the data processed with OLPv8.7.

One of the most important changes introduced in this new version of the pipeline is that data products are now derived using a new Uranus model in the LWS calibration files. The effect of the new model is that for a source decreasing in flux from short to longer wavelengths, the spectrum of this source is now 'flatter' in detectors SW1 and SW2. With the new model, both the RSRF and photometric calibration have been re-derived.

The photometric calibration of SW1, however, has been slightly degraded in the centre of the detector i.e. this is 10% higher than before as more of the detector was used to set the level. The photometric level of SW1 will be updated soon to replace it back to the OLP v7 level. The photometric levels of the other nine detectors remains the same as for OLP v7.

On checking all observations of Uranus against the model, a 'problem' has been found in the data. This has the effect that detectors SW1 and SW2 appear tilted down at short wavelengths and up at long wavelengths. This tilt has been noted for all observations after the LWS was switched off in the period corresponding to revolutions 380−442. Before this period the slope follows the model. This may indicate a change to the RSRF of these detectors during the switch off period but further investigation is needed before definitive conclusions can be made.

In addition, the OLPv8.7 LWS Fabry-Pérot products from AOTs LWS03 and LWS04 show a marked improvement in the flux calibration in comparison to their OLP v7 counterparts. As a consequence of this, the LWS04 mode was scientifically validated.

In OLP v7 the Fabry-Pérot LSAN file gave the flux per spectral resolution element (in units of W cm^{-2}). In OLP v8.7 the units will be W cm^{-2} μm^{-1}, where the throughput correction (i.e. the Fabry-Pérot transmission multiplied by the Fabry-Pérot resolution element) has been performed using Mars as calibrator.

The other noteworthy change in OLP v8.7 is that fixed dark currents are subtracted for all Fabry-Pérot observations, rather than those measured during

Table 9: Flux calibration accuracy of LWS OLPv8.7 data products per AOT

		LWS01 Grating	LWS02 Grating	LWS03 Fabry-Pérot	LWS04 Fabry-Pérot
Point sources	Bright	30%	30%	Unvalidated	n.a.
	Medium	10%	10%	Unvalidated	n.a.
	Faint	50%	50%	Unvalidated	n.a.
Extended sources	Bright	50%	50%	Unvalidated	n.a.
	Medium	30%	30%	Unvalidated	n.a.
	Faint	50%	50%	Unvalidated	n.a.

the observations themselves. These fixed set of detector dark currents originate from a series of dedicated measurements made in revolution 650.

Other minor changes were just oriented to ensure that LWS data will be Y2K compliant.

4.4.2 Current calibration accuracies and 'Error Budget' for LWS

A document describing the *LWS Calibration Status* as of November 1998 is available at:

`http://www.iso.vilspa.esa.es/users/expl_lib/LWS/LWS_Cal_Accuracy.html`

Although this report is based on OLPv7 data products, most of its content is still valid for OLP v8.7 data.

A summary of the main accuracy numbers is displayed in Table 9 as a function of the AOT and the brightness of the source observed. Note that the concept of 'bright', 'medium' and 'faint source depends on the observing mode. For the grating modes a 'bright' source means typically more than 1000 Jy at 120μm, while 'faint' could be a source with a flux density in the order of 10$-$50 Jy at 120μm. For the Fabry-Pérot modes these numbers have to be multiplied by a factor of 10 at least.

Some of the known sources of error affecting LWS grating observations are:

Dark current subtraction and memory effects: this especially affects spectra of faint sources. There is evidence that observation of a bright source before a faint one caused the dark current to be higher than expected and to be decaying during the subsequent observation. In addition, dark current variations have been observed within Fabry-Pérot measurements which are presently not fully understood.

Fringes: channel fringing is seen on the measured spectra of extended or off-axis point sources. Extensive modeling of the response of the instrument has been carried out using the ASAP optical design software showing that the fringes are produced by the interference between the reflecting surface of the LWS field mirror and its support structure as the diffraction pattern of the source falls off the edge of the field mirror itself. A quantitative model, however, is not yet available that would allow the removal of the fringes given knowledge of the spatial structure of the source. Instead, a method has been developed which performs a fit for the period, amplitude and phase of the sinusoid and removes it from the spectrum by division or subtraction.

Beam profile: the pipeline processing of LWS data makes no attempt to correct for the beam shape of the instrument. A model for the core of the beam profile has been obtained using spectra of Mars located at different positions with respect to the axis of the LWS as a function of wavelength. The observations show that the FWHM of the esentially gaussian beam profiles obtained are ~20% narrower than expected and assymetries and fringes are present in the wings. With the availability of the new model, it is now possible to convert from point source fluxes (Jy) to extended source fluxes (MJy sr^{-1}).

Non-linearity effects: Bright sources cause some of the detectors to become non-linear. The problem is complicated by photon curing of the detectors; this, in turn, causes the responsitivity of the detectors to change. An empirical method has been developed and implemented in the pipeline for the derivation of the photocurrent, and hence flux, from the voltage ramps which fits a first or second order polynomial automatically with no *a priori* assumptions about how the detectors respond, reducing the noise in the output spectra.

Time constants: The time constants of the detectors cause the shape of the spectrum (both lines and continuum) to be distorted under certain illumination conditions.

Poor order sorting: Spectra below 50 μm and between 83 and 90 μm might suffer from contamination owing to poor order sorting. An instrument model is required that will allow the determination and removal of the contamination.

Despite the significant advances achieved in the understanding of the Fabry-Pérot modes, some problems still remain to be addressed. These include:

Line asymmetry: The line profiles observed using AOT LWS04 are generally asymmetric, with the long wavelength wing at a higher level than the short wavelength one. This phenomenon is partially attributed to memory effects, also present in grating spectra. Various methods for removal of transient effects are being investigated. The effect on line flux depends on the line-to-continuum ratio. For example, for a line with no continuum, the line flux can change by as much as 30%. The effect on the velocity shift is relatively small (about ± 3 km s^{-1}). It is also possible that some of the profile asymmetry observed may well be due to loss of parallelism as the Fabry-Pérot line is scanned.

Velocity shifts: There appears to be a discrepancy in the measured and expected velocity shifts in LWS04 lines of up to ± 30 km s^{-1}, depending on the actual line being observed. At present the cause for this discrepancy is not known and is under investigation.

Removal of grating profile: Note that in the Fabry-Pérot modes, the problem with the underlying grating profile is not yet still fully solved. Removal of the grating response profile is complicated by the fact that the grating position is not known sufficiently accurately. This can result in a skewed spectrum. The user is recommended to refer to FP_PROC, the LWS Interactive Analysis (IA) Fabry-Pérot processing tool which removes the grating profile.

For LWS04 spectra the user can remove the skewness interactively, thereby deducing the actual grating position. For LWS03 observations, a least-squares fitting algorithm which minimizes the residuals in the overlap regions of spectra at adjacent grating positions is employed. The effect of not removing the grating profile on Fabry-Pérot line fluxes from LWS04 observations is likely to be very small, and this is why this mode was scientifically validated in v8.7 of the pipeline. However, for continuum fluxes in LWS03 observations the effect may not be negligible and is expected to be a function of the Fabry-Pérot scan extent.

The calibration accuracy of products manually processed with LIA does not strongly improve for the grating observing modes LWS01 and LWS02 for well-behaved data sets. The only changes expected concern LWS03 and LWS04. For bright sources observed with these AOTs there is an excess component in the signal that is most likely due to straylight.

A discussion on the individual contribution to the LWS photometry 'error budget' coming from the different steps involved in LWS data processing is contained in the document: *In-orbit performance of the ISO Long Wavelength Spectrometer* by Bruce Swinyard et al. (October 1998), available at:

`http://www.iso.vilspa.esa.es/users/expl_lib/LWS/HAWAII.PS`

Assuming a mean uncertainty in the Uranus model of ∼5% and a statistical error on the RSRF better than 0.01, for observations where the dark current is not a significant contribution to the signal, the uncertainty contributed to the measurement by the calibration process is estimated to be of the order of 7% for most detectors. In the case of faint sources, when the dark current becomes significant, the uncertainty in the measurement of the dark current begins to dominate.

Long term monitoring has shown that the reproducibility of the flux calibration is within 10% for all objects not influenced by the uncertainty in the dark current measurement.

For LWS the goals originally set before the mission (an accuracy of 30% or better in the grating mode and 50% in the Fabry-Pérot mode) have in most cases been achieved for well-behaved data sets. In some areas, however, problems remain and they are the subject of further investigation.

4.4.3 Future plans in LWS calibration

In the case of LWS it was decided that there will be no more pipeline version releases until the final one (OLP v10.0), expected in February 2001.

Meanwhile, the flux calibration accuracy of LWS is expected to improve significantly during the remaining post-operational phase.

Among the areas where improvements are expected in LWS calibration are:

- Drift correction

- RSRF changes before/after switch-off in revolutions 380−442

- Illuminator flash processing (new functionality)
- Strong source correction
- Intelligent Dark Current Subtraction (new functionality)
- Uranus/Mars models
- Glitch detection
- Fabry-Pérot wavelength calibration (velocity correction)
- LWS03 Fabry-Pérot observations
- Beam profile Cal-G files
- Uncertainty calculation
- Dark Current fixed values

Investigations are still on-going in order to decide which one of these improvements will finally be included in OLP v10.0. It may yet turn out that the solution is: a) not known; or b) not possible to include in a non-interactive pipeline (and thus is a candidate for LIA).

Solutions to other calibration problems are expected to be implemented only in LWS IA, like for:

- Transient correction
- Defringing
- Fabry-Pérot RSRF
- Straylight correction in Fabry-Pérot modes
- Grating profile removal from LWS03

Other LWS calibration items will only be documented, like the known problems with spurious features, filter leaks or the ghosts observed in Fabry-Pérot spectra.

Acknowledgements: Many people working at the ISO Data Centre and at the National Data Centres have contributed to the results here presented. They are too numerous to name individually but the improvements in ISO calibration would have never been possible without their enthusiastic dedication to the Project.